Detector Physics

G. Eigen, University of Bergen

HASCO July18-22, 2016 Göttingen

Introduction

- In particle physics, we build so-called multi-purpose detectors
- These are dedicated instruments that measure particular observables: vertex, track positions, particle IDs, momentum, energy, time, …
- In colliding-beam experiments, subdetectors are placed in layers around the interaction region in cylindrical geometry, like onion shells
- In fixed-target experiments, they are stacked behind the target in a fixed fiducial volume
- Though physics processes can be manifold and complex, we only encounter six particles in the final state: $e^{\pm}$, $\mu^{\pm}$, $\pi^{\pm}$, $K^{\pm}$, $p^{\pm}$, γ
- In matter, these particles interact electromagnetically

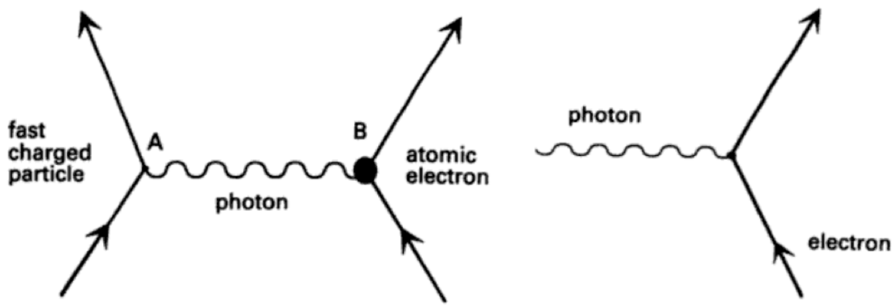

Multipurpose Detectors at LHC

- Each LHC experiment has about 100 million sensors
- Think that your 6MP digital camera takes 40 million pictures/s

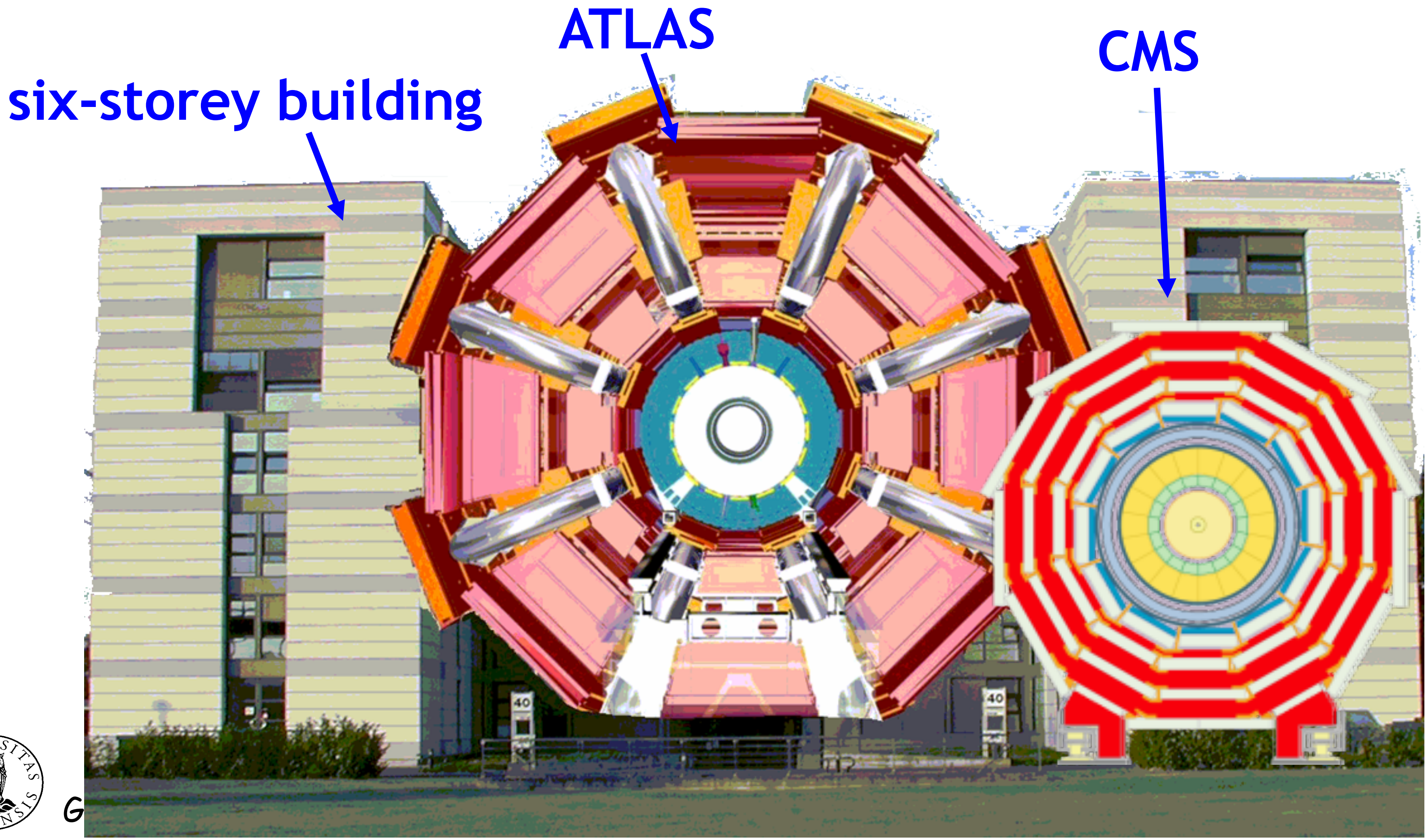

G

Outline

- Ionization, excitation & electron in gases
- Gaseous tracking detectors
- Momentum measurements
- Solid state detectors
- Electrons and Photons in Matter
- Electromagnetic Calorimeters
- Hadronic Calorimeters
- Particle Flow Calorimeters
- Particle identification detectors

Ionization, Excitation & Electrons in Gases

Energy Loss of Charged Particles

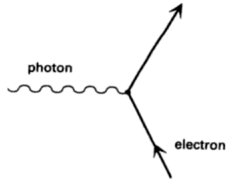

- Depending on the photon energy $\hbar\omega$, different processes occur:

1) For $\hbar\omega < E_{excitation}$ [optical region] $\approx$2 eV ⇨ ε>1 (real) → em shock wave

→ θ_c real for v > c/n

→ emission of real photon is possible if particle velocity is larger than phase velocity c/n of light (Cherenkov effect)

2) For 2 eV < $\hbar\omega$ < 5 keV, ε is complex with ε_1<1, ε_2>0

→ production of virtual photons only

→ excitation and ionization of medium

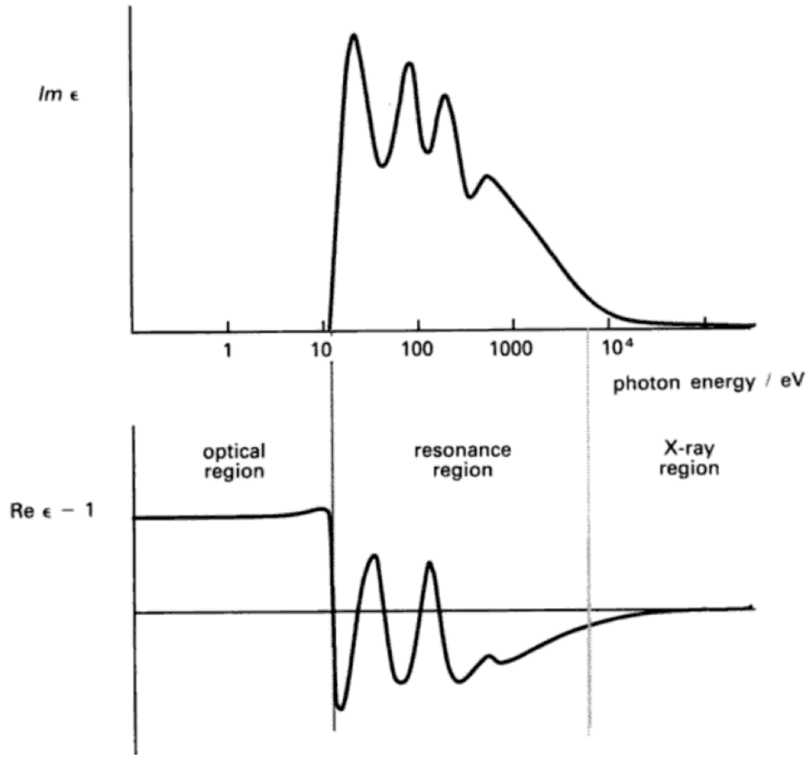

3) For $\hbar\omega$ > 5keV absorption becomes small: ε_2<<1, but ε_1<1

→ Threshold velocity for Cherenkov effect is larger than c

→ Radiation is emitted below this threshold if medium has discontinuities → transition radiation

Ionization and Excitation

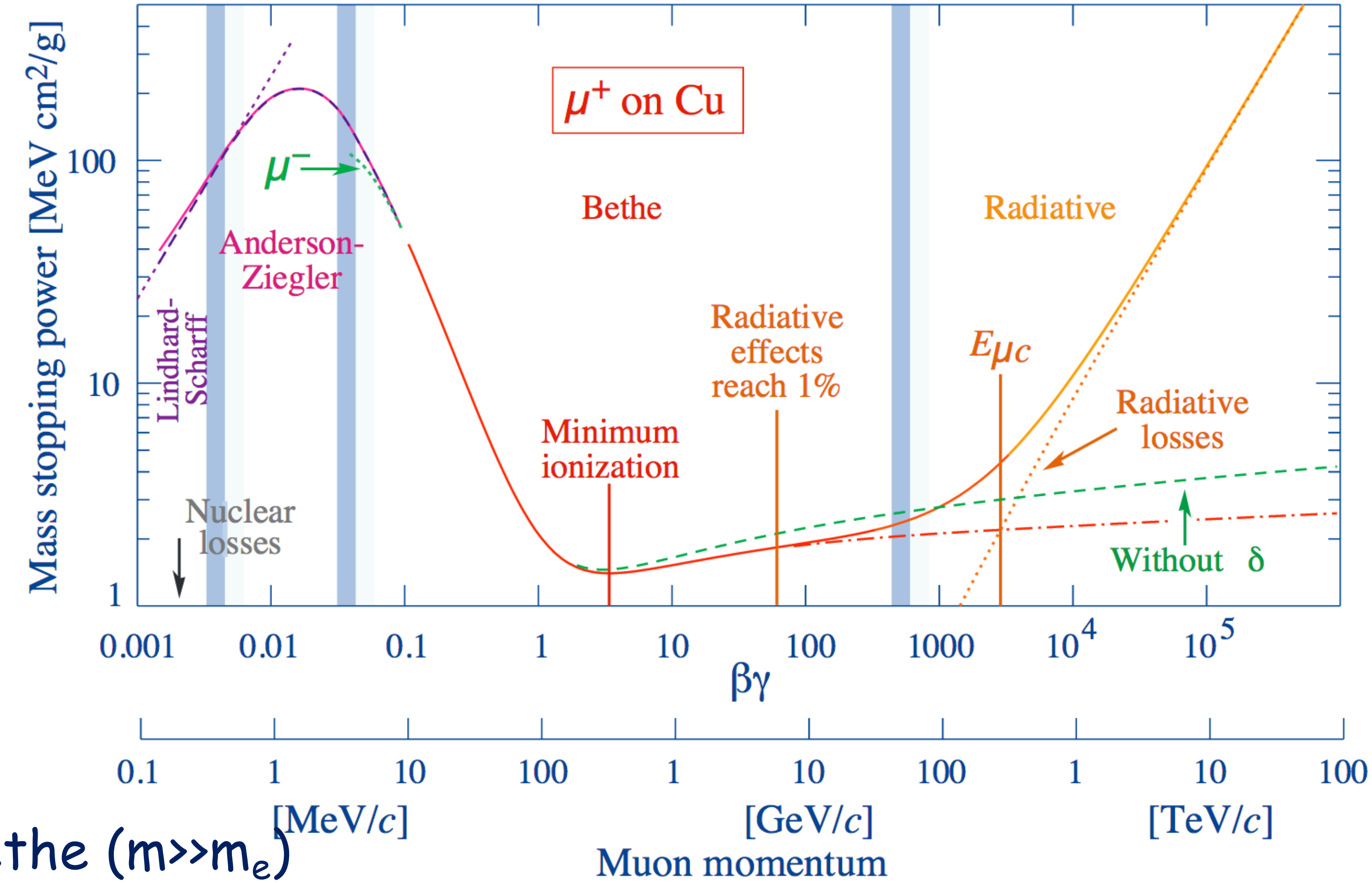

Medium

- A: atomic weight
- Z: atomic number
- ρ: density
- I: ionization potential
- $\alpha=1/137$
- m_e: electron mass

Particle

- T_{max}: maximum kinetic energy
- z: charge
- $\beta=|p|/E$
- $\gamma=E/m$

Bethe ($m>>m_e$)

$$-\left\langle\frac{dE}{dx}\right\rangle = Kz^2\rho\frac{Z}{A}\frac{1}{\beta^2}\left[\frac{1}{2}\ln\left(2m_e c^2\beta^2\gamma^2\frac{T_{max}}{I^2}\right)-\beta^2-\frac{\delta(\beta\gamma)}{2}-\frac{C}{Z}\right]$$

0.307 MeV cm²/g

Density effect

Shell correction

Energy Loss in Different Materials

- ❒ The mean energy loss shows minimum at ~ same $\beta\gamma$ value (3-4) for all materials
- ❒ Relativistic rise is higher in gases than in liquids and solids

Energy loss at minimum

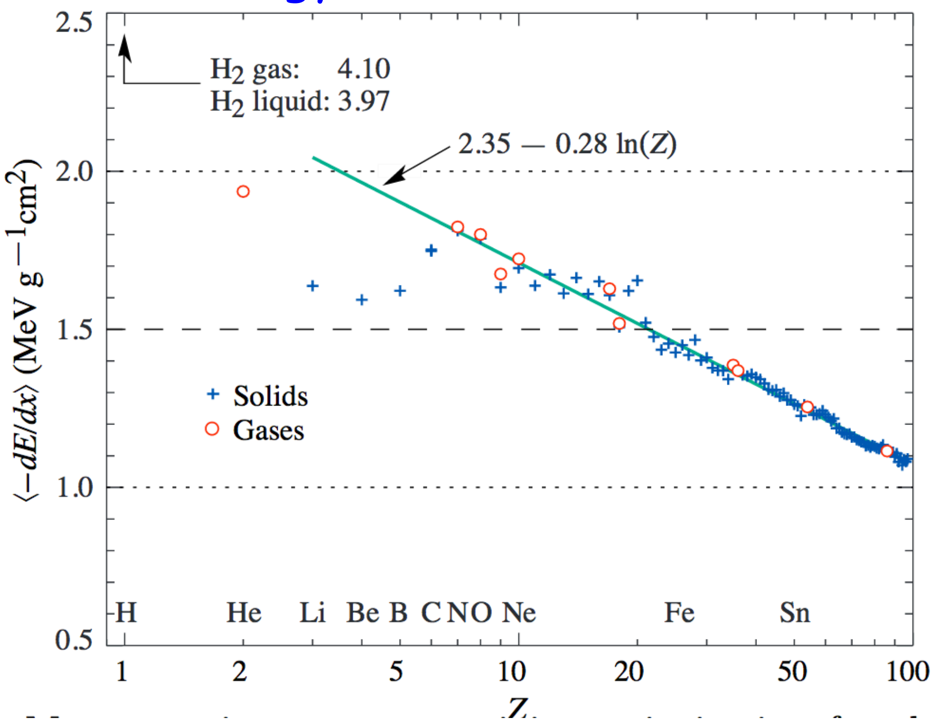

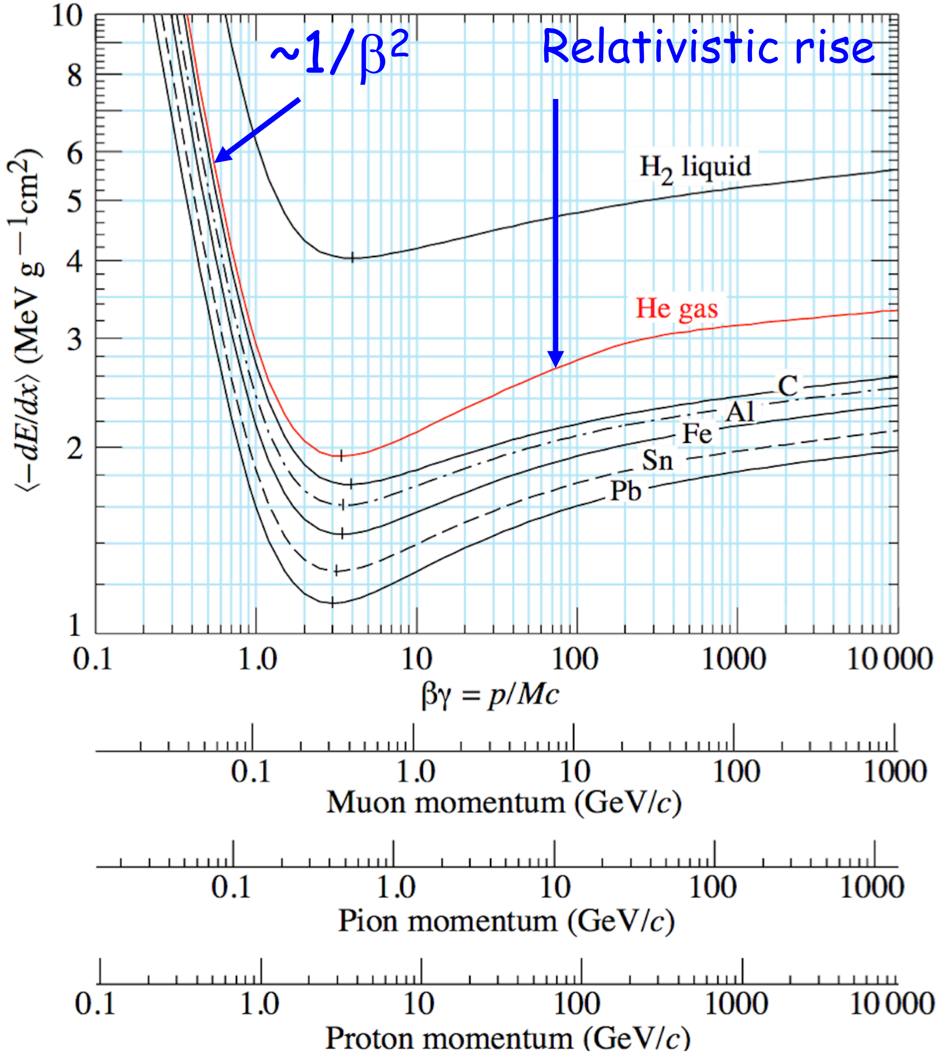

Minimum energy loss can be parameterized by: **2.35- 0.28 ln(Z)**

dE/dx for Particle Identification

- Measured energy loss in the ALICE TPC

- Landau distribution of dE/dx measurements Liquid Argon

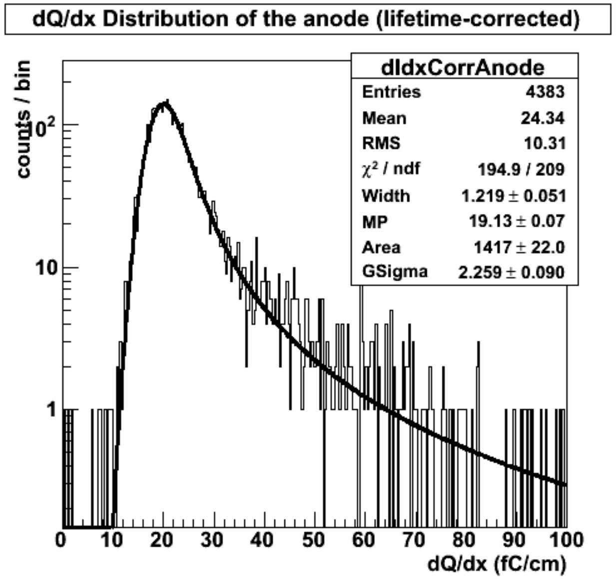

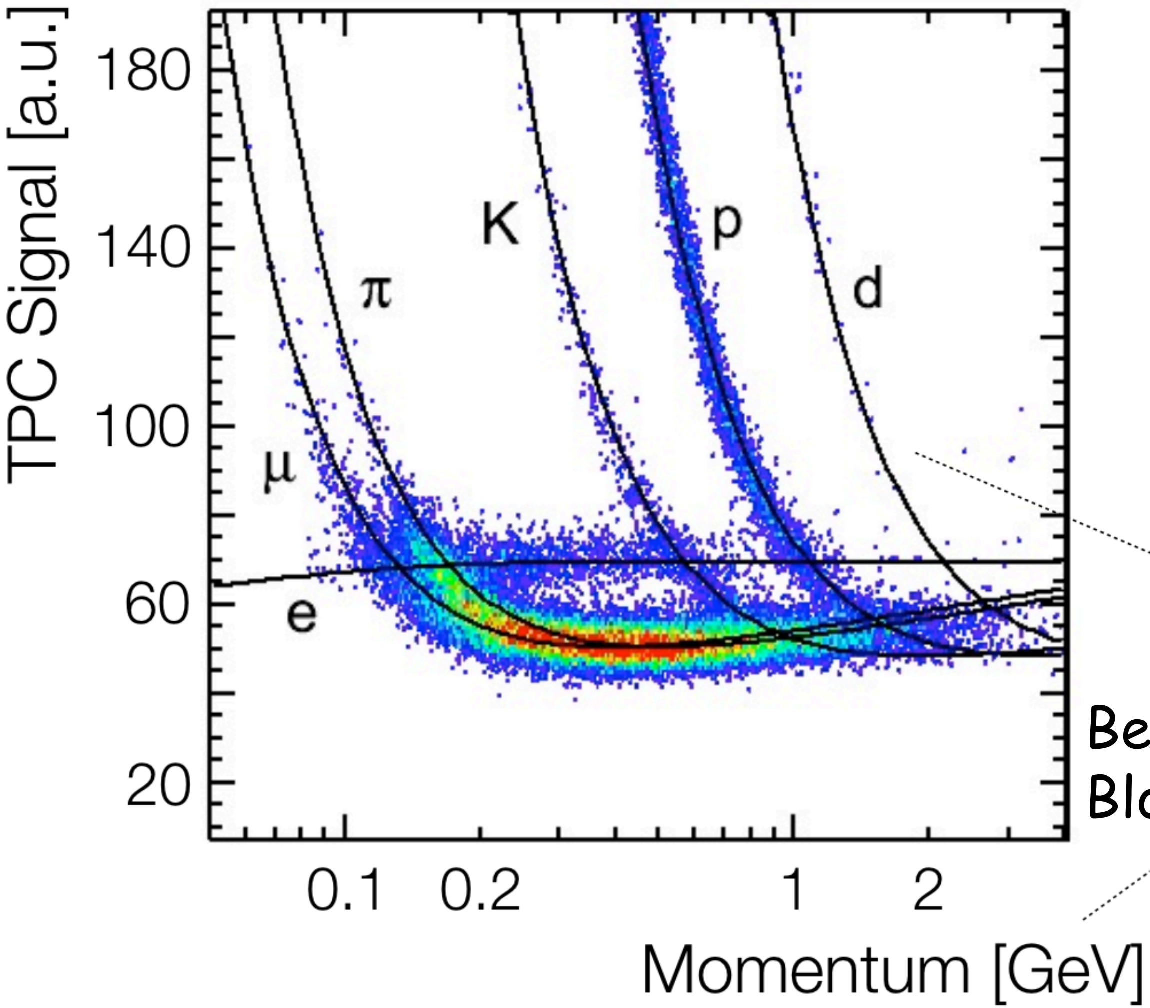

Bethe-Bloch

G. Eigen, HASCO 19-07-16 Göttingen

Mobility of Ions

- A charged particle traversing a gas produces $e^- i^+$ pairs
- A cloud of positive ions, i^+, placed in an electric field of strength $\vec{E}$, is accelerated by the $\vec{E}$ field and decelerated by collisions
  $\Rightarrow$ the motion can be described by a constant drift velocity $\vec{v}_D$
- According to measurements, $\vec{v}_D$ is proportional to $\vec{E}/P$

pressure

$$\vec{v}_D^{\,+} = \mu^+ \vec{E} \frac{P_0}{P}$$

where μ^+ is the ion mobility, units [$cm^2/(Vs)$] P_0=760 Torr

For $\vec{E}$=1kV/cm

- Examples:

He^+	in He:	μ^+= 10.2 $cm^2/(Vs)$		v_D^+= 0.01 cm/μs
Ar^+	in Ar:	1.7	"	0.0017 "
CH_4^+	in Ar:	1.87	"	0.00187 "
$(OCH_3)CH_2^+$	in $(OCH_3)CH_2$	0.26	"	0.00026 "

- Mobility is high (low) for small (big) atoms/molecules
- Drift velocities of electrons are 1-10 cm/μs

Drift Velocity

- The drift velocity can be expressed in terms of mean free path λ, thermal velocity u, electric field $\vec{E}$, charge q and particle mass m

$$\vec{v}_D = \frac{q\vec{E}}{m}\left\{\frac{2}{3}\left\langle\frac{\lambda_e(u)}{u}\right\rangle + \frac{1}{3}\left\langle\frac{d\lambda_e(u)}{du}\right\rangle\right\}$$

- For some gases $\vec{v}_D$ is independent of $\vec{E}$ in some range (C_2H_4) or is only slightly dependent on $\vec{E}$ (Ar)

- Electron drift velocities of are ~1-10cm/μs and e^- mean free paths are considerably larger: $\lambda_e = \lambda_{ion} \cdot 5.66$

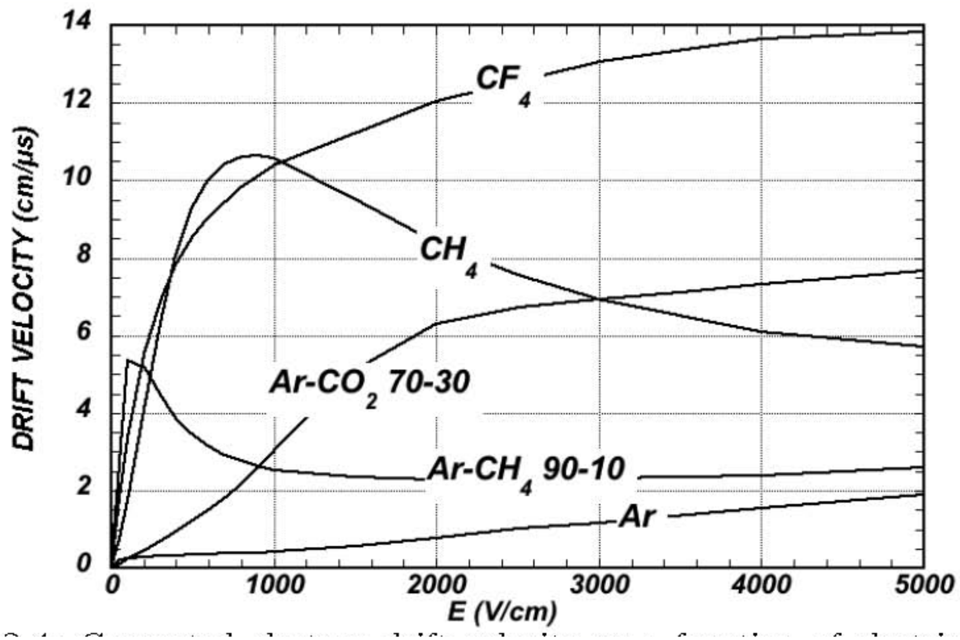

Drift of Electrons in $\vec{E}$ & $\vec{B}$ Fields

- A charge in an electromagnetic field moving through a gas-filled volume is subject to the force

$$m\dot{\vec{v}} = q(\vec{E} + \vec{v} \times \vec{B}) + m\vec{A}(t)$$

Coulomb Lorentz Langevin

- Stochastic acceleration averaged over time compensates translational acceleration where τ is average time between 2 collisions

$$\left\langle \vec{A}(t) \right\rangle = -\frac{\vec{v}_D}{\tau}$$

- In a constant $\vec{E}$ field we have

$$\vec{v}_D = \frac{\mu}{1+\omega^2\tau^2}\left[\vec{E} + \frac{\vec{E}\times\vec{B}}{|\vec{B}|}\omega\tau + \frac{(\vec{E}\cdot\vec{B})\cdot\vec{B}}{|\vec{B}|^2}\omega^2\tau^2\right]$$

- In the presence of $\vec{E}$ & $\vec{B}$ fields the drift velocity has 3 terms
  - i) one parallel to $\vec{E}$
  - ii) one parallel to $\vec{B}$
  - iii) one perpendicular to plane spanned by $\vec{E}$ & $\vec{B}$

$$\vec{\omega} = -\frac{q}{m}\vec{B}$$

Cyclotron frequency

$$\frac{\omega}{B} = 17.6\,\mathrm{MHz} / \mathrm{G}$$

- If $\vec{E}$ and $\vec{B}$ are not parallel, there is angle between $\vec{v}_D$ and $\vec{E}$ called Lorentz angle

$$\tan\alpha = \omega\tau$$

Diffusion of Ions in a Field-free Gas

- A charge distribution Q(t) localized at (0,0,0) at t=0 is diffused by multiple scattering

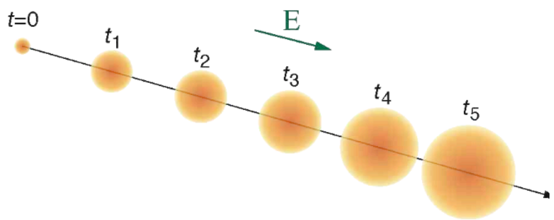

- At time t, Q(t) is Gaussian with center at origin

Charge density distribution for 5 equidistant time intervalls:

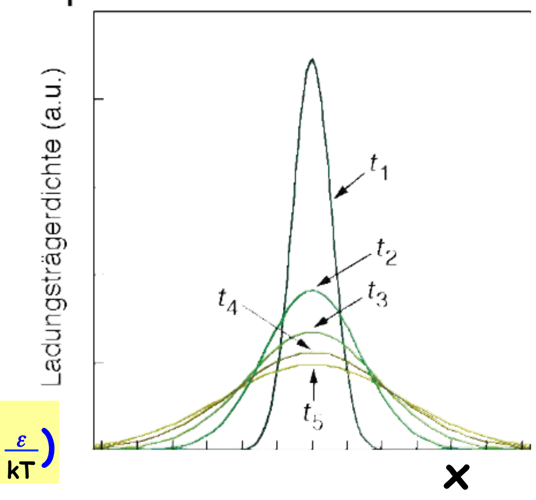

- The rms spread is proportional to the diffusion coefficient: $D = \frac{1}{3}\int u\lambda(\varepsilon)F(\varepsilon)d\varepsilon$

  with Maxwell-Boltzmann distribution $F(\varepsilon) = c\cdot\sqrt{\varepsilon}\cdot\exp(-\frac{\varepsilon}{kT})$

- For energy-independent λ we obtain $D = \frac{1}{3}u\lambda$

ε: kinetic energy

- For a classical ideal gas we have $\lambda(\varepsilon) = \dfrac{1}{N\sigma(\varepsilon)}$

where $\sigma(\varepsilon)$ is the collision cross section and N is number of molecules per unit volume

$$N = 2.69\times 10^{19}\,\frac{P}{760}\,\frac{273}{kT}\;\frac{\text{molecule}}{\text{cm}^3}$$

Diffusion of Electrons in $\vec{E}$ & $\vec{B}$ Fields

- Diffusion parallel (L) and perpendicular (T) to the drift direction depends on the nature of the gas
- Typically faster gases yield smaller diffusion than slower gases
- The spatial resolution is depends on time and the diffusion coefficient

$$\sigma = \sqrt{2Dt}$$

- Since $t=L/v_D$ & $D=u\lambda/3$ we get in absence of a magnetic field

$$\sigma = \sqrt{\frac{2L}{3v_D}}\sqrt{u\lambda}$$

- In the presence of a magnetic field spatial resolution improves by

$$\left(1+\omega^2\tau^2\right)^{-1}$$

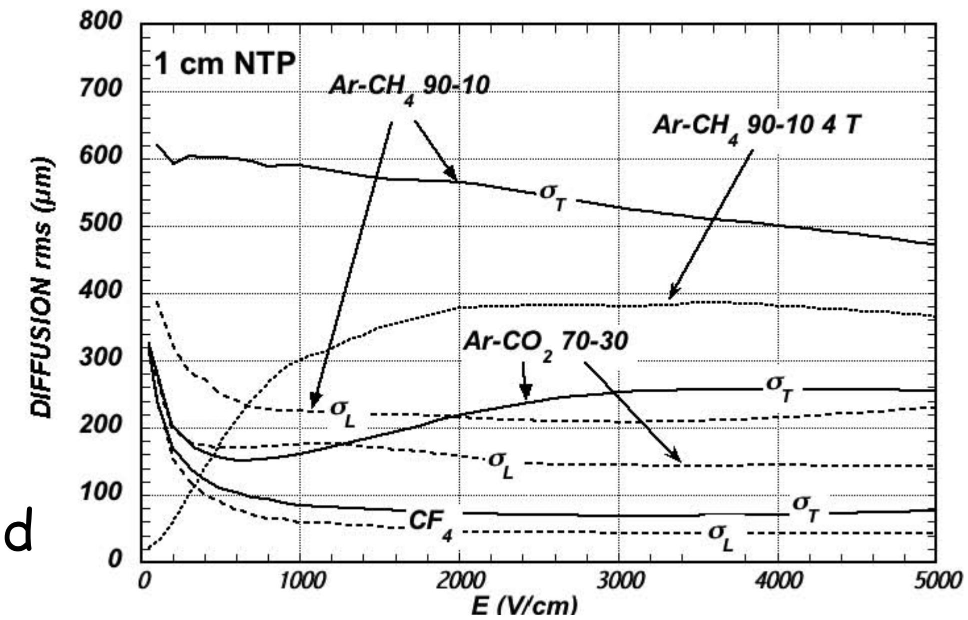

Figure 28.5: Electron longitudinal diffusion (σ_L) (dashed lines) and transverse diffusion (σ_T) (full lines) for 1 cm of drift. The dotted line shows σ_T for the P10 mixture at 4T [67].

τ: time between 2 collisions

Gaseous Tracking Detectors

Proportional Counter

- If we apply a high electric field between anode wire and cathode cage (10^4-10^5 V/cm), electrons from the primary ionization gain enough energy between 2 collisions to cause further ionizations

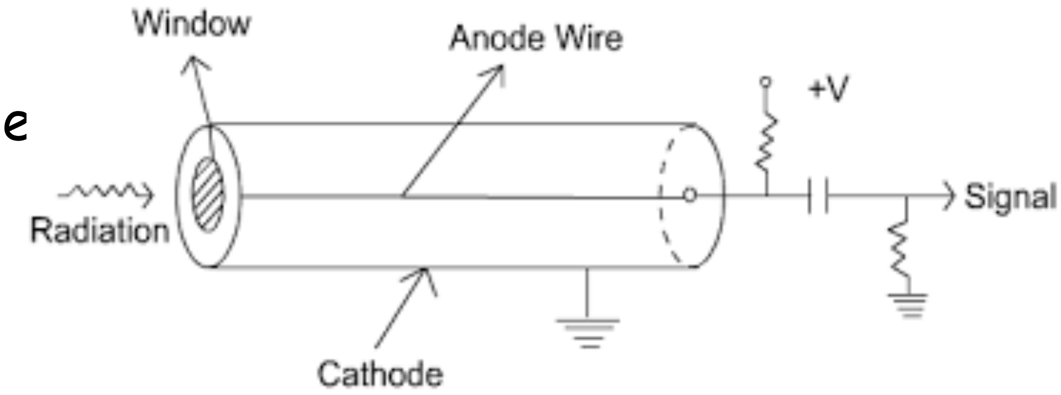

- For certain $\vec{E}$ fields & gas pressures, ***A*** is independent of the amount of primary ionization ⇨ observed signal is proportional to primary ionization

- This domain of field strengths is called proportional region ⇒ here *A* $\approx 10^4$-10^6

- Achieve high field strengths with thin wires (20 μm-100 μm) as anode

- Amplification will start in close vicinity to anode

First Townsend Coefficient

- The number of e^--i^+ pairs formed by an electron along a 1cm path is called 1. Townsend coefficient $\alpha = \sigma_i N$
  where σ_i is ionization cross section and N=2.69×10^{19} atoms/cm^3
  (atomic density of noble gases)

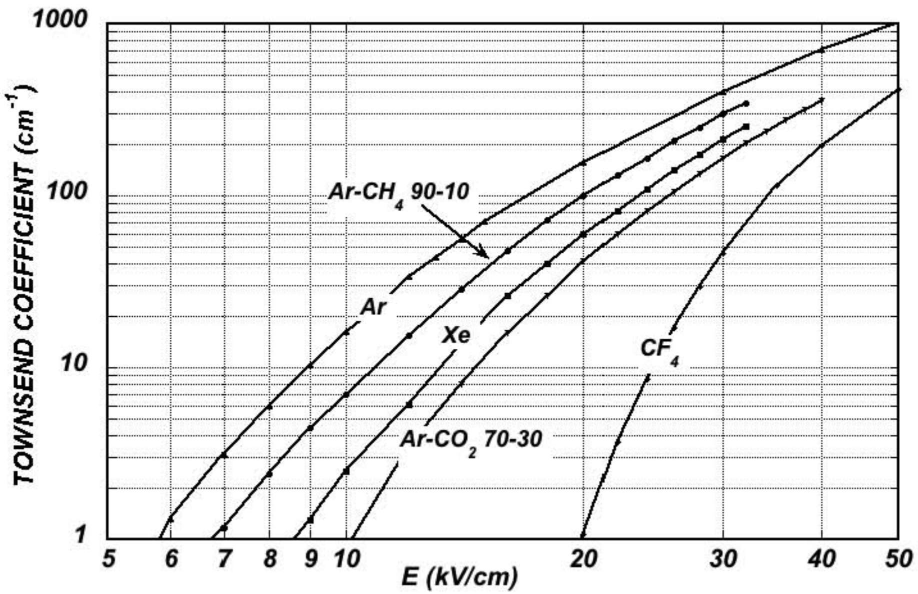

- If N_0 is number of primary e^- at x=0 and N(x) is number of e^- at path x

  $\Rightarrow$ $$dN(x) = N(x)\alpha dx$$

- So $$N(x) = N_0 \exp \int_x \alpha(x')dx'$$

  and gas amplification is since $\alpha(x)=1/\lambda(x)$

  $$A(x) \propto \exp \int_x \alpha(x')\,dx' = \exp \int_x \frac{dx'}{\lambda(x')}$$

- For fast gases, Townsend coefficients are considerably smaller than those for slow gases

Gas Amplification

- In addition to the secondary electrons, ionization processes due to UV photons contribute

- These UV photons originate from de-excitations of atoms excited in collisions & produce e^- via photoeffect in gas atoms or cathode

⇨ Assume that in avalanche formation $N_0 \cdot A$ electrons are produced from N_0 primary electrons

⇨ From UV photons additional $N_0 \cdot A \cdot \gamma$ photoelectrons are formed ($\gamma \ll 1$)

⇨ By gas amplification these photoelectrons produce $N_0 \cdot A^2 \cdot \gamma$ electrons

⇨ From them another $N_0 \cdot A^2 \cdot \gamma^2$ photoelectrons are formed which in turn produce $N_0 \cdot A^3 \cdot \gamma^2$ electrons, and so on

- Summing up all terms we get the total gas amplification factor A_γ

$$N_0 A \sum_{n \geq 0} \left(A\gamma\right)^n = \frac{N_0 A}{1 - A \cdot \gamma} := N_0 A_\gamma$$

- For $A \cdot \gamma \to 1$, A_γ diverges & signal no longer depends on primary ionization ⇨ This is called Geiger-Müller region ($A_\gamma \sim 10^8$-10^{10})

Multi-Wire Proportional Chamber

- In a multi-wire proportional chamber (MWPC) a plane of anode wires is sandwiched between cathode planes

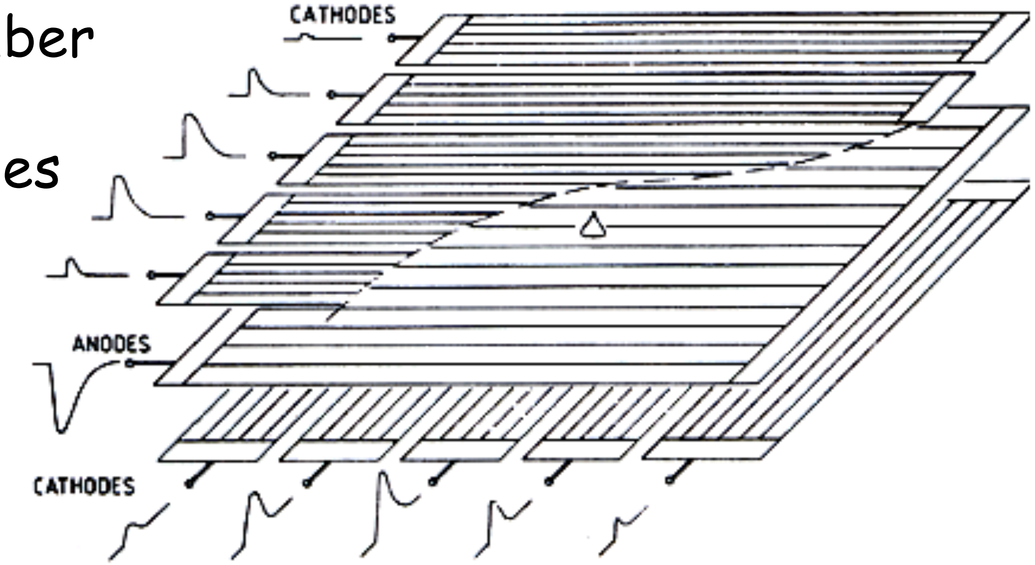

- Cathode planes are segmented into strips; strips in one (other) plane run parallel (perpendicular) to the anode wires
- A traversing charged particle liberates e^- i^+ pair along its path
- e^- are accelerated towards the anode wire & i^+ towards cathode plane
- The $\vec{E}$ field is chosen sufficiently high so that secondary ionization sets in and an avalanche is formed near the anode wire and signals are induced on the cathode strips
- anode wires: 20 μm thick Au-plated W, Al; 2 mm spacing
  counting gas: Ar, Kr, or Xe with admixture of CO_2, CH_4, isobutane, …
  amplification: 10^5; efficiency: ~100%
  with cathode readout measure x and y positions

Position Determination

- Position is usually obtained by center-of-gravity method

$$y = \frac{\sum_i (Q_i - b) y_i}{\sum_i (Q_i - b)} \qquad (4.2)$$

y-position of wire i

Charge of wire i

Small bias voltage to correct for noise

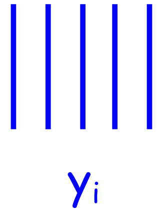

- Position along the wire is obtained via charge division

⇨ Need to read out both wire ends

- Achieve resolutions of 110-170 μm, 35 μm in small chamber

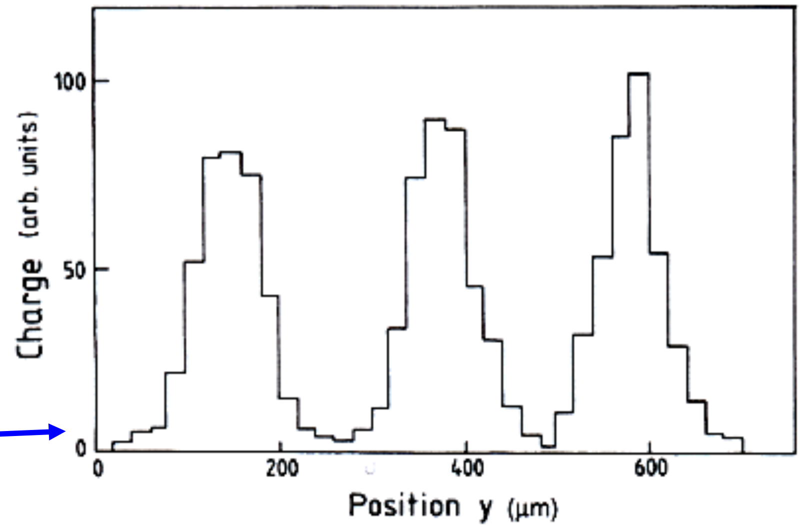

- For charge measurements Q_A & Q_B obtain position along the wire

$$x = L \frac{Q_A - b}{Q_A + Q_B - 2b}$$

- Accuracies are ~0.4% of wire length

Drift Chamber

- We can obtain spatial information by measuring the drift time of electrons produced in ionization processes
- The drift time Δt between primary ionization t_0 & the time t_1 when e^- enters the high $\vec{E}$ field generating an avalanche is correlated with the rising edge of the anode pulse
  ⇨ For constant drift velocity $\vec{v}_D^-(t)$ drift distance for this Δt interval is

$$z = v_D^- \left(t_1 - t_0\right) = v_D^- \Delta t$$

- Constant $\vec{v}_D$ results from constant E

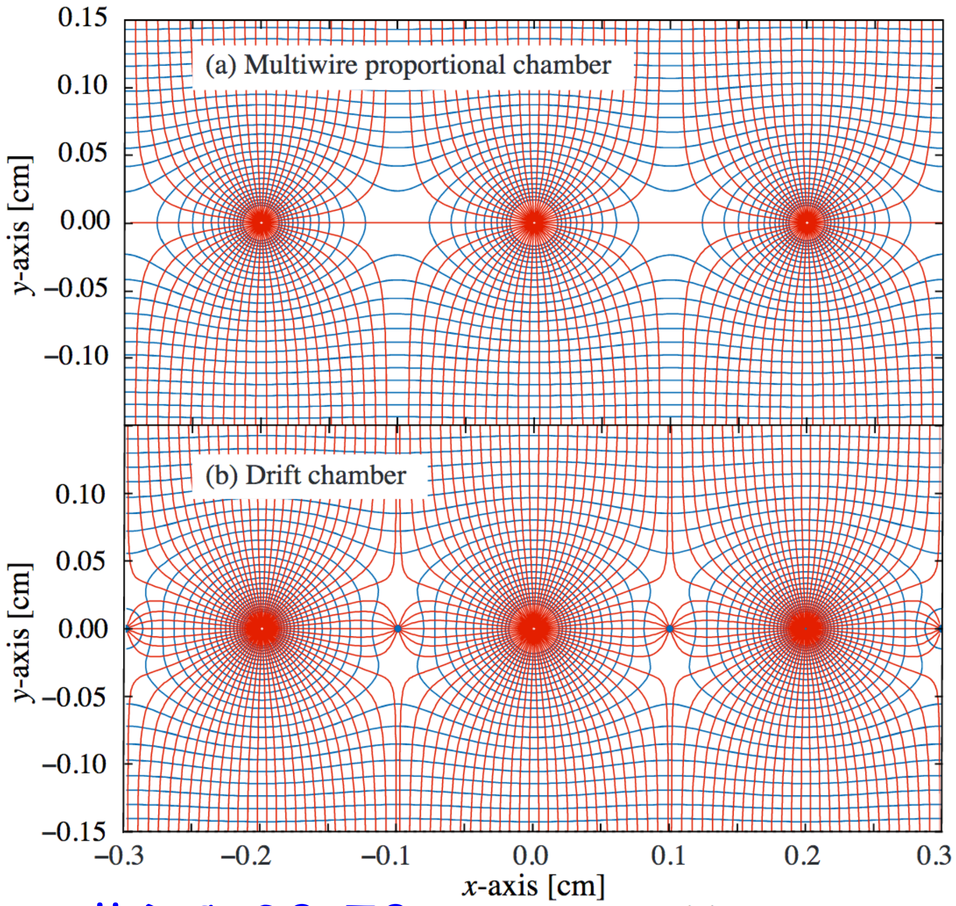

- This is not achieved in MWPCs
  ⇨ Need to introduce a field wire at potential -HV1 between anode wires
- Choice of gas Ar-C_4H_{10} (purity)
  Use slower $\vec{v}_D^-$ to optimize spatial resolution ⇨ large DC: 55-200 μm, small DC: 30-70 μm

Cylindrical Drift Chamber

- $\vec{E}$ field lines lie in the r-φ plane, perpendicular to axial $\vec{B}$ field
- The $\vec{E}$ field is generated by a suitable arrangement of potential wires, which are parallel to each other surrounding a single signal wire

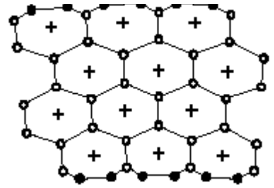

- A large fraction of layers (typically ≥ 50%) have wires running parallel to $\vec{B}$ field (axial layers) & rest have wires running skew under stereo angle $\gamma=\pm$few ^{0} wrt $\vec{B}$ field axis (stereo layer)
- Axial wires only give r-φ position, stereo wires allow to get z position
- One determines r-φ position from all axial wires, then the stereo wires are added by moving along z-position till the r-φ fits with that of axial layers
- For each signal wire t_0 and the time-to-distance relation need to be measured

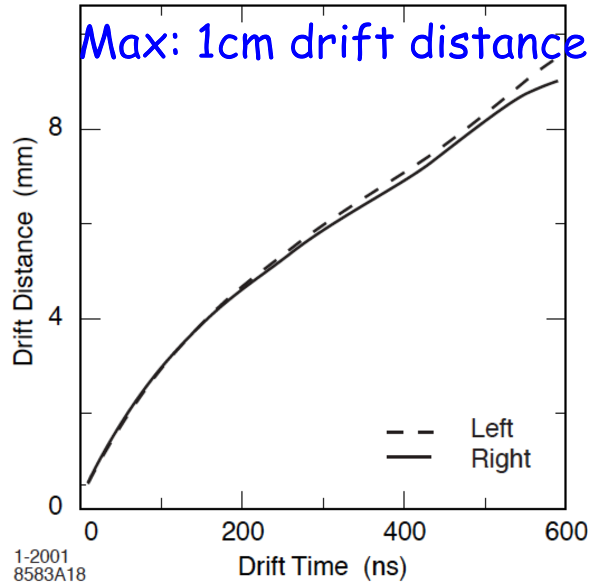

BABAR drift chamber: 40 layers, $\sigma_{r\varphi}\approx 125\ \mu m$

Time Projection Chamber

- The Time Projection Chamber combines principles of a drift chamber & proportional chambers to measure 3-dimensional space points
- A high $\vec{E}$ field is placed parallel to a high $\vec{B}$ field (1.5 T)
  ➔ no Lorentz force on drifting e^-

ALICE TPC

- $845 < r < 2466$ mm
- drift length 2 x 2500 mm
- drift gas Ne, CO_2, N_2 (85.7/9.5/4.8)
- gas volume 95 m^3
- 557568 readout pads

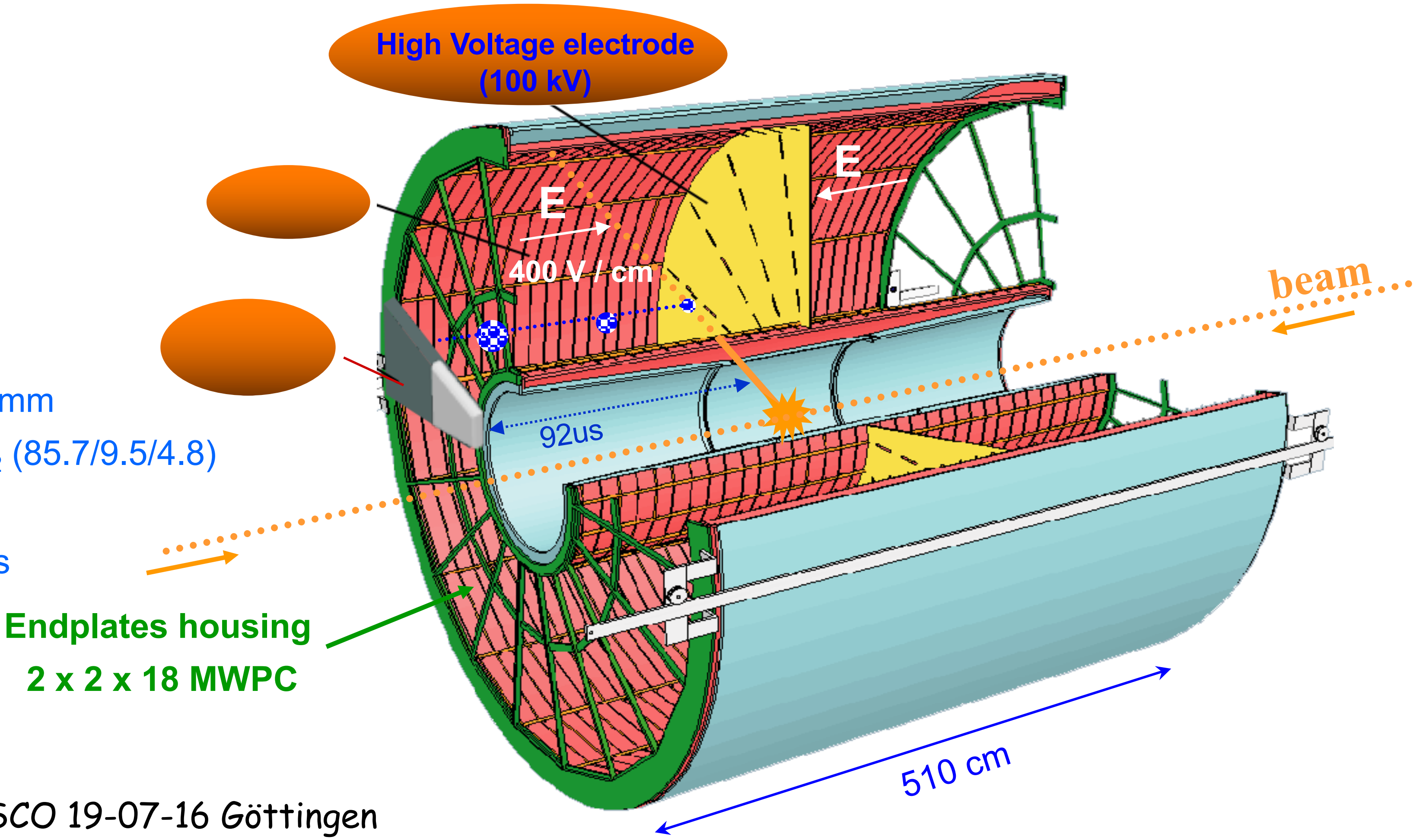

Time Projection Chamber

- Electrons produced by ionization of a charged track traversing volume drift towards endcap
- Image is broadened by diffusion during drift process
- Broadening is considerably reduced by strong $\vec{B}$ field
- e^- are forced to perform helical movement around $\vec{B}$ field lines
- Transverse diffusion coefficient is reduced by $1/(1+\omega^2\tau^2)$, with $\omega=(e/m)|\vec{B}|$ & τ is mean free time between 2 collisions
- Spatial resolution: 150-200 μm

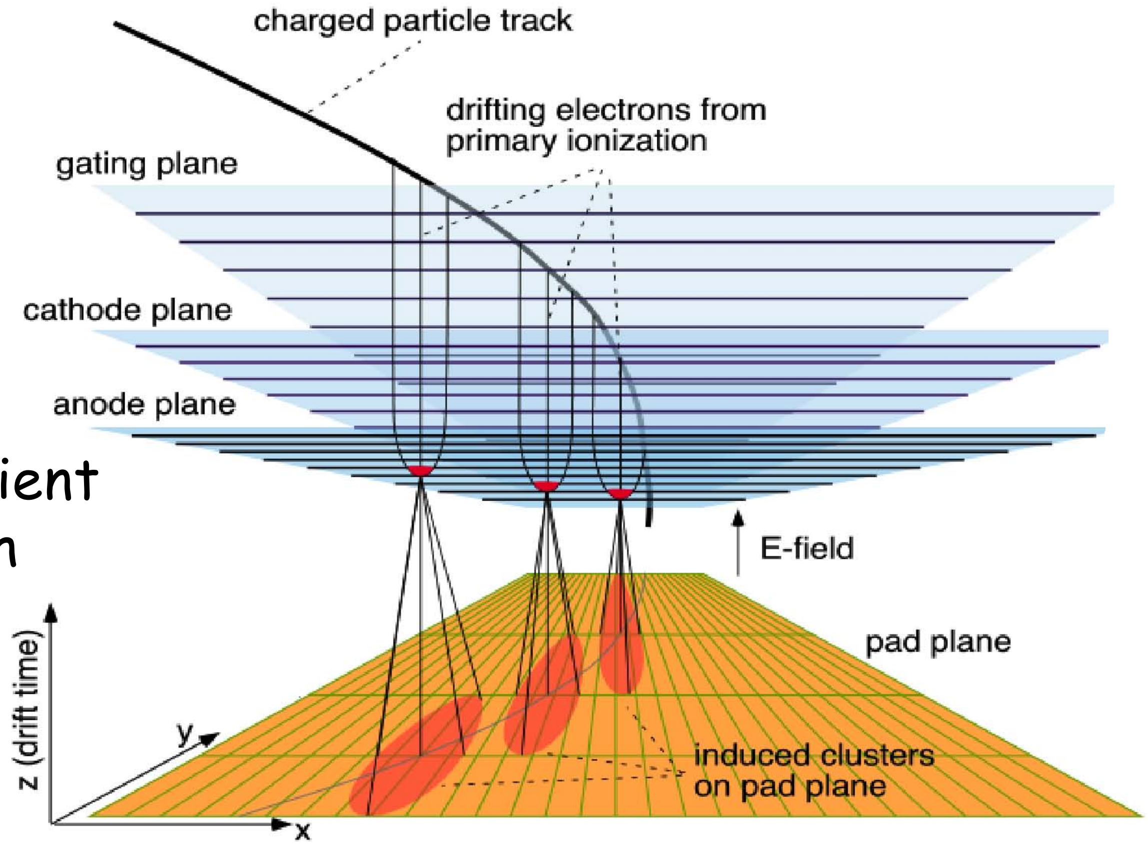

Gas Electron Multiplier

- Position-sensitive gas detectors based on wire structure are limited by diffusion processes and space charge effects to accuracies of 50-100 μm
- A GEM detector consist of a thin Cu-Kapton-Cu sandwich into which a high density of holes is chemically processed: 25-150 μm ⌀, 50-200 μm pitch
- A high E field 50-70 kV/cm is applied across holes
  ⇨ electron produces avalanche in hole
- Coupled with a drift electrode above and a readout electrode below it acts as a highly performing micro amplifying detector
- Amplification and detection are decoupled
  ⇒ operate readout at zero potential
- With several layers gain of 10^4 is achievable
- GEMs have higher rate capability than MWPCs

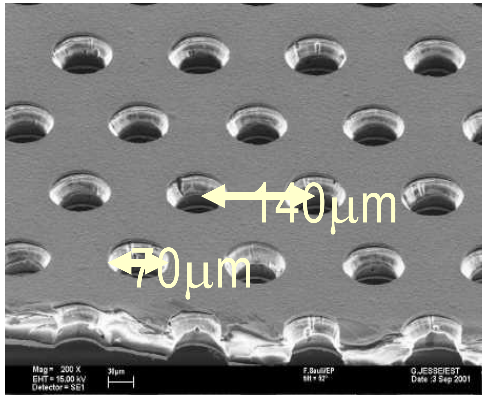

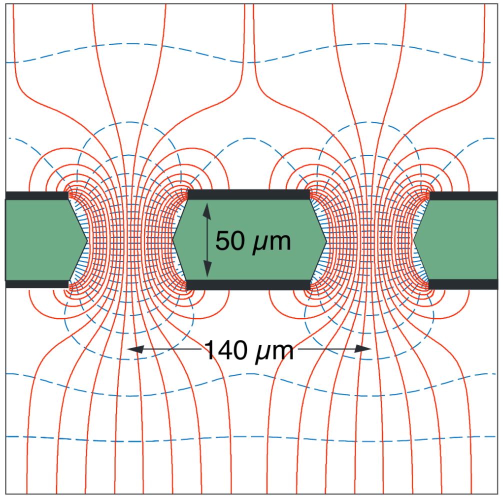

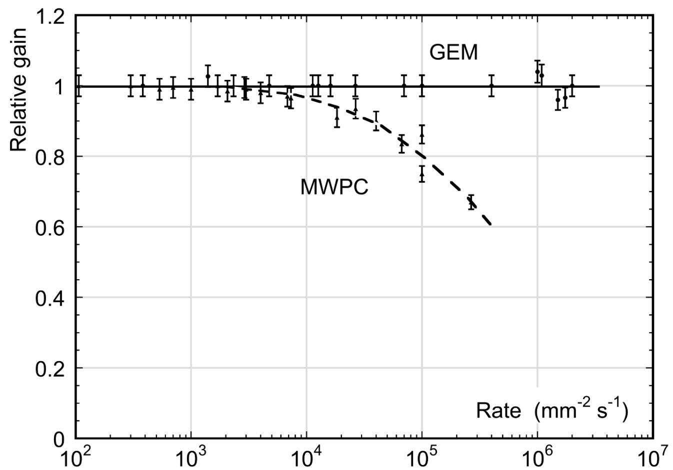

Micro-Mesh GAseous Structure

- The micro-mesh gaseous structure is a thin parallel-plate avalanche counter
- It has a drift region & a narrow amplification gap (25-150 μm) between a thin micro mesh & the readout electrode (conductive strips or pads printed on insulator board)
- Primary e^- drift through mesh holes into amplification gap where they are amplified

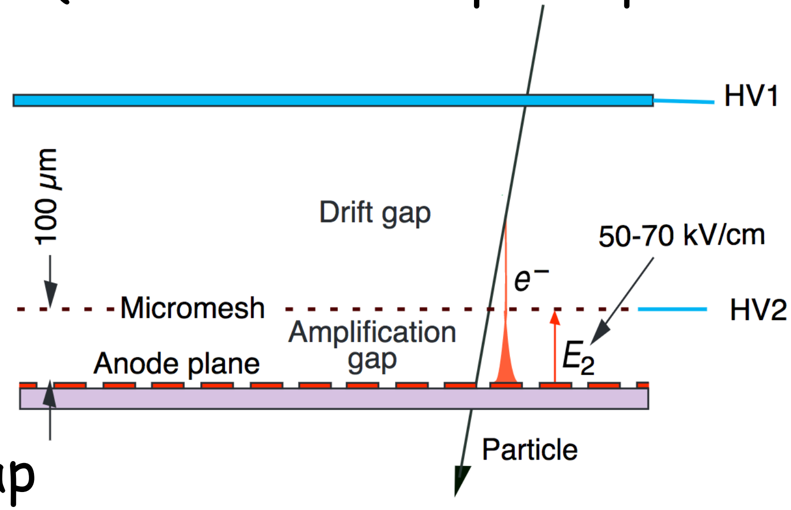

- Homogeneous E fields, 1 kV/cm in drift region & 50-70 kV/cm in amplification gap
- Excellent spatial resolution of 12 μm, good time resolution and good energy resolution for 6 keV X-rays of 12% at FWHM
- New developments of MicroMEGAS with pixel readout will integrate amplification grid with the CMOS readout, use 1 μm Al grid above 50 μm ⇨ expect excellent spatial and time resolutions

Momentum Measurements

Deflections in Magnetic Fields

- Particles with momenta p_x, p_y « p_z placed in a magnetic field $\vec{B}=(0,B_y,0)$ are deflected along a circular orbit with radius $R = p/(e|\vec{B}|)$

- If magnetic field is active on length L_t, the angular deflection is $$2\sin\frac{\theta}{2} = \frac{L_t}{R} = -\frac{eB_yL_t}{p}$$

- This leads to a change in transverse momentum by $$\Delta p_x = p \cdot \sin\theta \approx -eB_yL_t = -e\int B_y\, dz$$ in good approximation for small deflection angles

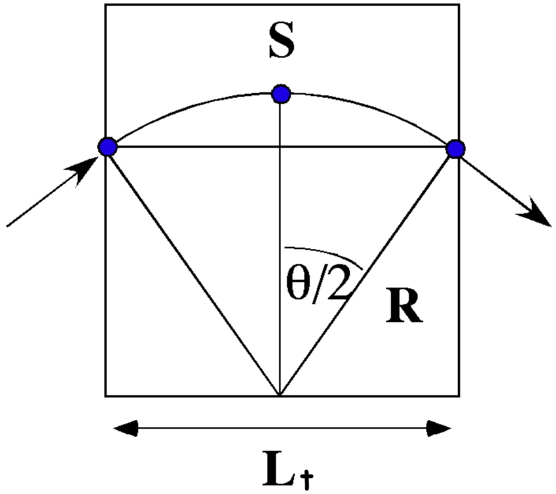

projected (transverse) length

- The error in position measurement σ(x) leads to an error in the momentum measurement via

$$\frac{\sigma_p}{p} = \frac{2p}{\Delta p_x}\frac{\sigma(x)}{h}$$

where h is lever arm for angle measurement before & after magnet

e.g.: for |B|=0.5 Tm, σ(x)=300 μm & h=3cm

➔ σ_p/p~1.3% for p= 100 GeV/c, → σ_p/p^2 ~1.3×10^{-4}/GeV

Momentum Resolution

- The momentum resolution typically has a contribution from the position measurement and one from multiple scattering

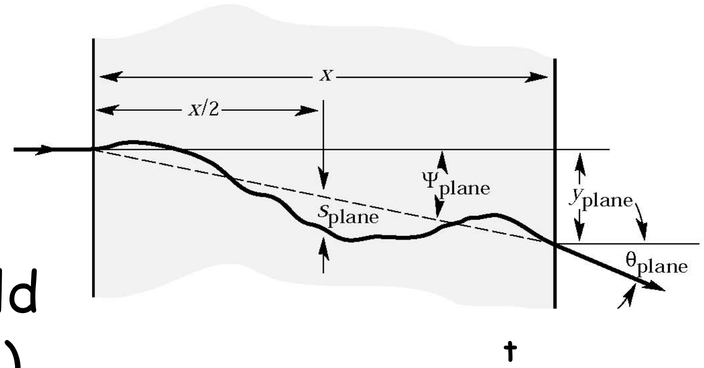

- We focus on important case of solenoidal field
  - ➔ Here we have cylindrical geometry (r, φ, z) where $B=(0, 0, B_z)$

- If position is measured at 3 equidistant points along the track L_t, the sagitta s of circular orbit is

$$s = R - R\cos\frac{\theta}{2} \approx \frac{R\theta^2}{8}$$

- Since $R=p/(0.3\cdot B) \rightarrow \theta \approx L_t/R \approx 0.3\cdot B\cdot L_t/p$, yielding

$$s = 0.3\frac{BL_t^{\,2}}{8p}$$

that is is determined by 3 measurements to precision

$$\sigma_s = \sqrt{3/2}\,\sigma_x$$

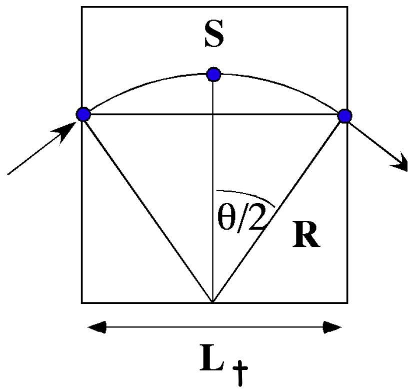

- For N measurements we get statistical factor of $\sqrt{\frac{720}{N+4}}$ instead of $\sqrt{\frac{3}{2}}$

Momentum Resolution

- If $\sigma_{r\varphi}$ is measurement error in (r-φ) plane, momentum component in that plane, p_t, is measured with errors:

$$\left(\frac{\sigma_{p_t}}{p_t}\right)^M = \frac{\sigma_{r\varphi} p_t}{0.3BL_t^2}\sqrt{\frac{720}{N+4}}$$

B field

Transverse length in m

# of measured points along track at uniform spacing

- Multiple scattering yields mean transverse p change

$$\Delta p_t^{MS} = 21\text{MeV}\left(\frac{L_t}{X_0}\right)^{1/2}$$

Transverse path length in Fe

- This leads to an multiple scattering error of

$$\left(\frac{\sigma_{p_t}}{p_t}\right)^{MS} = \frac{0.05}{BL_t}\sqrt{\frac{1.43L_t}{X_0}}$$

Solid State Detectors

Properties of Silicon

- Si has 4 valence e^-

⇨ Each valence e^- is coupled to e^- of neighboring atom via covalent bound

- At T=0, all e^- are bound & cannot conduct any current

⇨ full valence band, empty conduction band, separation: 1.1 eV

- At room temperature thermal energy is sufficient to liberate e^- into conduction band ($10^{11}/cm^3$)

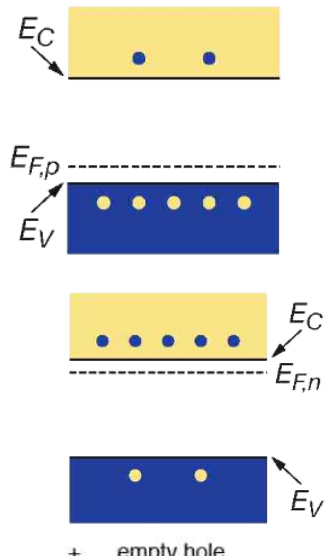

- However, usually we add controlled level of impurities

  i) Elements with 3 valence e^- (p-type)
  B, Ga, In ⇒ hole carriers, acceptor impurity

  ii) Elements with 5 valence e^- (n-type)
  Sb, P, As ⇒ e^- carriers, donor impurity

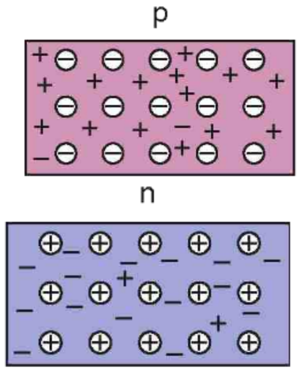

- Concentration of electrons (n) and holes (p) satisfies

$$n \cdot p = N_c N_v \exp\left(\frac{E_g}{kT}\right) = const$$

N_v: # of allowed levels in valence band

N_c: # of allowed levels in conduction band

E_g: energy gap

p—n Junction

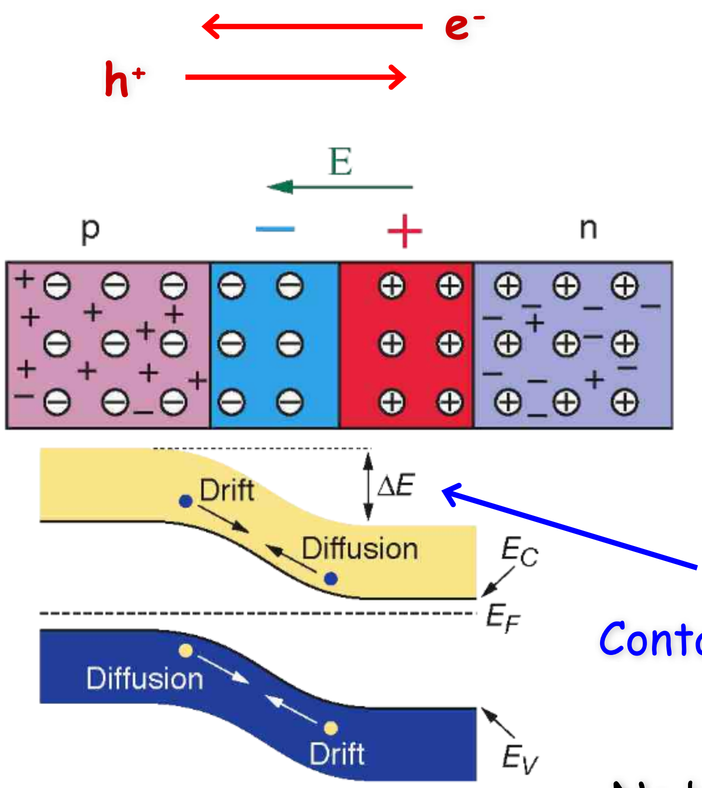

Contact potential V_0

No bias voltage

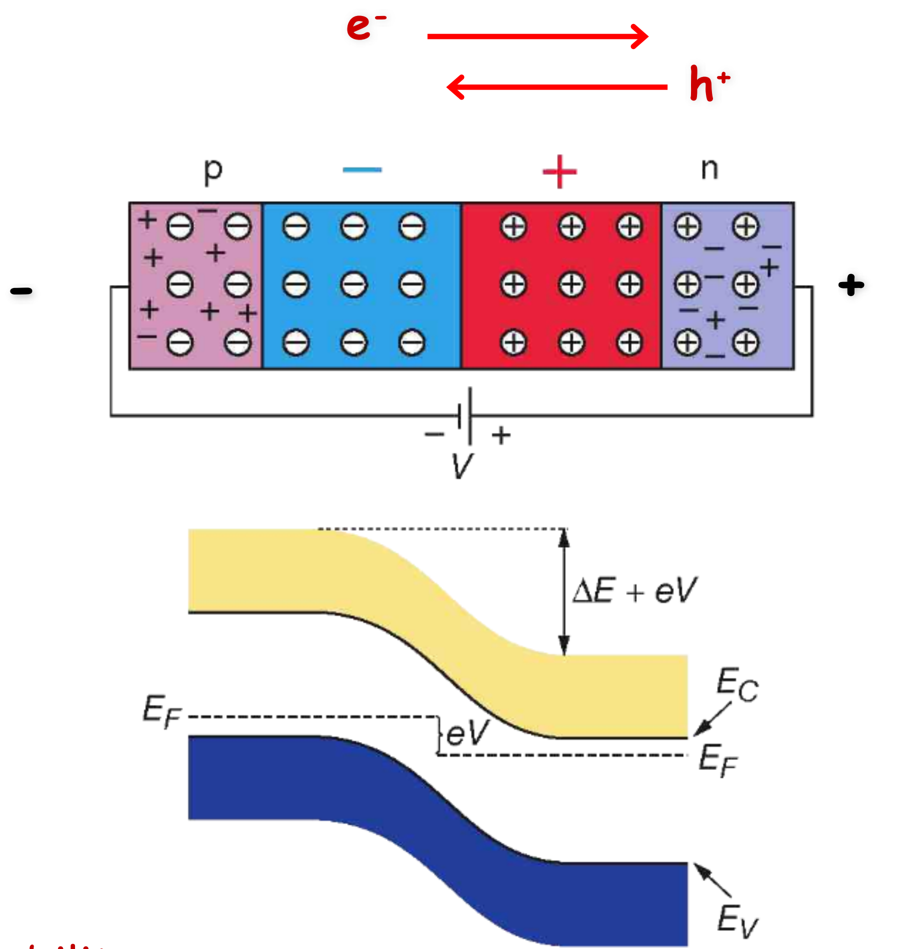

With reverse bias voltage V_b

- Depletion layer

$$d \cong \left(2\varepsilon\varepsilon_0 \rho_n \mu_e (V_0 + V_b)\right)^{1/2}$$

μ_e: electron mobilit
ρ_n: n-region resistivity
ε: dielectric constant

- When ionization liberates charge in depletion layer, e^- & h^+ drift apart due to strong internal field & produce a current

Si Microstrip Detectors

- A typical n-type Si microstrip detector has
  - p^+n junction: $N_p \approx 10^{15}\mathrm{cm}^{-3}$, $N_n \approx 1\text{-}5 \times 10^{15}\mathrm{cm}^{-3}$
  - N-type bulk: $\rho > 2$ kΩcm, thickness 300 μm
  - Operating voltage < 200 V
  - n^+ layer on the backplane to improve ohmic contact
  - Aluminum metalization
- About 30000 e^-h^+ pairs are liberated by a traversing charged particle via $dE/dx|_{ion}$
- Charges drift towards electrodes where they produce a signal on that strip
- Each strip is coupled to a preamplifier

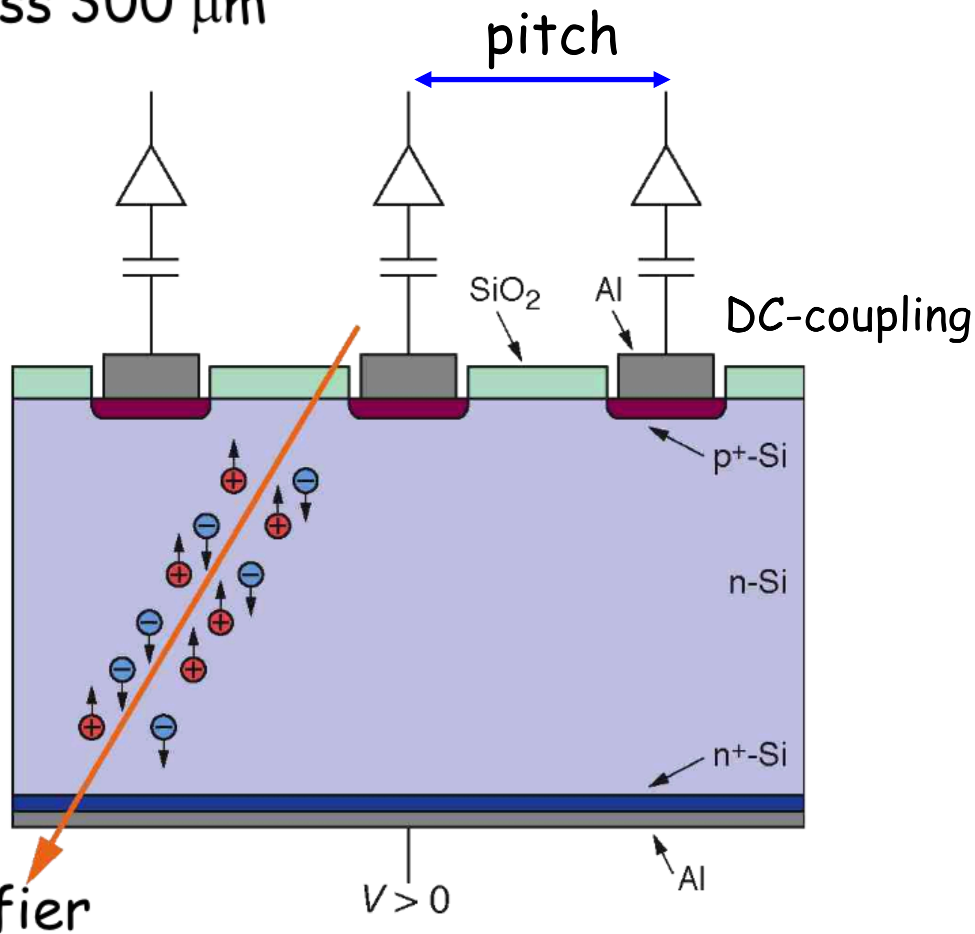

Use of AC-coupling blocks leakage current from preamplifier

Noise

- The main source of noise is due to statistical fluctuations in the number of carriers, leading to changes in conductivity

- The most important noise contributions are (Equivalent Noise Charge)
  - leakage current (ENC_I)
  - detector capacity (ENC_C)
  - detector parallel resistor (ENC_{Rp})
  - detector serial resistor (ENC_{Rs})

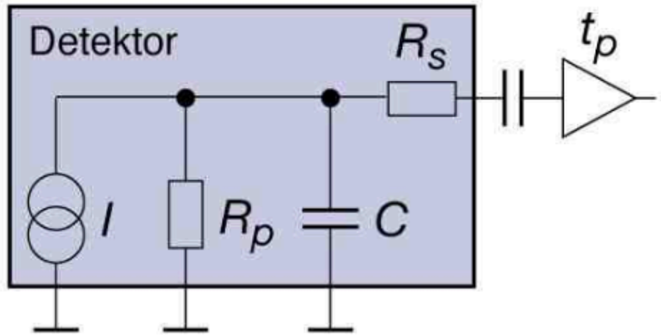

Alternate circuit diagram of a silicon detector.

- The overall noise is the quadratic sum of all contributions

- The detector capacity is typically the dominant noise source

$$\overline{ENC_C^2} \cong 8kTC_d / f_T\tau_f$$

time constant of filter

frequency for unity gain of amplifier

kT=25.85 T/300K [meV]

- For typical values of f_T=1GHz and τ_f=100 ns we estimate $ENC=1.13\times10^2\,C_d^{1/2}$ [rms e^-] with C_d in pF

Signal: 30,000e^-

for C_d=1pF ➔ ENC≈113 e^-, for C_d=100pF ➔ ENC≈1130 e^-

Position Resolution

- The dE/dx energy loss produces a Landau-like distribution that is different for pions and protons of the same momentum

- For a single strip the position resolution is

$$\sigma_x = \frac{p}{\sqrt{12}}$$

- For two or more strip hits we use the center-of-gravity method

- Here, a large signal-to-noise ratio improves the spatial resolution

$$\sigma_x \propto \frac{p}{S/N}$$

- Diffusion broadens the spatial resolution
  ⇨ broadening depends on the drift length

Pions and Protons:

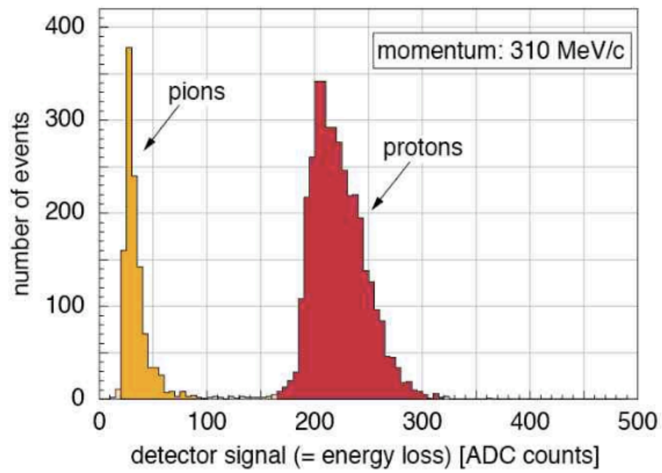

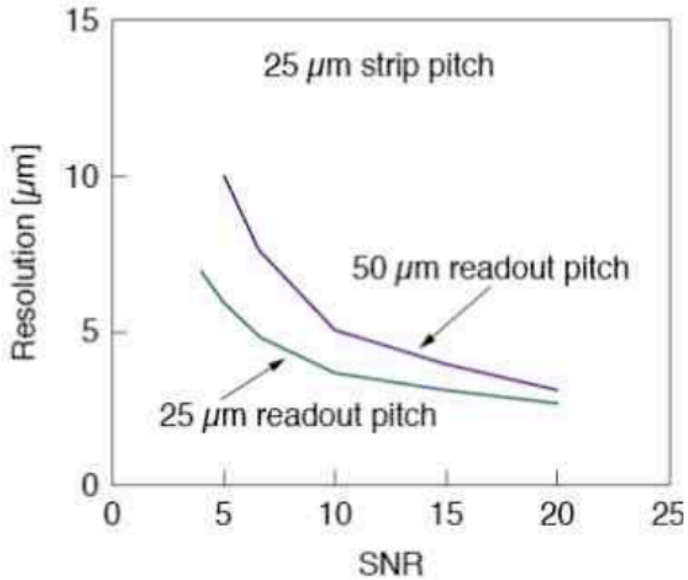

ATLAS Semi-Conductor Tracker

- 4 layers with 2 planes each, r-φ strips and r- φ strips slightly tilted by 40 mrad

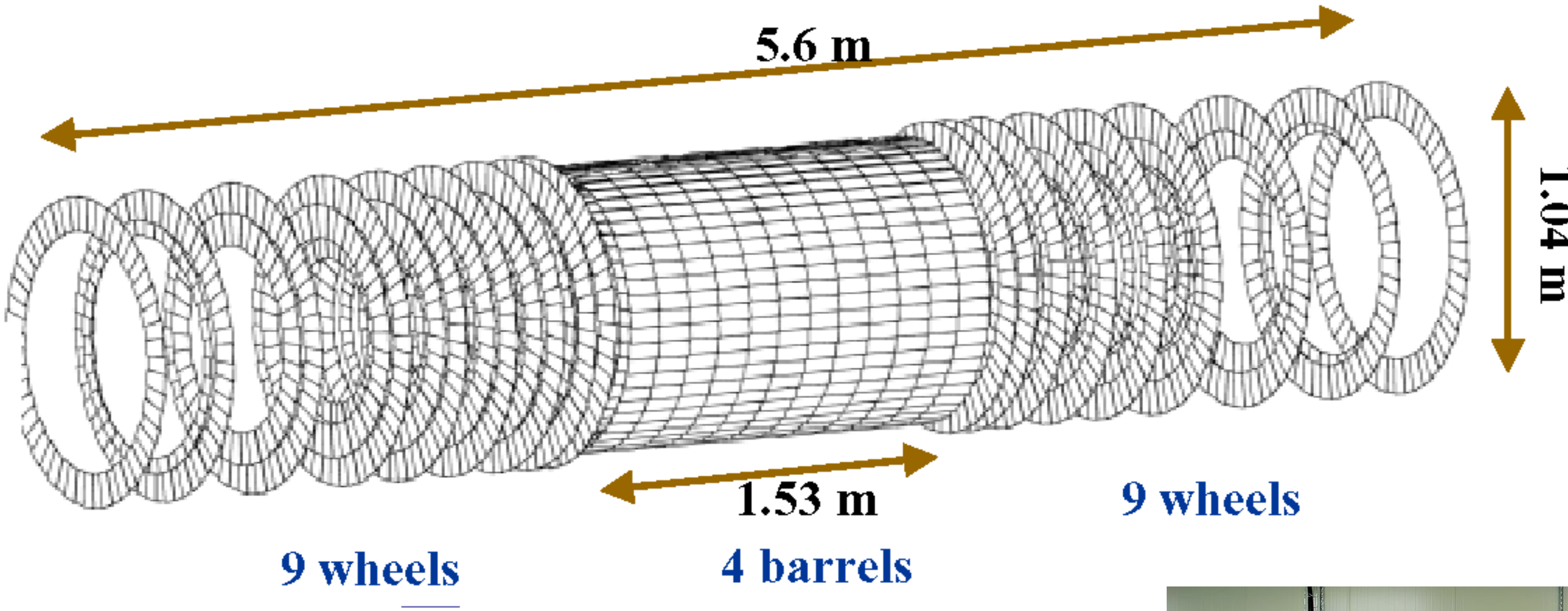

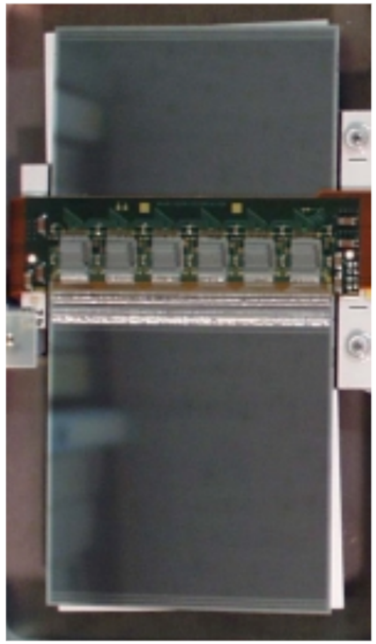

SCT module

Due to radiation issues ATLAS uses p-in-n Si

- In ϕ, modules are tilted wrt to surface of support structure by (11^0, 11^0, 11.25^0 & 11.5^0)
- ~ 61 m^2 of Si (15392 Si wafers)
- ~6.3×10^6 readout channels

Sensor thickness: 285 μ, 80 μm pitch

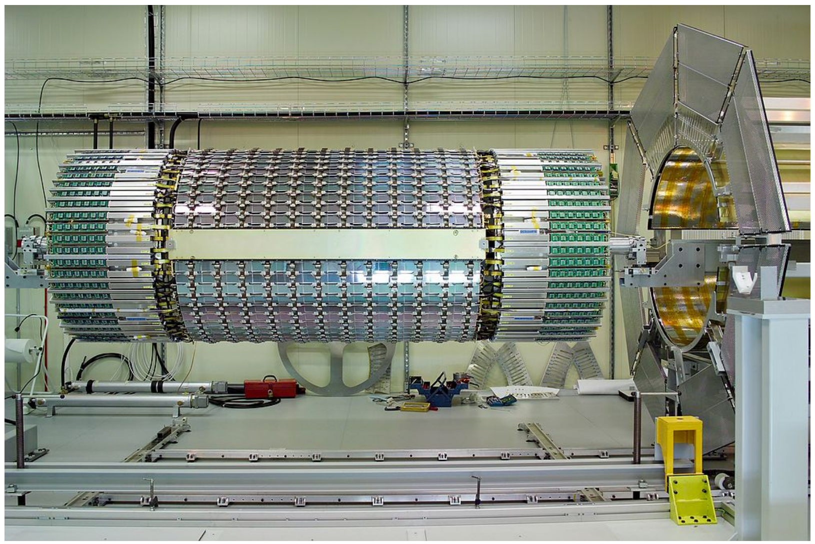

ATLAS SCT Performance

- Cluster width

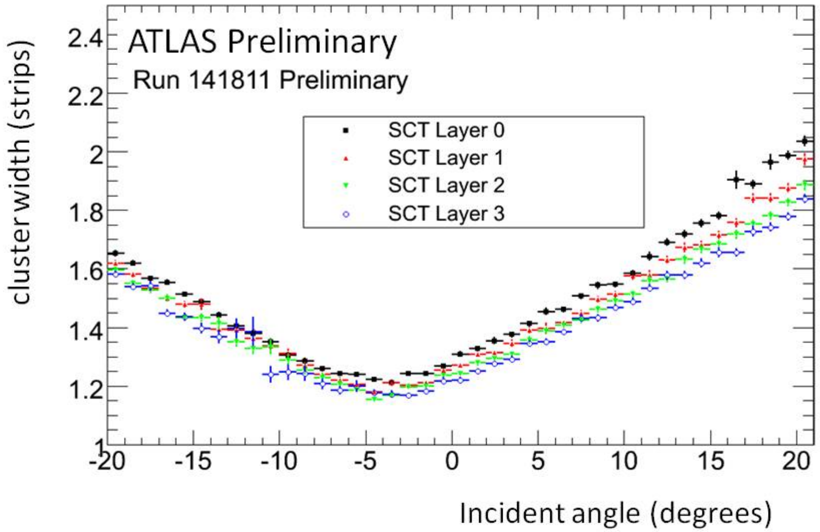

- Hit efficiency in barrel (2009)

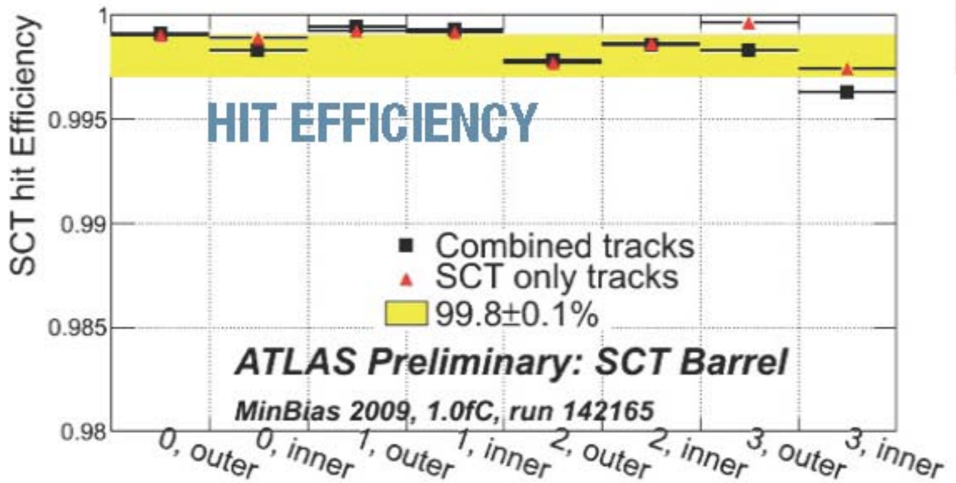

- # SCT hits per track

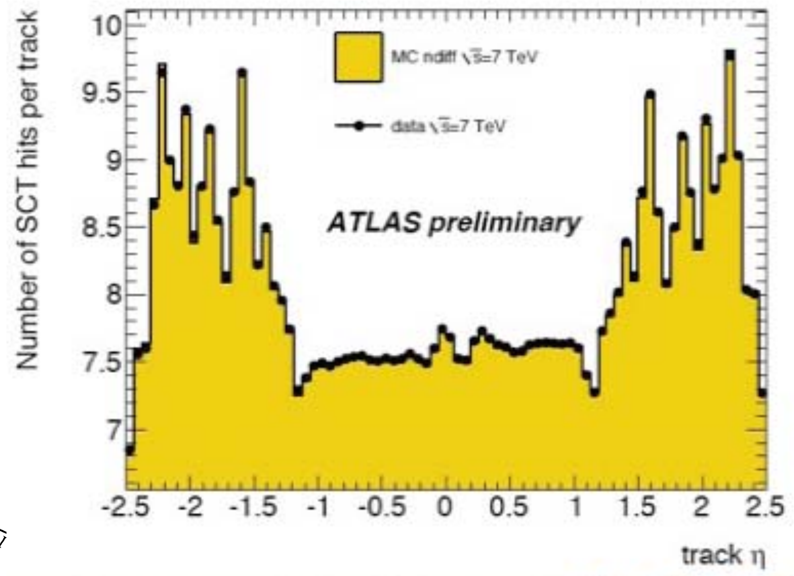

- Impact parameter

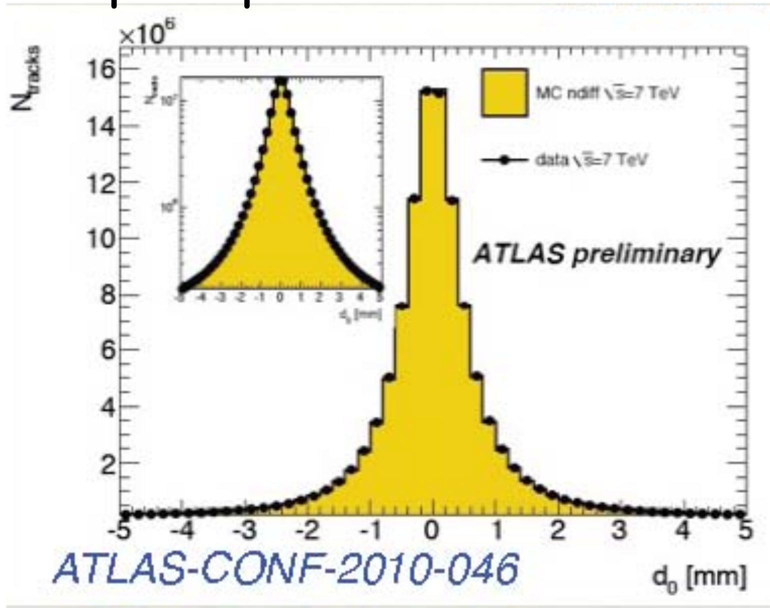

$\eta = -\ln[\tan(\theta/2)]$

Power of Microstrip Detectors

- The power of Si vertex detector measurements (ALEPH)

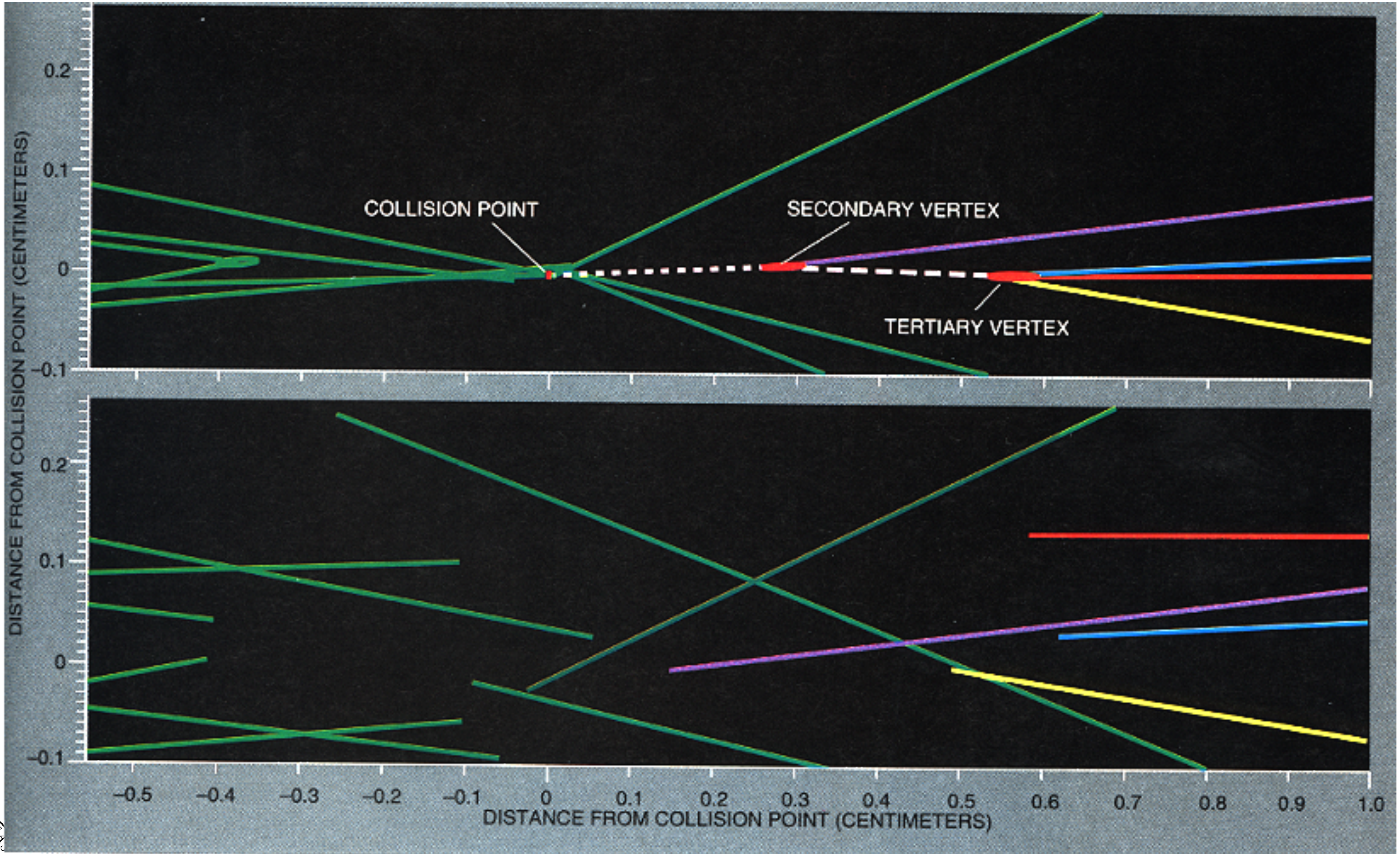

Pixel Detectors

❒ Pixel detectors are made of an array of small Si pixels, i.e. physically isolated pads, providing both r-φ & z measurements

❒ Pixels are bump-bonded to a pixellated readout chip

❒ Advantage: excellent 2-track resolution, take high occupancies

❒ They are used in colliding beam experimen e.g. WA97, DELPHI, ATLAS, CMS, …

❒ Typical pixel dimensions:

WA97: 75×500 μm² ⇒ 5×10⁵ pixels
DELPHI: 320×320 μm² ⇒ 1.2×10⁶ pixels
ATLAS: 50×300 μm² ⇒ 8.×10⁷ pixels
CMS: 150×150 μm² ⇒ 3.9×10⁷ pixels

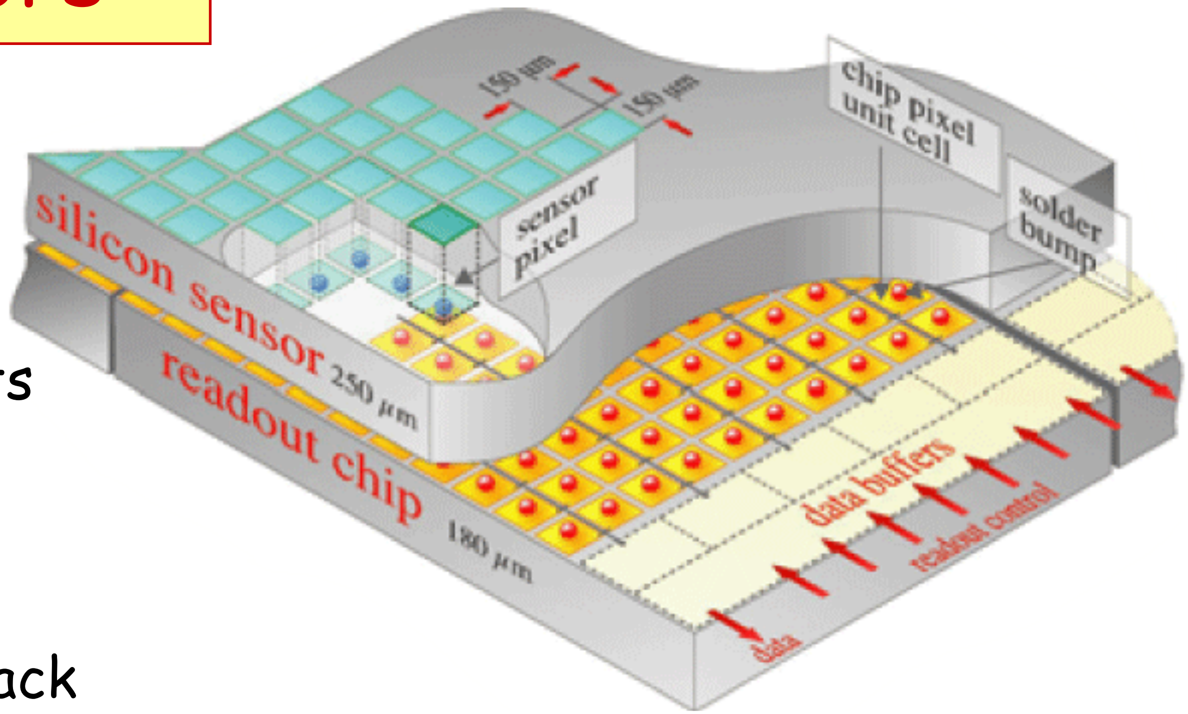

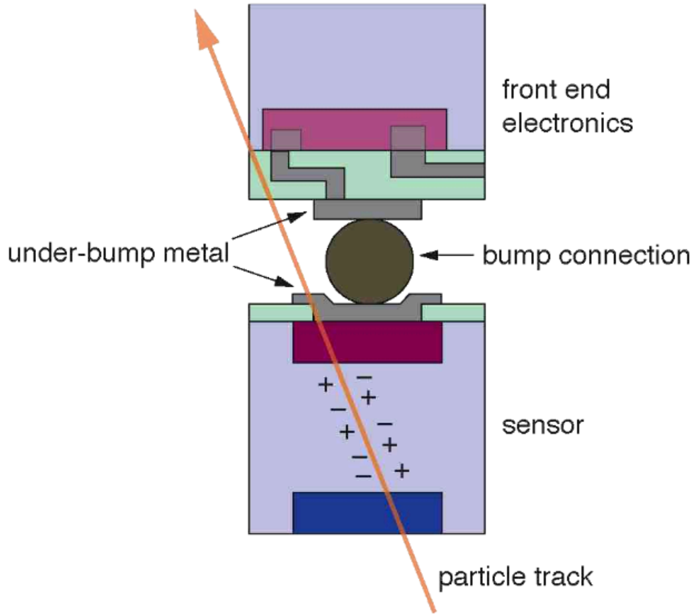

ATLAS Pixel Detector

- ATLAS Pixel detector

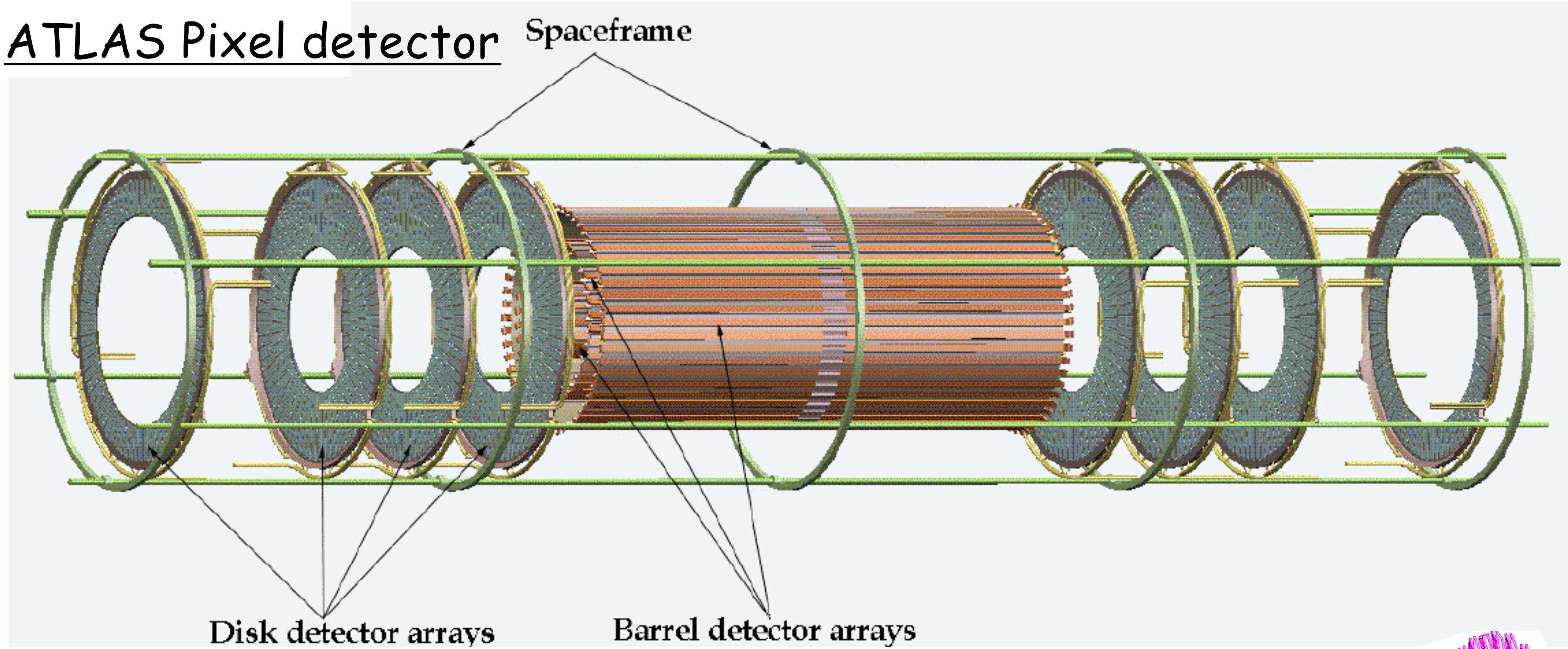

Barrel: r=5.05 cm, 8.85 cm, 12.25 cm

Endcap: z=±49.5 cm, ±56 cm, ±65 cm

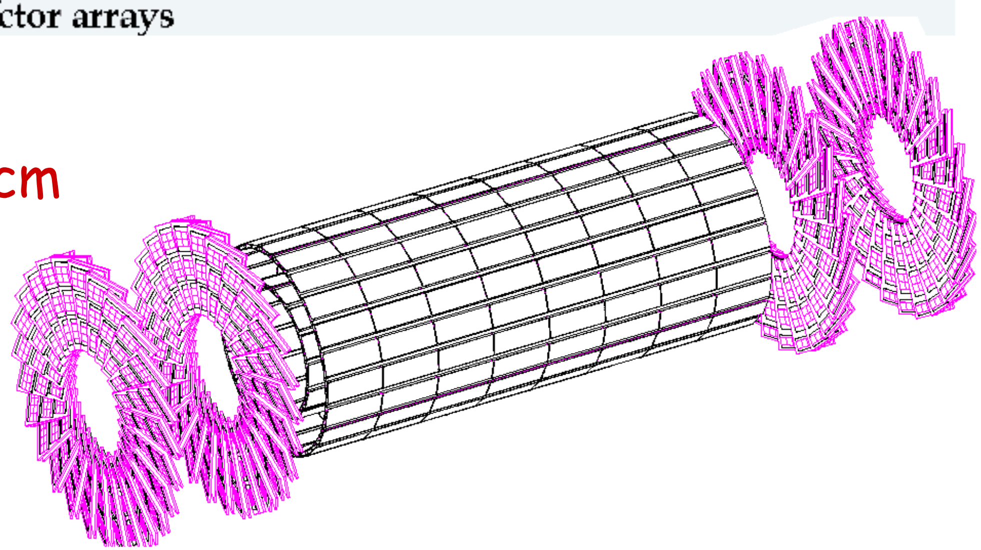

- CMS Pixel detector

Barrel: r=4.4 cm, 7.5 cm, 10.2 cm

Endcap disks at ±34.5 cm,±46.5 cm

ATLAS Pixel Detector Performance

- Cosmic muon traversing through the pixel detector and SCT

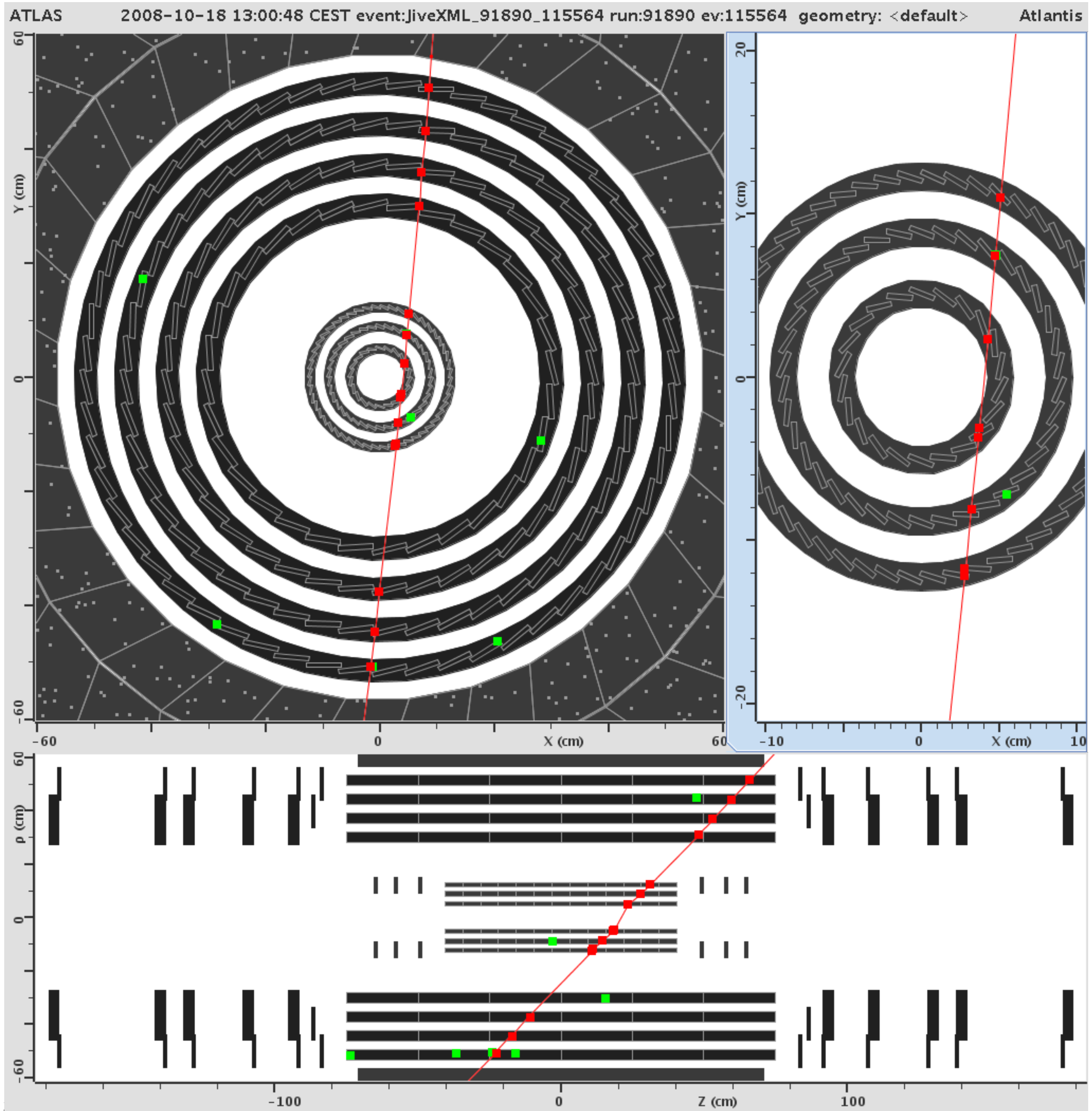

3D Si Detectors

- 3D sensor concept

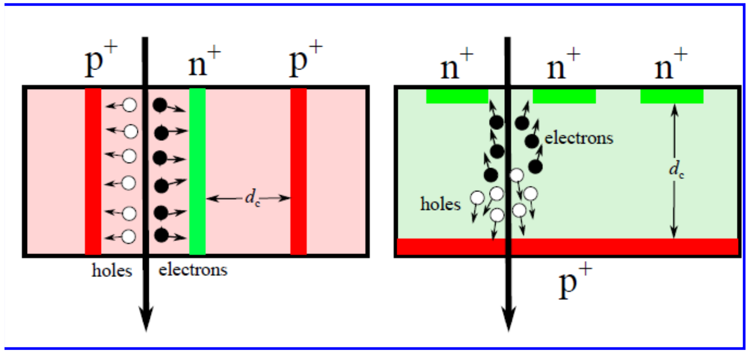

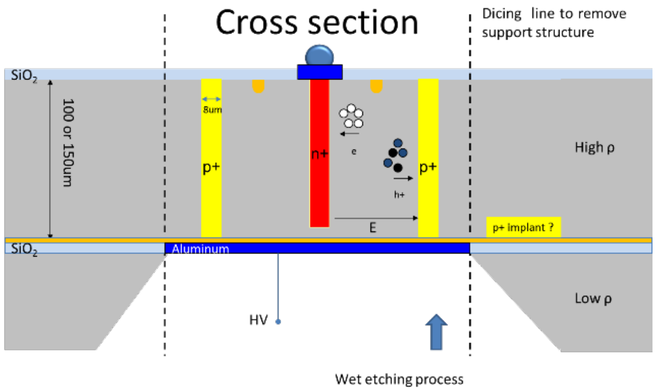

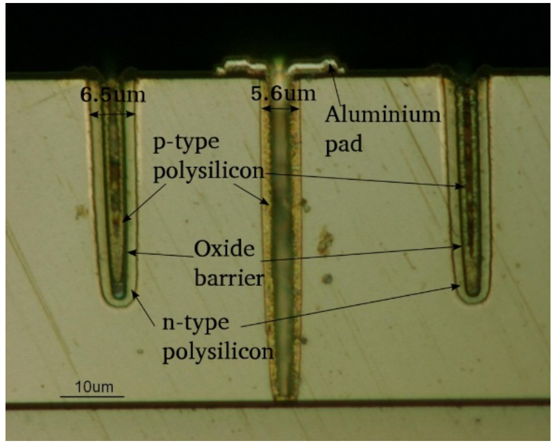

- Advantage: low depletion voltage, small drift length
- Need to be cooled to -30° C to achieve high efficiency after radiation

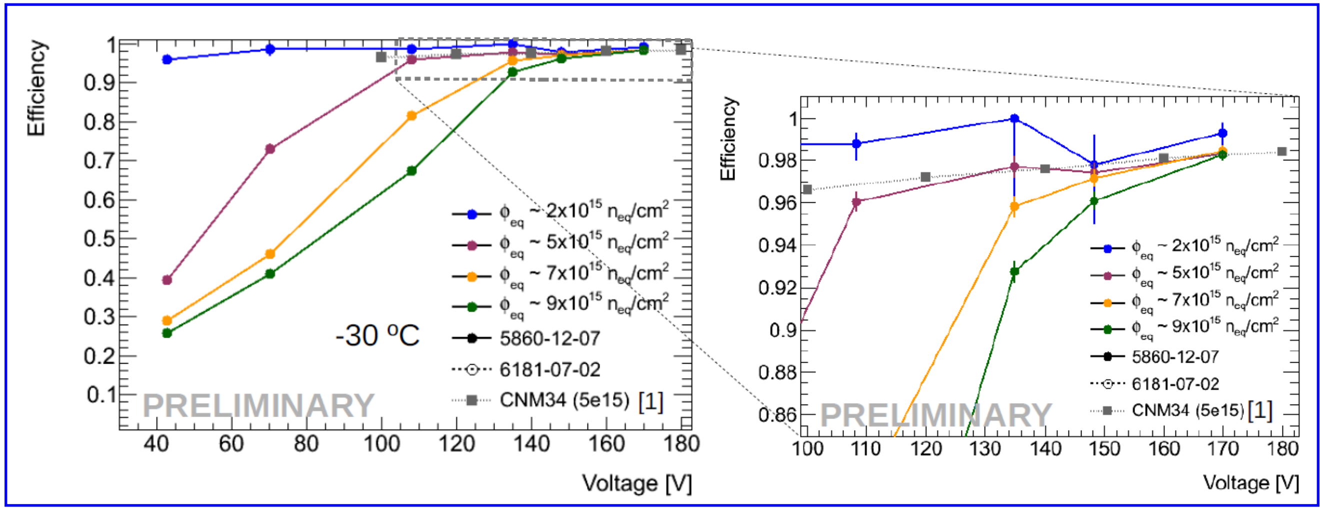

Electrons and Photons in Matter

Energy Loss of Electrons & Positrons

- Electrons & positrons suffer energy losses by radiation in addition to the energy losses by collisions (ionization)
- Thus
$$\left(\frac{dE}{dx}\right)_{tot} = \left(\frac{dE}{dx}\right)_{rad} + \left(\frac{dE}{dx}\right)_{coll}$$
- The basic mechanism of energy loss via collisions is also valid for $e^{\pm}$, but Bethe-Bloch must be modified for 3 reasons:

  i) their small mass $\Rightarrow$ incident particle may be deflected

  ii) For e^- we have collisions between identical particles
  $\Rightarrow$ we must take into account indistinguishable particles

  $\Rightarrow$ Obtain some modifications, e.g. $T_{max}=T_e/2$

  iii) e^+ and e^- are fermions while heavy particle are typically bosons

Critical Energy and Radiation Length

- Critical energy E_c is the energy where $(dE/dx)_{rad}=(dE/dx)_{coll}$ for each material

- Approximate formulae

$$E_c = \frac{610}{Z+1.24} \text{ for solids} \qquad E_c = \frac{710}{Z+0.92} \text{ for gases}$$

E.g. Pb: E_c=7.3 MeV
Air: E_c=102 MeV

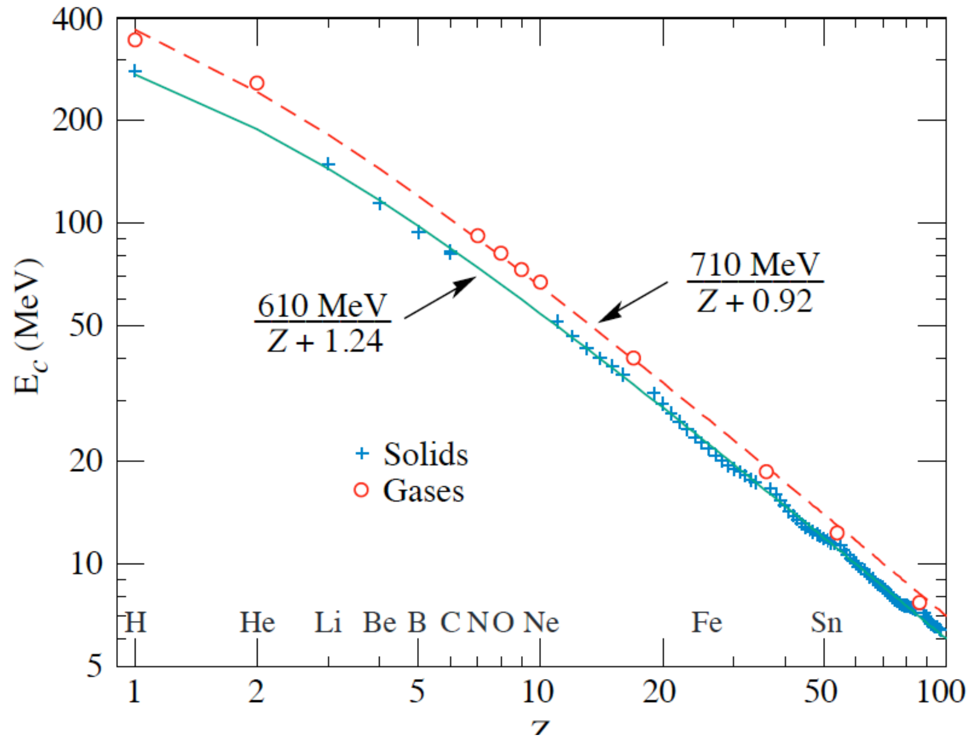

- Radiation length X_0 is the distance over which the electron energy is reduced by $1/e \approx 37\%$ due to radiation loss only

- The radiation length depends only on parameters of the material

$$\frac{1}{X_0} \cong 4\alpha r_e^2 \rho \frac{N_0}{A}\left\{\underbrace{Z^2\left[\ln(184.15 \cdot Z^{-\frac{1}{3}}) - f(Z)\right]}_{\text{protons}} + \underbrace{Z\ln(1194 \cdot Z^{-\frac{2}{3}})}_{\text{electrons}}\right\}$$

N_0: Avogadro's # 6.022×10^{23} mole^{-1}

Detection of Photons

- A photon traversing a medium can experience different processes
  - i) Photoelectric absorption
  - ii) Rayleigh scattering
  - iii) Compton scattering
  - iv) Pair creation in nucleon/electron field
  - v) Photonuclear interaction

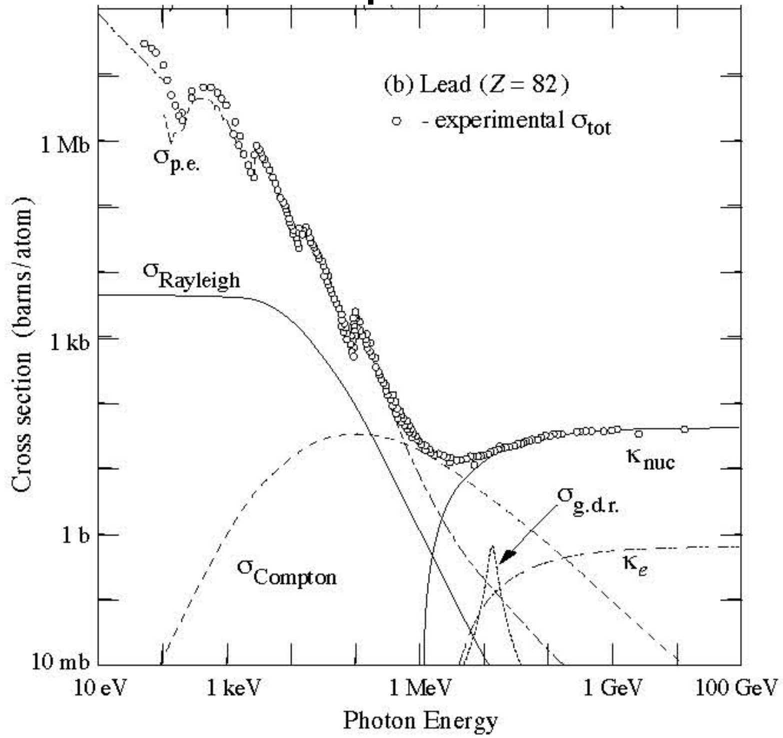

- All processes reduce initial intensity

$$I(z) = I_0 \cdot \exp(-\mu z)$$

where μ is linear absorption coefficient that is related to photon absorption cross section σ by $\mu = \sigma N_0 \rho / A$

- Photoelectric absorption decreases as $\sim 1/E_\gamma^{3.5}$ & increases as Z^5 (e.g. for energies between K&L)

- Compton scattering decreases as $1/E_\gamma$ & increases as Z

- Pair creation requires minimum energy of $E \geq 2m_e c^2$

Electron-Photon Showers

- At high energy a photon is likely to convert into e^+e^-
- $e^\pm$ particles loose energy via bremsstrahlung producing new γ's that are likely to convert into e^+e^-
- Result is a cascade or shower of e^+, e^-, & γ's
- Process stops once energies of e^+, e^-, & γ's become so small that energy loss of γ's occurs preferentially via photoelectric absorption & that energy loss of e^+ & e^- occurs preferentially via ionization

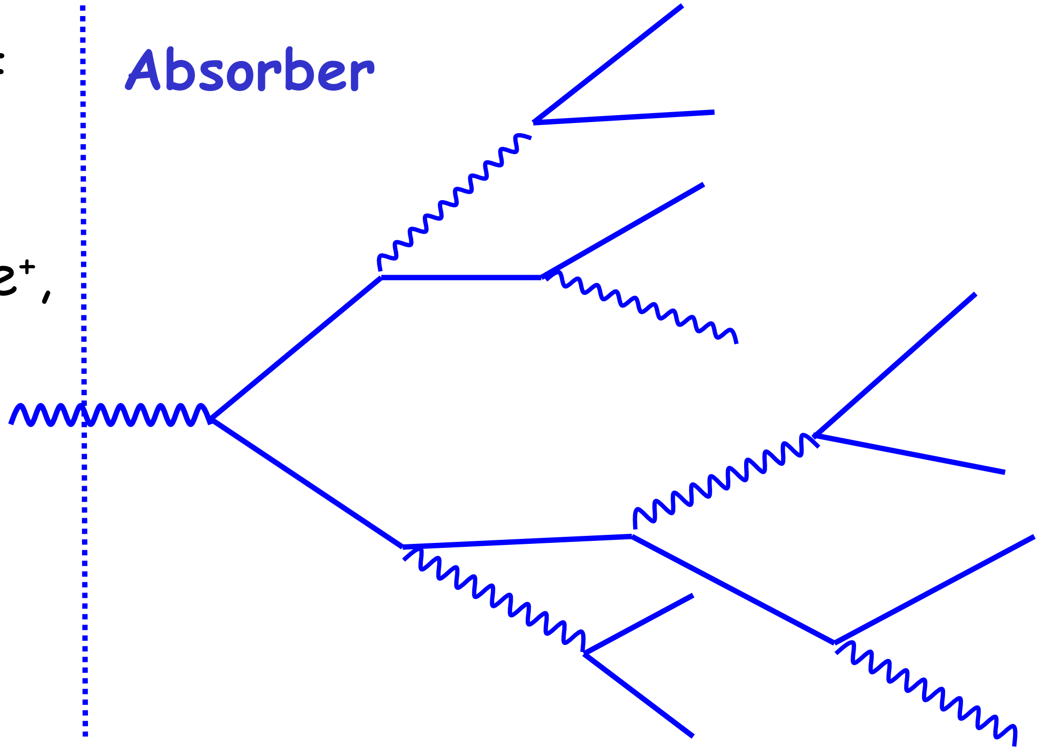

- A similar shower is obtained if we start with a high-energy e^- or e^+

Model for Electron-Photon Showers

- High energy photons & e^- produce a shower of γ, e^+ & e^- via e^+e^- pair creation & bremsstrahlung
- This process stops if energy of γ, e^+ & e^- approaches the critical energy
- A simplified model of an em shower looks like this:
  - An initial photon of energy E_0 produces e^+e^- pair with probability of 7/9 after passing a $1X_0$ thick layer of material
    $\Rightarrow$ e^+ & e^- each have average energy of $E_0/2$
  - If $E_0/2 > E_c$, e^+ & e^- loose energy via bremsstrahlung
    $\Rightarrow$ Energy decreases to $E_0/(2f)$ after traversing second X_0 of material
    $\Rightarrow$ Radiated photon has energy $E_\gamma = E_0/2 - E_0/(2f)$ $[E_0/2 > E_\gamma > E_0/(2f)]$
  - So after $2X_0$ average # of particles is 4: e^+, e^-, γ, γ
    $\Rightarrow$ Each photon produces another e^+e^- pair & each e^+ & e^- radiate another γ after passing through another X_0 thick layer
  - After n generations corresponding to thickness $n \cdot X_0$ we obtain $N_p = 2^{n_{max}} = E_0/E_c$ particles at shower maximum with average energies of $E_0/(2^{n_{max}})$, where $n_{max} = \ln(E_0/E_c)/\ln 2$
  - Cascade breaks off if $E_0/(2n) \approx E_c$

Electromagnetic Calorimeters

Characteristics of e^{-}-γ Shower

- The most exact calculations of detailed shower development is obtained with MC simulations (EGS)

- We obtain the following properties of the e^{-}-γ shower
  i) Number of particles at shower maximum, N_p, is proportional to E_0
  ii) Total track length s of e^{-} & e^{+}, is proportional to E_0
  iii) Depth at which shower maximum occurs, X_{max}, increases as log

$$\frac{X_{max}}{X_0} = \ln\left(\frac{E_0}{E_c}\right) + t$$

  where $t=-0.5$ for e^{-} & $t=0.5$ for photons

- Example: 1 GeV photon in NaI crystal: X_0=2.59 cm, E_c=12.5 MeV
  $\Rightarrow$ N_p=80, n=6.3, & X_{max}=11.8 cm

- Basically 2 types of em calorimeters
  1) homogeneous shower counter (inorganic crystals [NaI, CsI(Tl), BGO, BaF_2, $PbWO_4$, LSO, LYSO], Pb glass, liquid noble gases [Ar, Kr, Xe])
  2) sampling shower calorimeter

Longitudinal & Transverse Distributions

- Longitudinal energy distribution is parameterized by $\frac{dE}{dt} = E_0 C t^{\alpha} e^{-\beta t}$ with $\beta=0.5$, $\alpha=\beta t_{max}$ and $c=\beta^{\alpha+1}/\Gamma(\alpha+1)$
- Transverse shower dimensions results from MS of low-energy e^+ & e^-
- Useful unit for transverse shower is Molière radius $R_M = 21\ MeV\ X_0 / E_c$
- Transverse energy distribution in units of R_M independent of material
  ➔ inside $1R_M$ 90% of shower is contained ➔ inside $3R_M$, 99% of shower

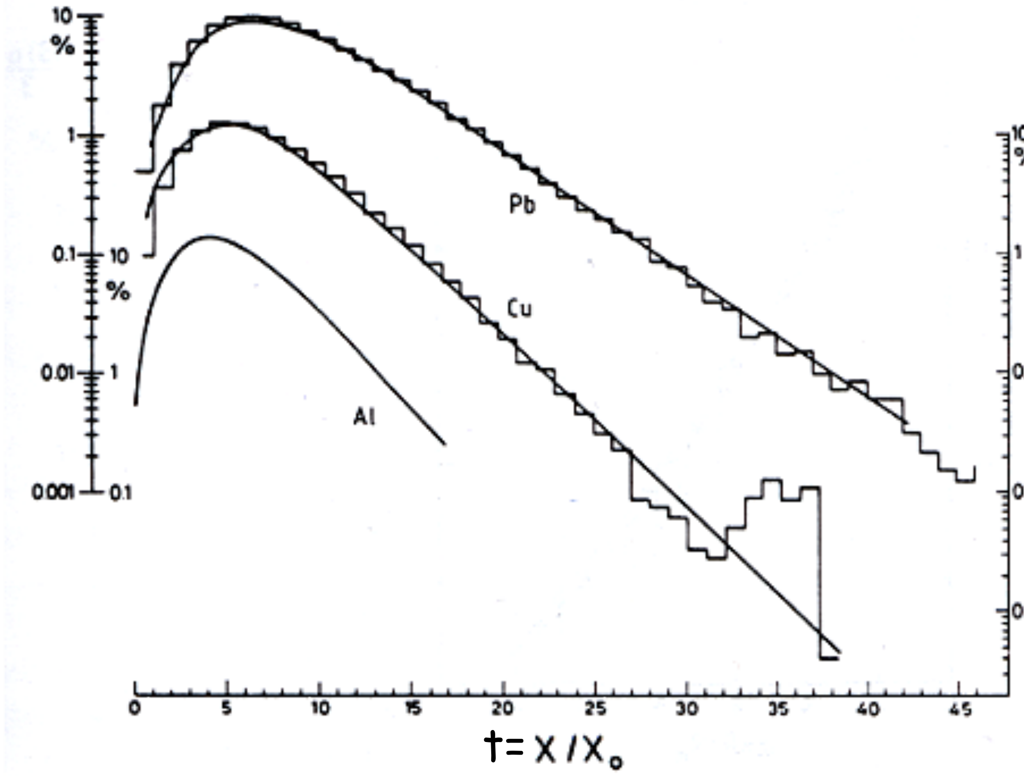

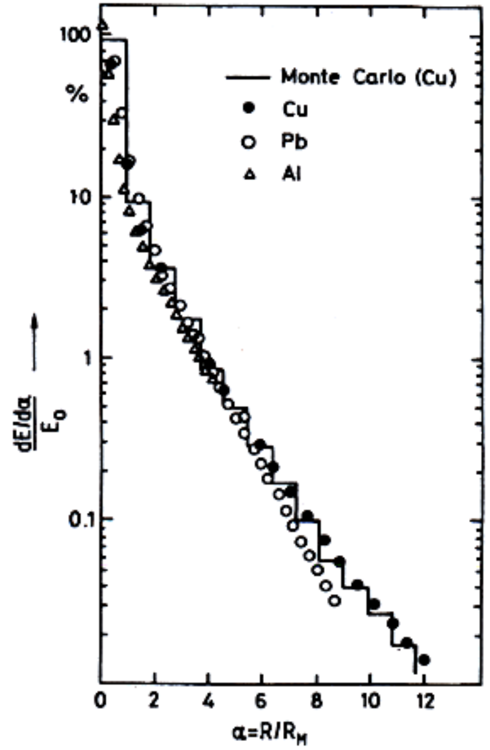

Energy Resolution of Homogeneous Calorimeter

- The energy resolution of a crystal calorimeter is given by:

$$\left(\frac{\sigma_E}{E}\right)^2 = \frac{\sigma^2_{noise}}{E^2} + \left(\frac{a}{\sqrt{E}}\right)^2 + \overbrace{\tilde{b}^2 + \underbrace{\sigma^2_{FL} + \sigma^2_{SL} + \sigma^2_{RL}}_{\text{leakage terms}}\, f(E) + \sigma^2_{NC}}^{b^2} \qquad (7.10)$$

noise term

stochastic term

leakage terms front, side, rear

nuclear counter term particles passing through detector

term for intercalibration, inhomogeneity

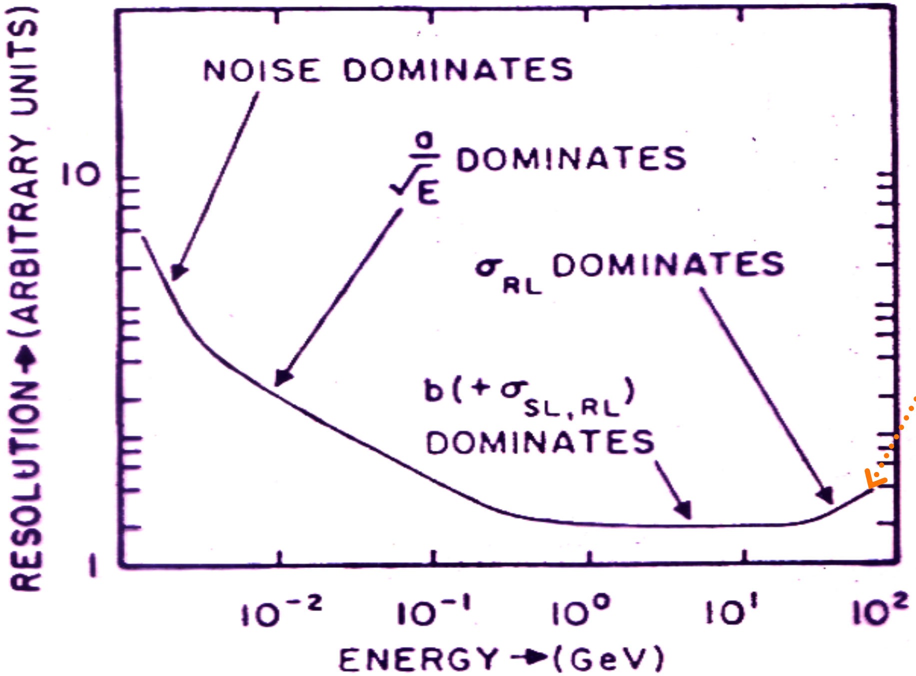

- $F(E) = 1 + c_1 E + c_2 E^2 + \ldots$
- For a sufficiently long calorimeter, $F(E) \approx 1$
- All energy-independent terms are typically parameterized by one constant b
- For CsI(TL) stochastic term is $1/\sqrt[4]{E}$

BABAR EMC Performance

- ❒ Energy & angular resolution of BABAR CsI(Tl) crystal calorimeter
  - ➢ Use photons & electrons from physics processes
  - ➢ Low-energy point is obtained from radioactive source

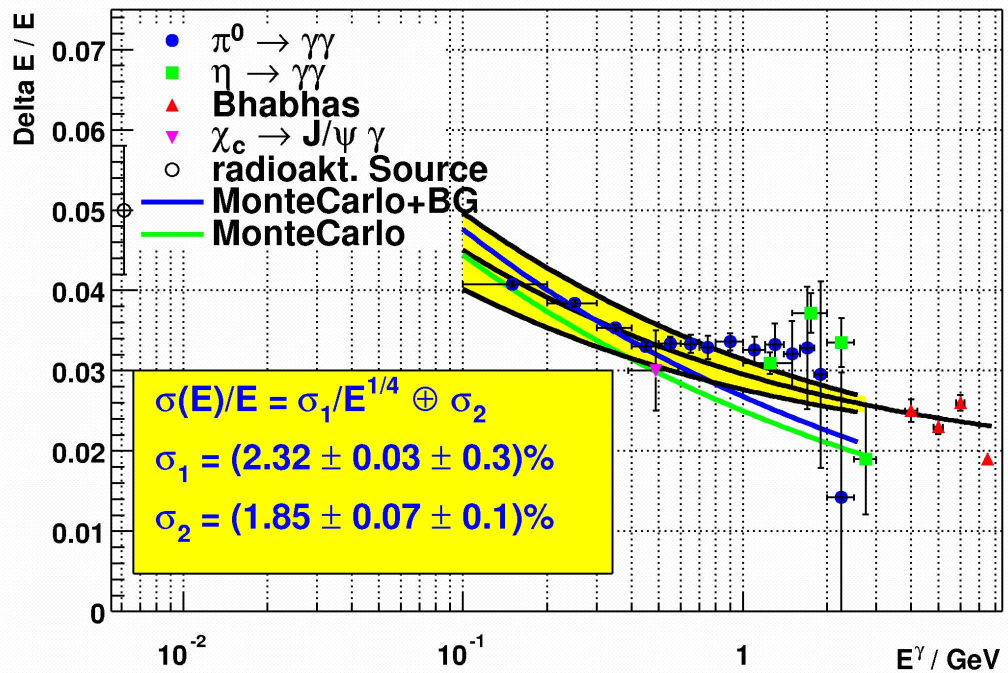

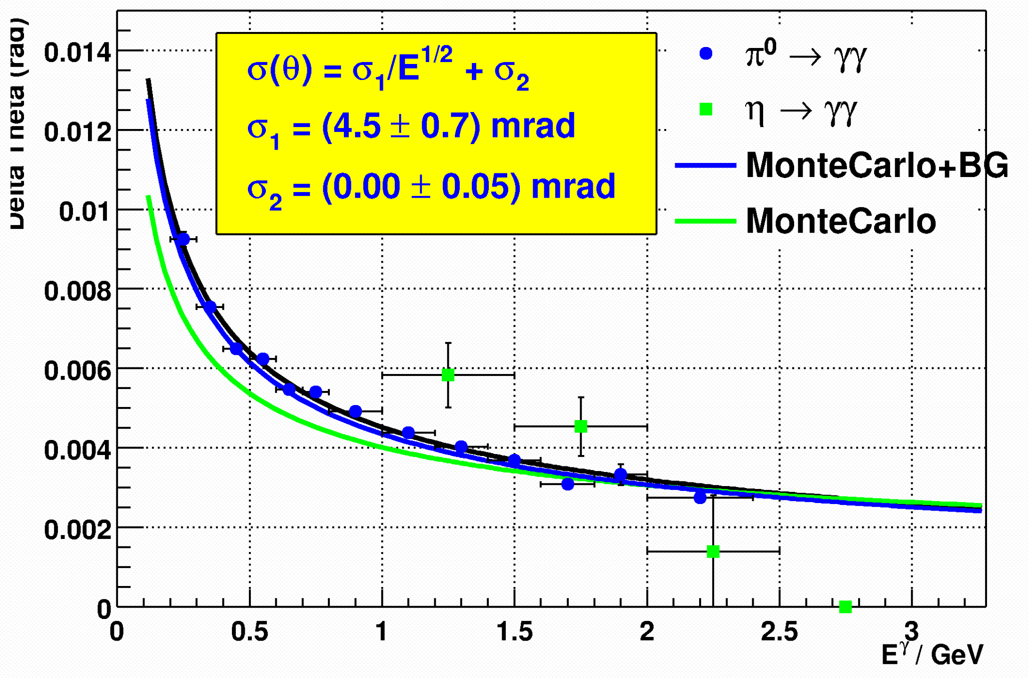

SAMPLING SHOWER DETECTORS

- Sampling calorimeters are devices in which the fluctuations of energy degradation & energy measurement are separated in alternating layers of different substances

- The choices for passive absorber are plates of Fe, Cu, W, Pb, U

- For energy measurement a gas mixture, liquid noble gases, or plastic scintillators are used

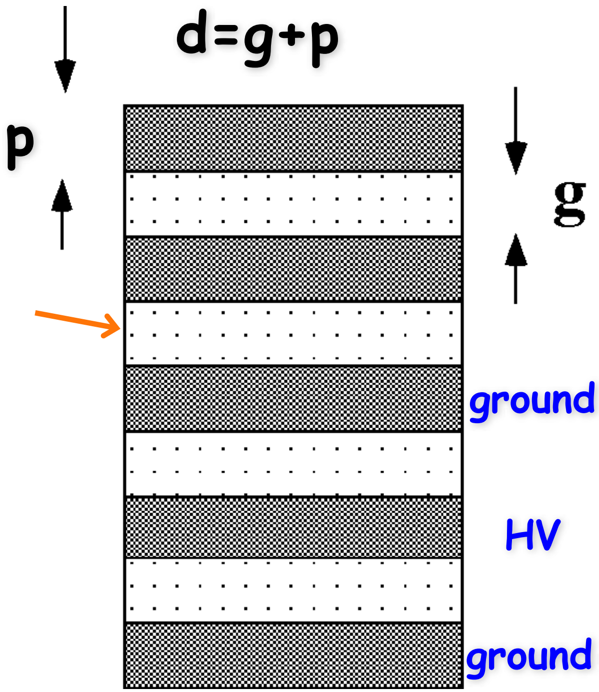

- This allows to build rather compact devices & permits optimization for specific experimental requirements ⇒ e^{-} - π discrimination
  - ⇒ longitudinal shower profile
  - ⇒ good angular measurements
  - ⇒ good position measurements

- Plate thickness p ranges from fraction of X_0 (EM) to few X_0(hadronic)

- Disadvantage is that only a fraction of total energy of em shower is detected (sampling) in active planes resulting in additional sampling fluctuations of the energy discrimination

Energy Resolution of Sampling Calorimeter

- The total energy resolution of a sampling calorimeter is

$$\left(\frac{\sigma_E}{E}\right)_{tot} = \left[\left(\frac{\sigma_E}{E}\right)^2_{sampling} + \left(\frac{\sigma_E}{E}\right)^2_{Landau} + \left(\frac{\sigma_E}{E}\right)^2_{path\ length}\right]^{1/2}$$

where

$$\left(\frac{\sigma_E}{E}\right)_{sampling} \geq 3.2\% \left[\frac{\Delta E\ [\mathrm{MeV}]}{F(\xi)\cos\left(\frac{21\ \mathrm{MeV}}{E_c\pi}\right)E\ [\mathrm{GeV}]}\right]^{1/2}$$

$$\left(\frac{\sigma_E}{E}\right)_{Landau} = \left[\frac{3}{\sqrt{N_x} \times \ln\left(1.3 \times 10^4 \delta\right)}\right]$$

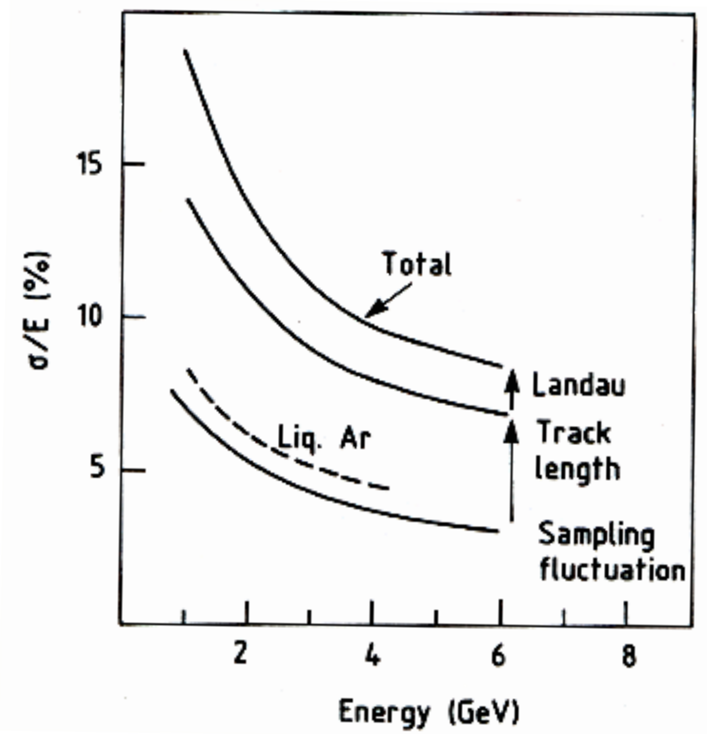

- The sampling fluctuations include multiple scattering and effects of an energy cut-off

N_x: number of crossings in sampling calorimeter=total track length divided by distance between active plates

$$N_x = \frac{E_0 X_0}{E_c d} = \frac{E_0}{\Delta E}$$

- The path length fluctuations depend on the density of the medium

An Simulated EM Shower

❒ Simulation of em shower using EGS IV

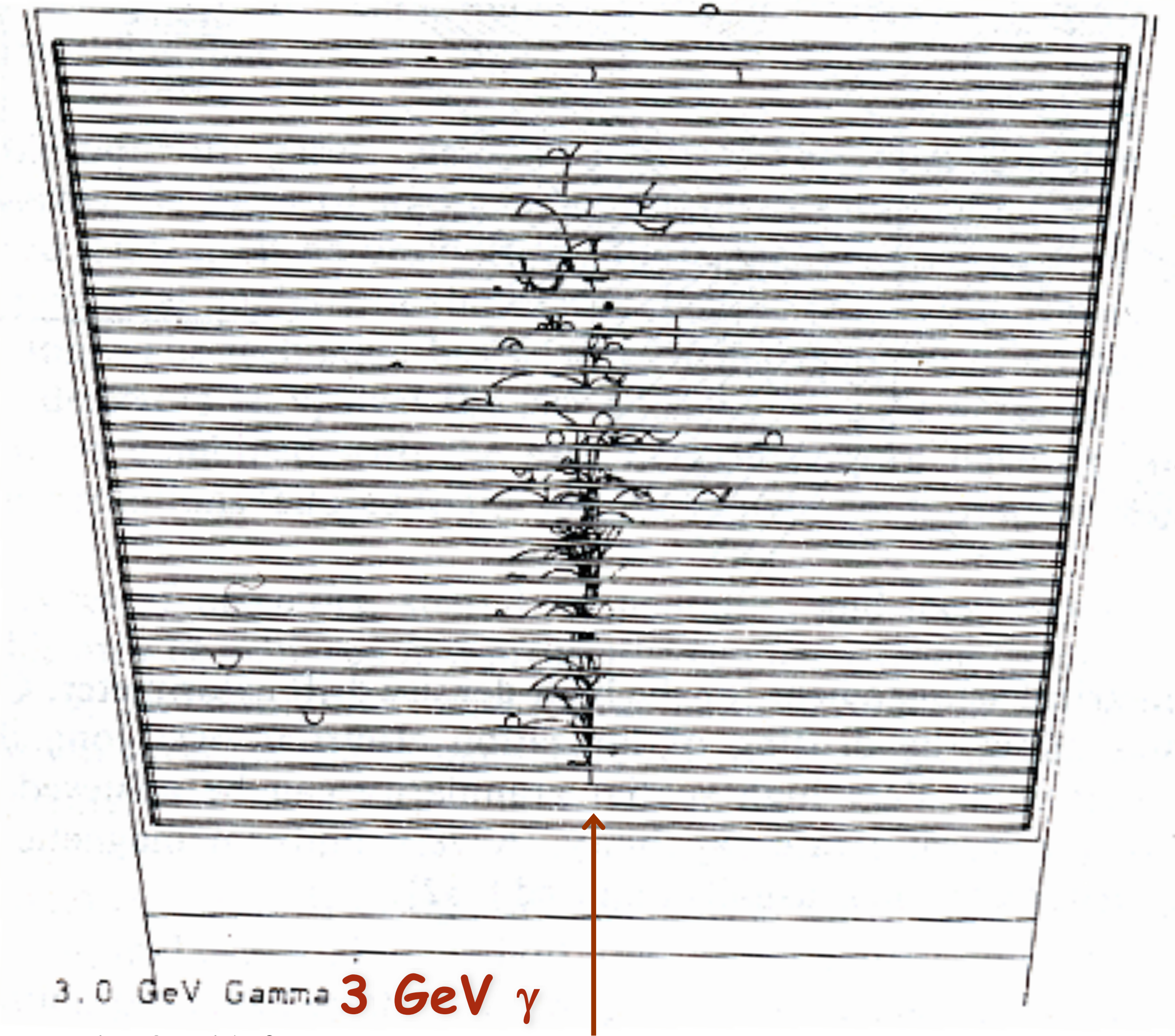

ATLAS Liquid Argon ECAL

- ATLAS Pb-LiAr sampling calorimeter

$$\eta = -\ln\left|\tan\frac{\theta}{2}\right|$$

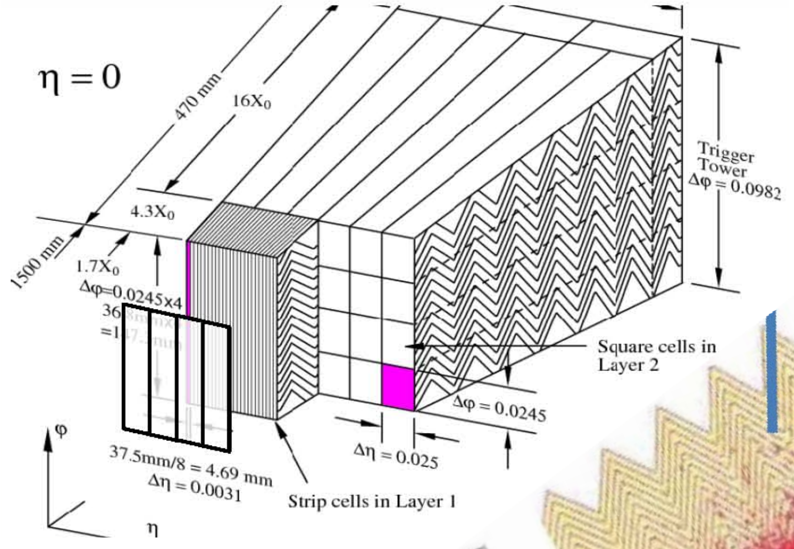

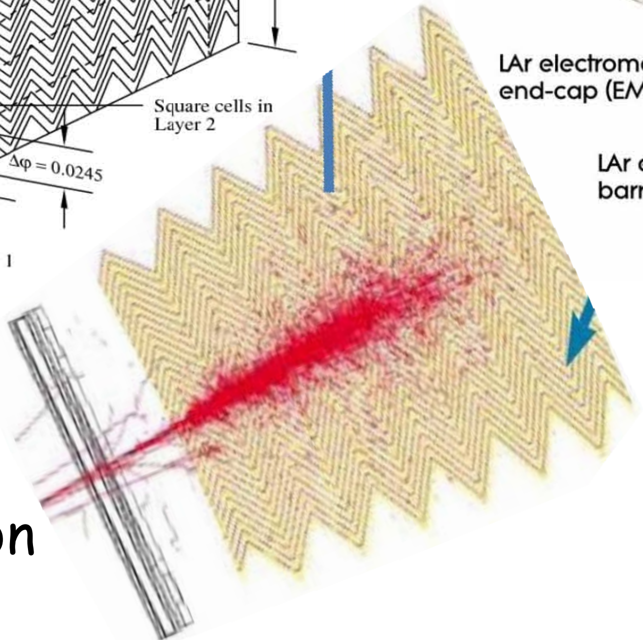

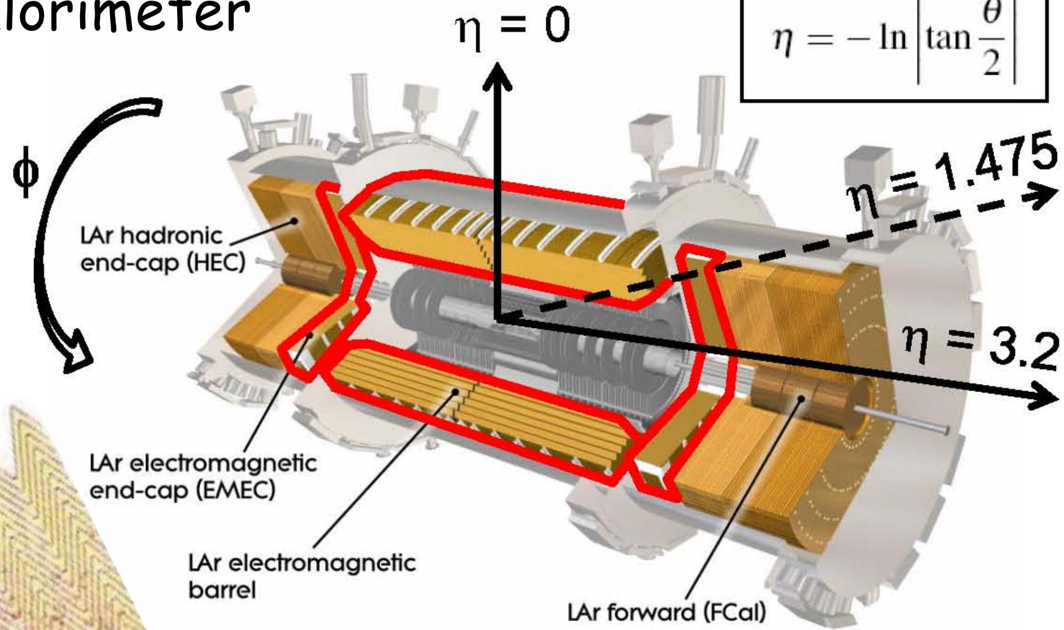

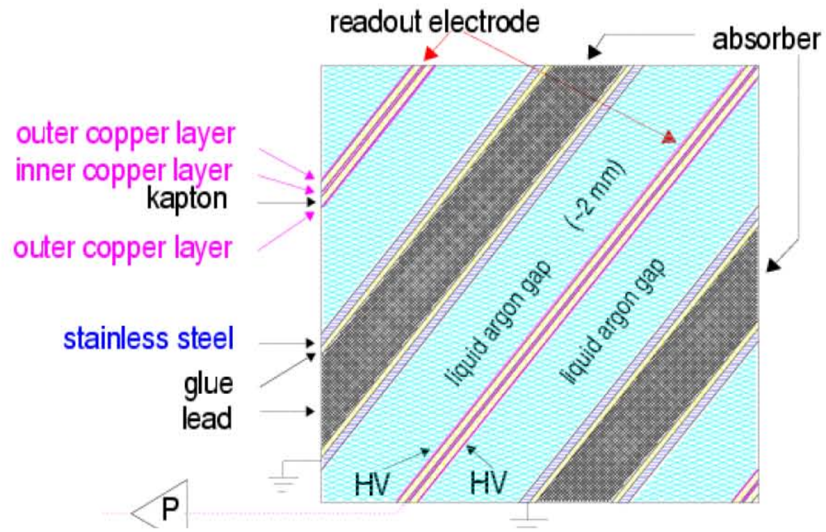

- Use accordion geometry
- Full ϕ coverage w/o cracks
- 3 layers with |η|<3.2
- 173312 readout channels (98.5% work)

ATLAS LiAr ECAL

- The ATLAS LiAr calorimeter works well

Energy Linearity from test beam

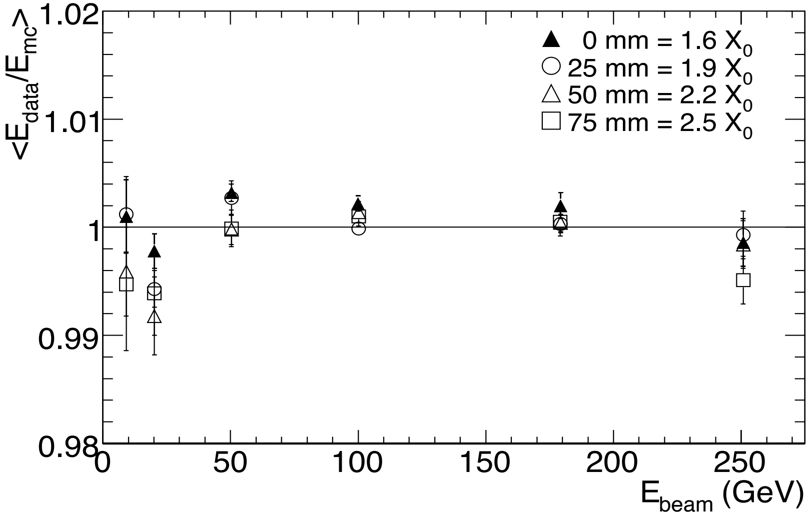

Energy Resolution from test beam

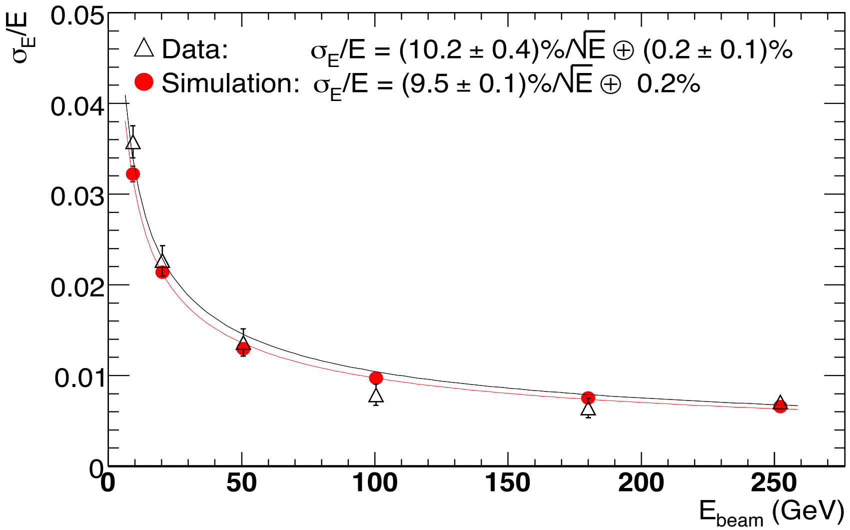

- Energy response is linear

- Energy resolution is

$$\frac{\sigma_E}{E} = \frac{0.1}{\sqrt{E}} \oplus 0.007$$

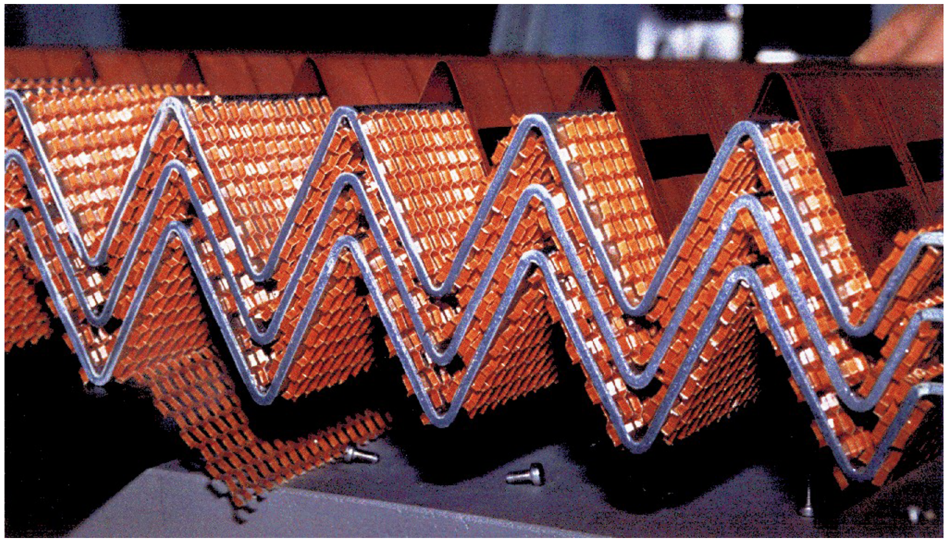

Hadronic Calorimeters

Hadron Showers

- Conceptually, energy measurement of hadronic showers is analogous to that of electromagnetic showers, but due to complexity & variety of hadronic processes, a detailed understanding is complicated
- Though elementary processes are well understood, no simple analytical description of hadronic showers exist
- Half the energy is used for multiple particle production ($\langle p_t \rangle \cong 0.35$ GeV), the remaining energy is carried off by fast, leading particles
- 2 specific effects limit the energy resolution of hadronic showers

i) A considerable part of secondary particles are π^0's, which will propagate electromagnetically without further nuclear interactions Average fraction of hadronic energy converted into π^0's is

- $f_{\pi^0} \approx 0.1 \ln(E)$ [GeV] for few GeV $\leq E \leq$ several 100 GeV
- Size of π^0 component is largely determined by production in first interaction & by event-by-event fluctuations about the average value

ii) A sizable amount of available energy is converted into excitation or breakup of nuclei $\rightarrow$ only a fraction of this energy will be see

Intrinsic Energy Resolution

- The intrinsic hadronic energy resolution is:

$$\left(\frac{\sigma_E}{E}\right)_{\text{intrinsic}} \cong \frac{0.45}{\sqrt{E\ [\text{GeV}]}}$$

holding for materials from Al to Pb (exception ^{238}U)

- The level of nuclear effects & level of invisible energy is sensitively measured by comparing the calorimeter response to e & h at the same available energy
  - Ideally, one wants e/h≅ 1
  - Typical values are e/h≅1.4
  - e/h drops to ~0.7 below 1 GeV
- Unless event-by-event fluctuations in the EM component are not corrected for, $\sigma_E/E \cong 0.45\ E^{-1/2}$
- This applies likewise to homogeneous & to sampling calorimeters

e/h ratio in different hadron calorimeters

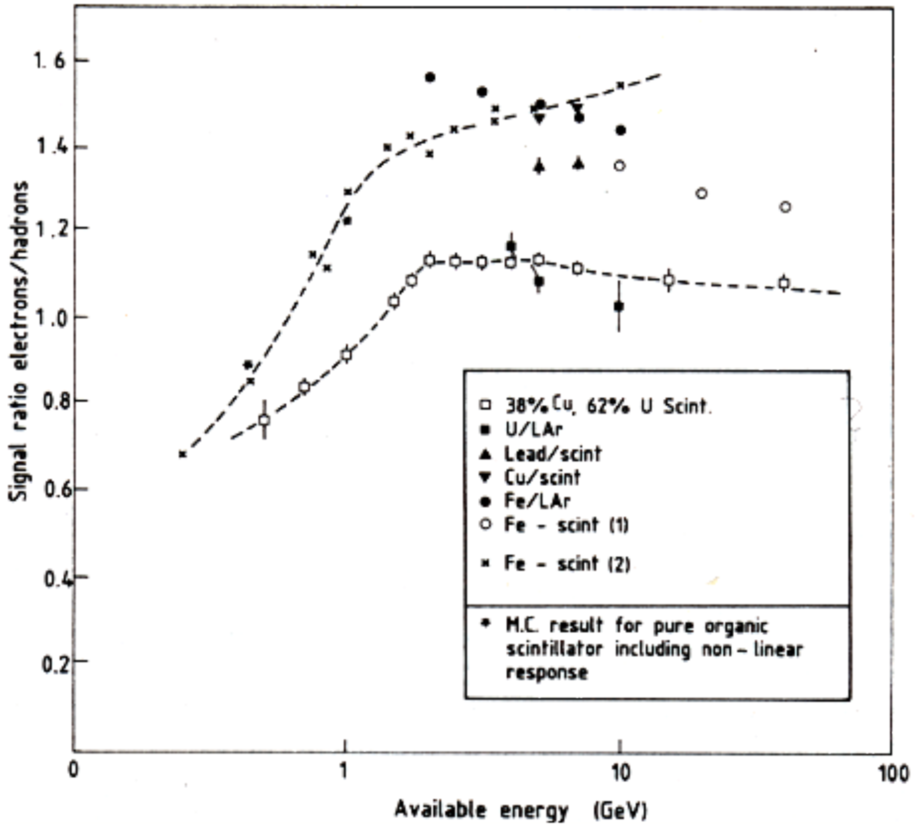

Compensation Fluctuations

- To cure these fluctuations we need to equalize response for e^- & h
  $\Rightarrow$ either decrease e^- response or boost h response
- The latter can be achieved in U-scintillator calorimeters
  - Due to nuclear break-up one gets neutron-induced fission liberating about 10 GeV of fission energy
  - Just need to detect 300-400 MeV to compensate for nuclear deficit measure either the few MeV γ component or the fission neutrons
- Intrinsic resolution for ^{238}U is $$\left(\frac{\sigma_E}{E}(U)\right)_{\text{intrinsic}} \cong \frac{0.22}{\sqrt{E\ [\mathrm{GeV}]}}$$
- This was achieved in the ZEUS calorimeter (U-scintillator)
- In addition sampling fluctuations contribute to the total energy resolution where ΔE is energy loss per unit sampling for MIPs $$\left(\frac{\sigma_E}{E}\right)_{\text{hadronic sampling}} \cong 0.09\sqrt{\frac{\Delta E[MeV]}{E[GeV]}}$$
- Hadronic sampling fluctuations are approximately twice as large as EM sampling fluctuations

Shower Containment

- In analogy to X_0 define a hadronic interaction length λ as the length in which a hadron has interacted with probability of 63%
- Longitudinal shower distributions parametrized in λ are similar for different materials
- Shower maximum

  $$l_{max}(\lambda) \sim 0.2 \ln E[GeV] + 0.7$$

- 95% longitudinal shower containment $L_{0.95}(\lambda) = l_{max} + 2.5\lambda_{att}$

  where $\lambda_{att} \cong \lambda \cdot (E[GeV])^{0.13}$

  ⇨ $L_{0.95}(\lambda)$ describes data in few GeV $\leq$ E $\leq$ few 100 GeV within 10%

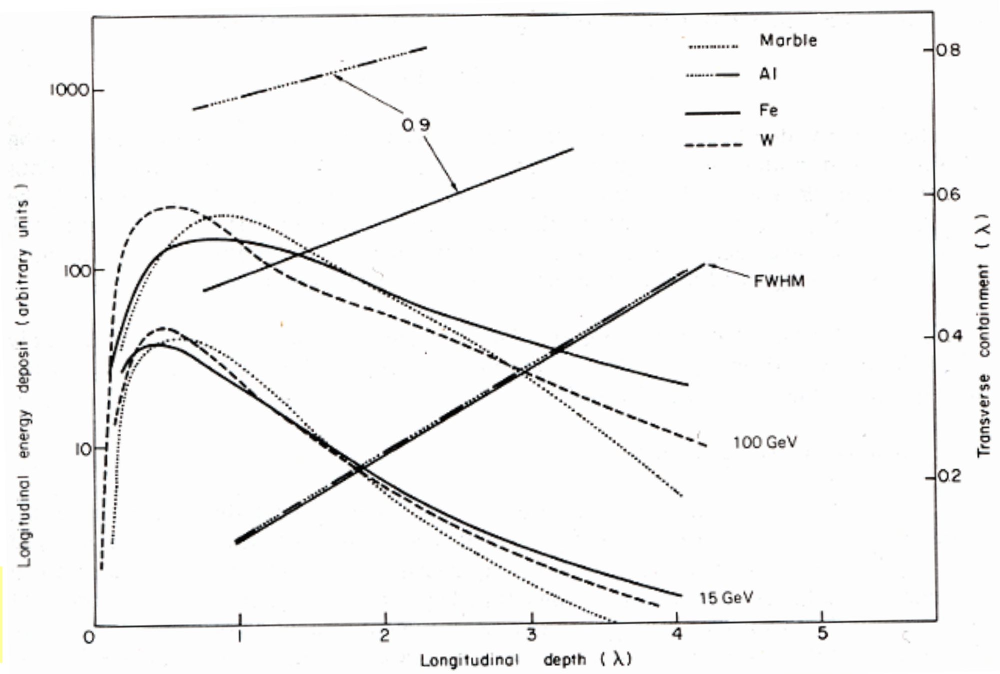

- 95% radial shower containment is $R_{0.95} \leq 1\lambda$
- Useful parameterization of longitudinal shower development

  $$dE/ds = K\left[w \cdot t^a e^{-bt} + (1-w) l^c e^{-dl}\right]$$

a,b,c,d: fit parameters
$t = s/X_0$, $l = s/\lambda$, f: fraction

ATLAS Hadron Calorimeters

- Steel-scintillator sampling calorimeter (total thickness ~11λ)
  - 14 mm thick steel plates
  - 460 000 3 mm thick scintillator tiles
  - Calorimeter is built in 3 sections: barrel and 2 extended barrels

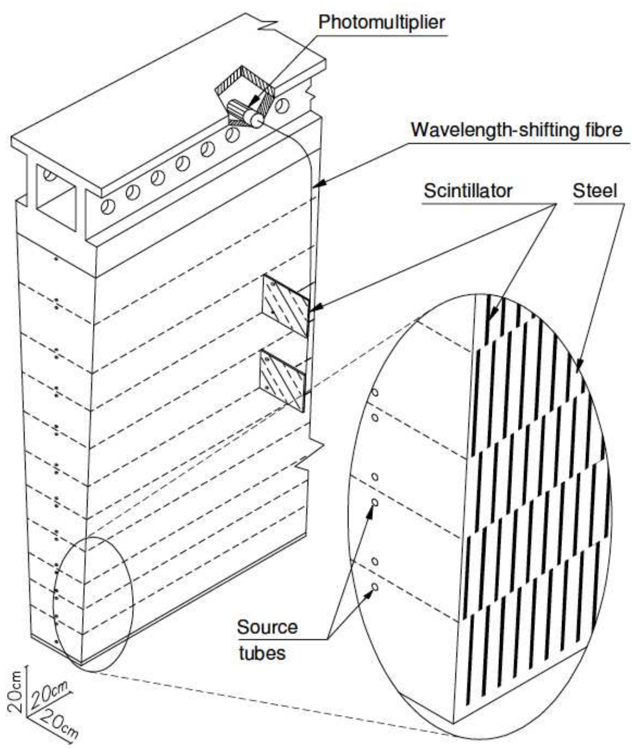

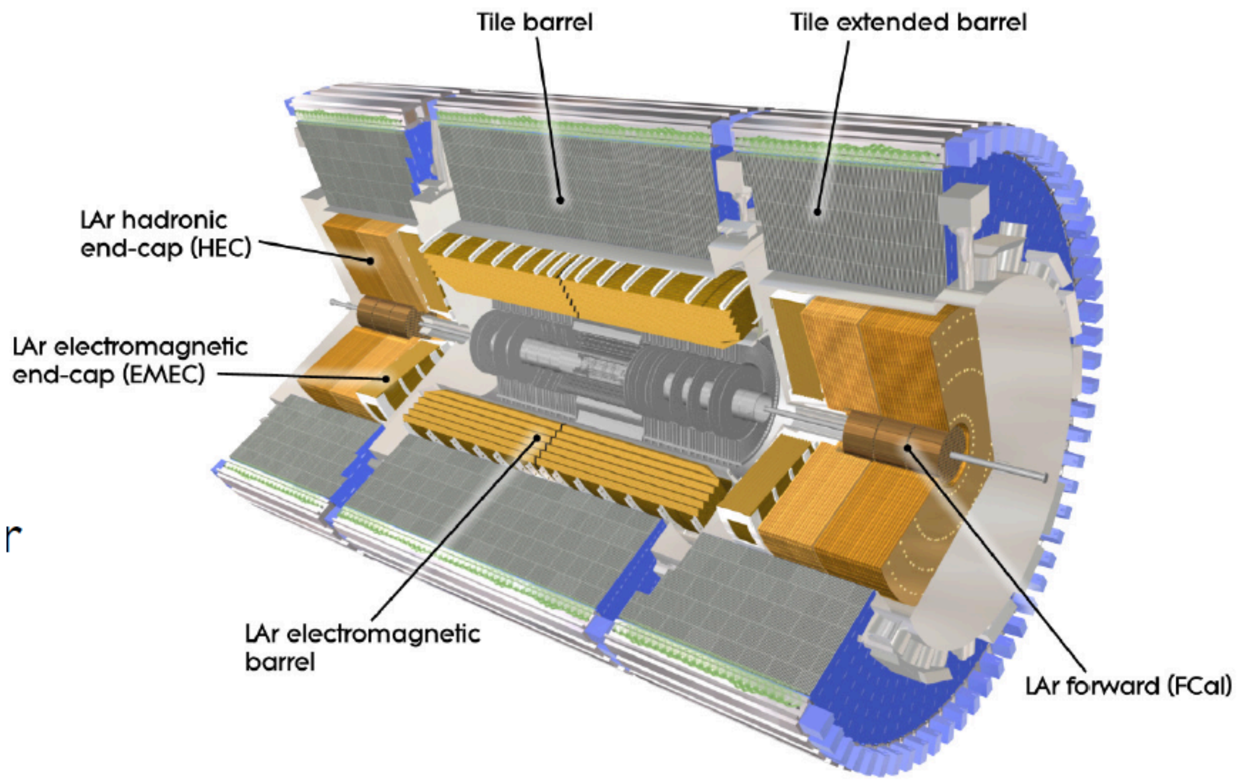

Characteristics of Hadron Showers

- Energy response in a cell of the ATLAS tile calorimeter showing noise plus showers

- Mean energy response is uniform in η and ϕ

- Mean energy deposit is determined by random triggers

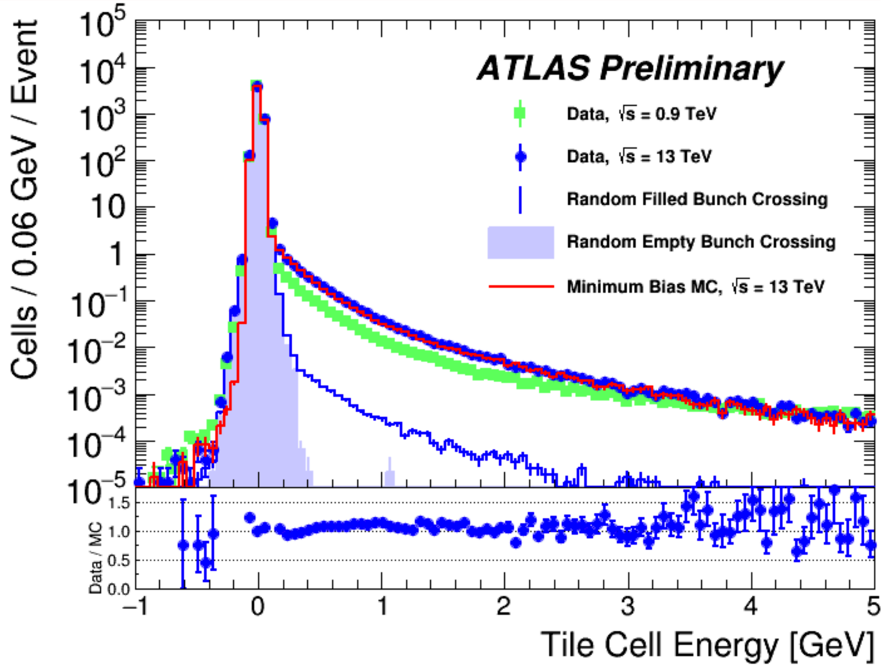

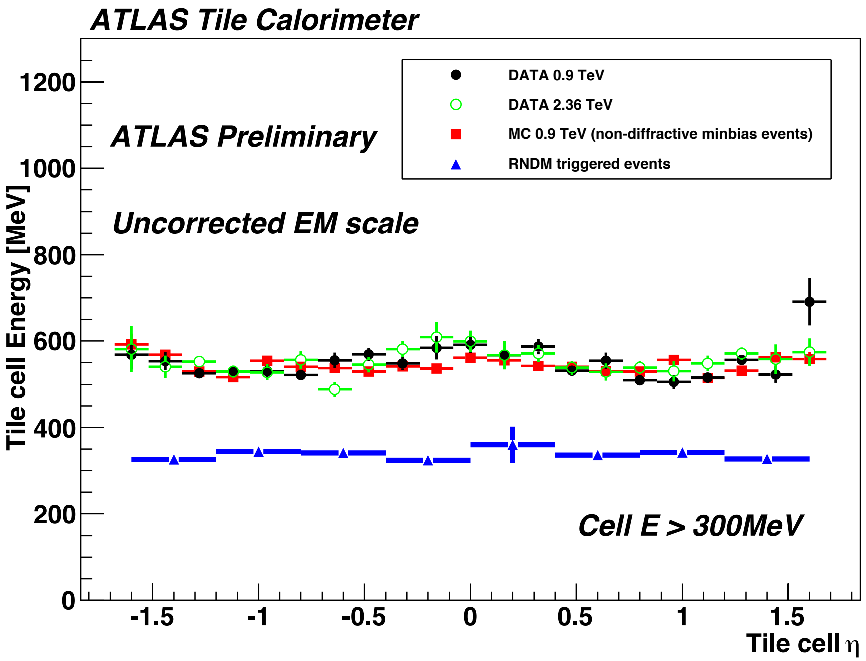

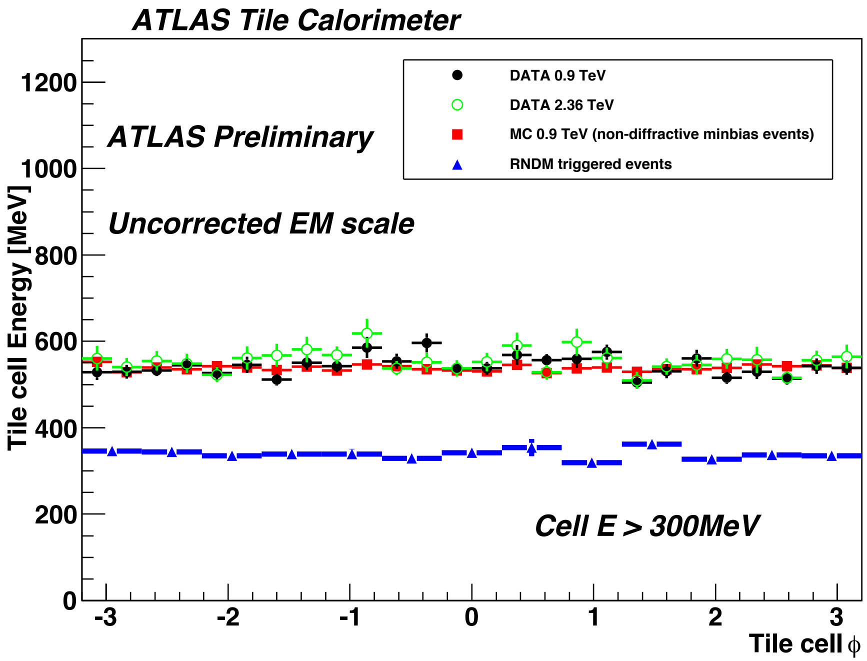

Observed Energy Resolution

- Energy resolution of the ATLAS hadron calorimeter
- Fe-scintillator tile calorimeter: covers barrel region
  - Test beam measurements yield

Data: $\left(\frac{\sigma_E}{E}\right) = \frac{52.1\%}{\sqrt{E}} \oplus 3.0\% \oplus \frac{1.8\ GeV}{E}$ MC: $\left(\frac{\sigma_E}{E}\right) = \frac{48.0\%}{\sqrt{E}} \oplus 3.3\% \oplus \frac{1.5\ GeV}{E}$

- e/h ratio is larger than 1 and varies over energy range

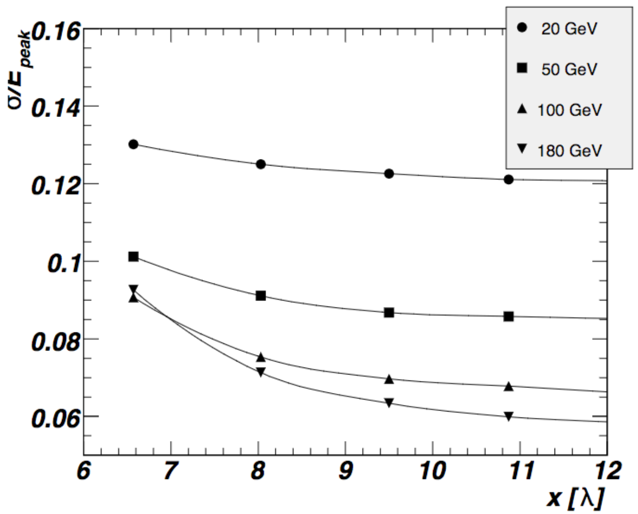

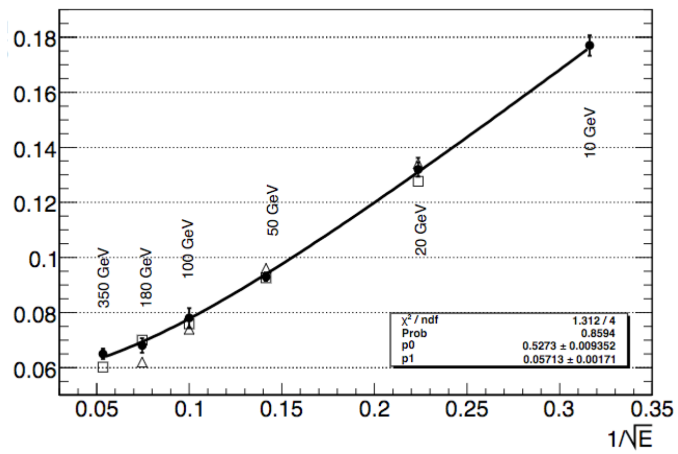

e/h ratio

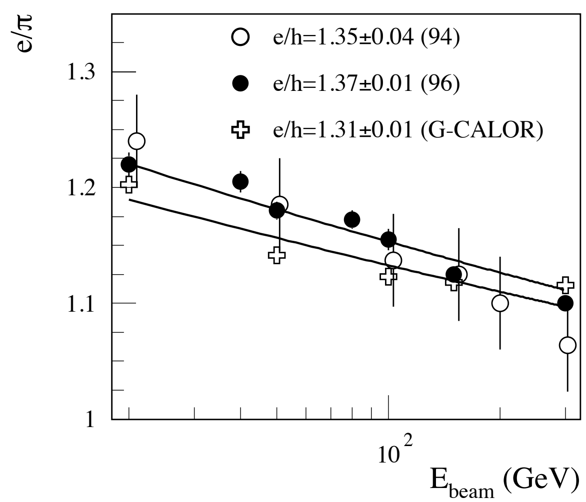

Particle Flow Calorimeters

New Concepts: Particle Flow

- At the international linear collider (ILC) an excellent jet-energy resolution is crucial to study new particles
- Simulate $e^+e^- \to W^+W^-$ & $e^+e^- \to ZZ$ for LEP-like detector & LC design with factor of 2 improvement

LEP-like detector

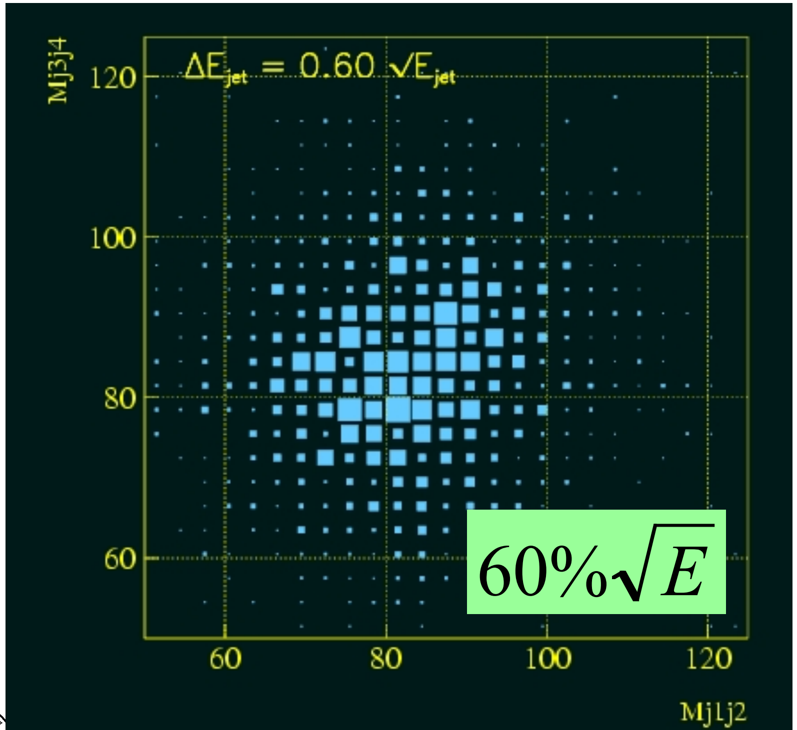

LC design goal

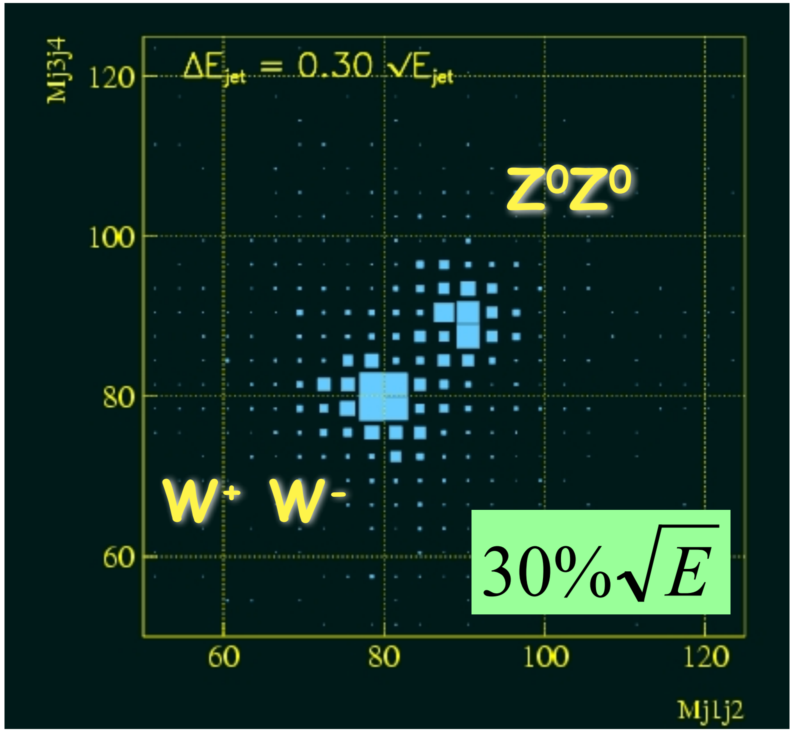

H.Videau

Particle Signatures

- Different particles show characteristic signatures in the detector

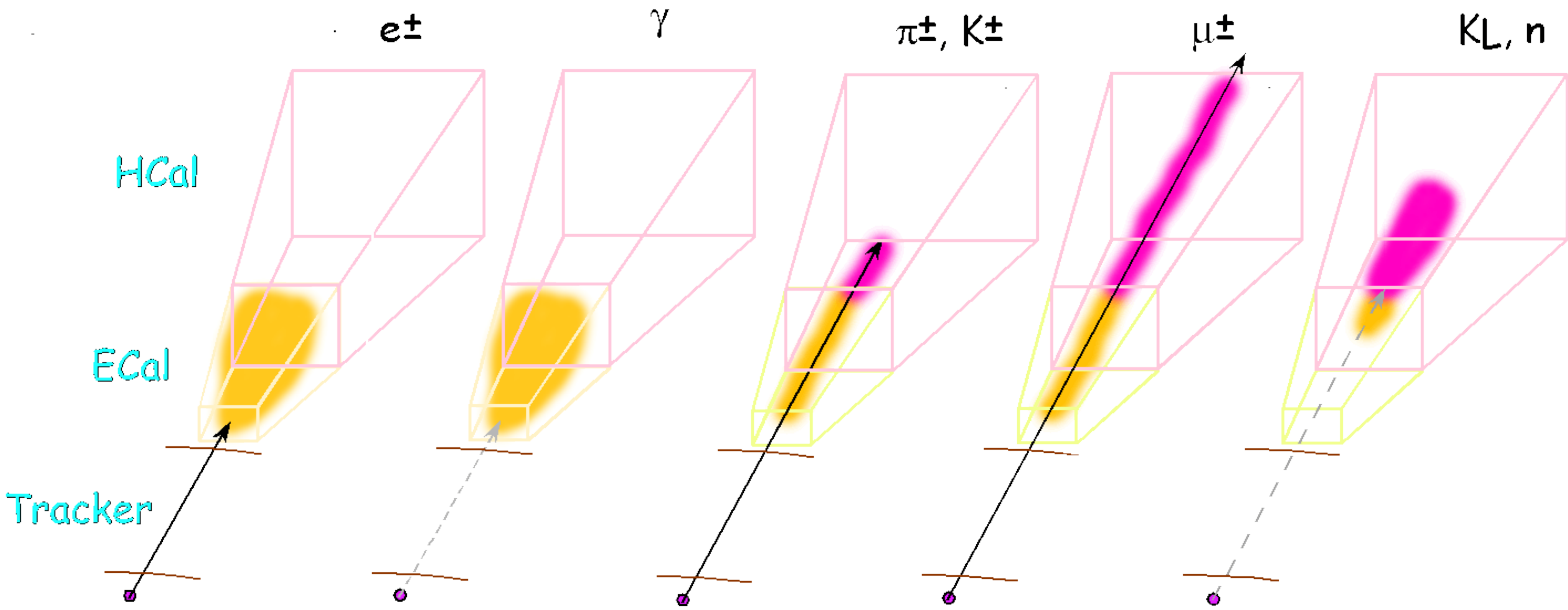

- Need appropriate segmentation in ECal & HCal to separate these

Jet Energy Resolution

- Jet energy: $\mathrm{E}_{\mathrm{jet}} = \mathrm{E}_{\mathrm{charged}} + \mathrm{E}_{\mathrm{photons}} + \mathrm{E}_{\mathrm{neut.\,had.}}$

  65% 25% 10%

- Implementing particle flow we have get jet energy resolution

$$\sigma^2_{\mathrm{E_{jet}}} = \sigma^2_{\mathrm{E_{charged}}} + \sigma^2_{\mathrm{E_{photons}}} + \sigma^2_{\mathrm{E_{neut.had.}}} + \sigma^2_{\mathrm{confusion}}$$

- With anticipated resolutions

$$\sigma^2_{\mathrm{E_{charged}}} \approx \left(5\times10^{-5}\right)^2 \sum \frac{\mathrm{E}^4_{\mathrm{charged}}}{\mathrm{GeV}^2} \approx (0.02\ \mathrm{GeV})^2\, \tfrac{1}{10} \sum \left(\frac{\mathrm{E}_{\mathrm{charged}}}{10\ \mathrm{GeV}}\right)^4$$

$$\sigma^2_{\mathrm{E_{photons}}} \approx (0.10)^2 \sum \mathrm{E}_{\mathrm{photon}} \cdot \mathrm{GeV} \approx (0.52\ \mathrm{GeV})^2 \sum \left(\frac{\mathrm{E}_{\mathrm{jet}}}{100\ \mathrm{GeV}}\right)$$

$$\sigma^2_{\mathrm{E_{neutral\ hadrons}}} \approx (0.50)^2 \sum \mathrm{E}_{\mathrm{neutral\ hadrons}} \cdot \mathrm{GeV} \approx (1.6\ \mathrm{GeV})^2 \sum \left(\frac{\mathrm{E}_{\mathrm{jet}}}{100\ \mathrm{GeV}}\right)$$

- Ignoring the (typically) negligible tracking term:

$$\sigma^2_{\mathrm{E_{jet}}} \approx (0.17)^2 \left(\mathrm{E}_{\mathrm{jet}} \cdot \mathrm{GeV}\right) + \sigma^2_{\mathrm{confusion}} \approx (0.3)^2 \left(\mathrm{E}_{\mathrm{jet}} \cdot \mathrm{GeV}\right)$$

- $\sigma^2_{\mathrm{confusion}}$ is the largest term of all >25%

SiW EM Calorimeter

- Si-W ECAL, 3 W structures
- 15 active layers (Si)
- 1 cm×1 cm Si pixels
- CMS has adopted design for upgrade of ECAL ECs

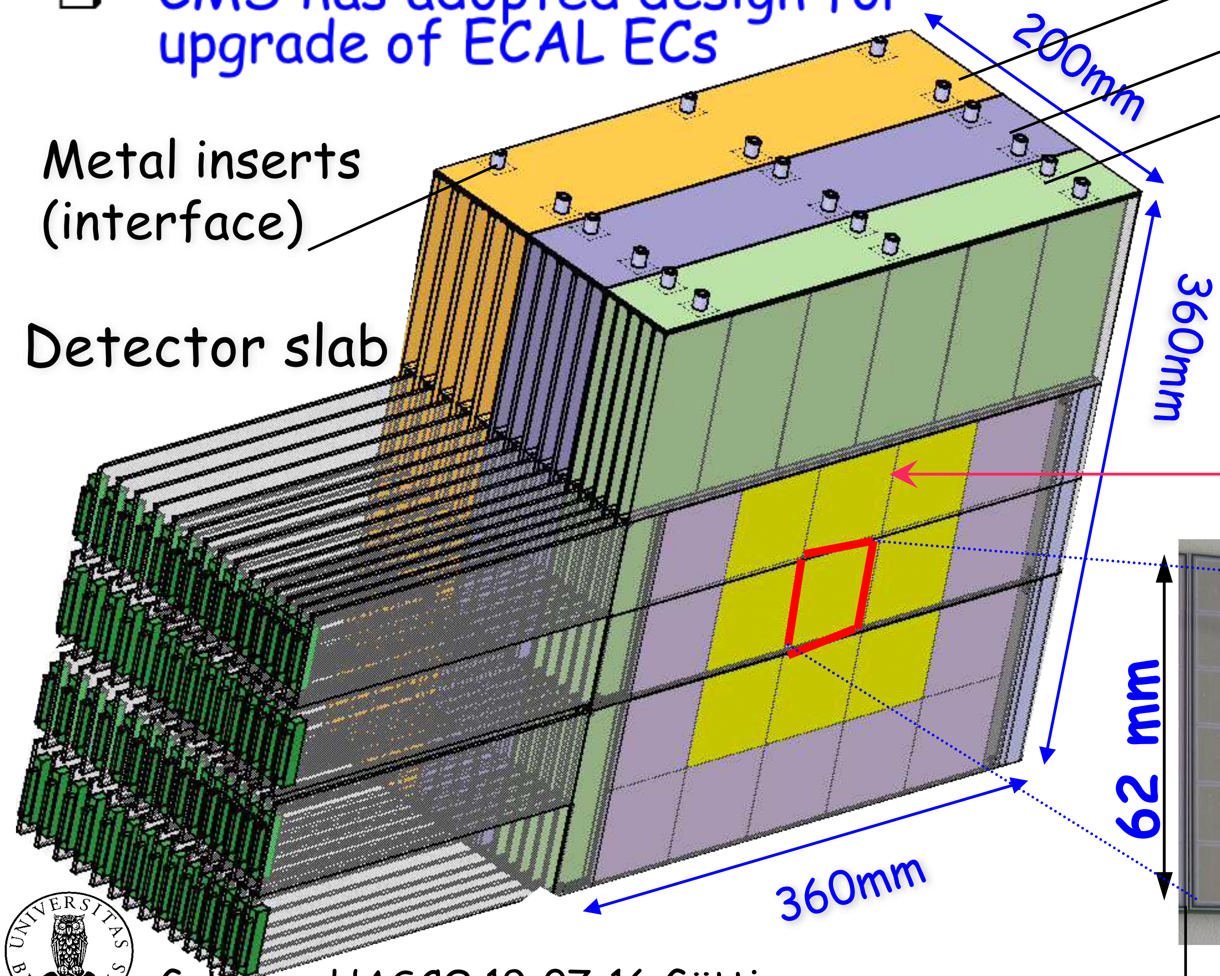

active area (18×18 cm^2)

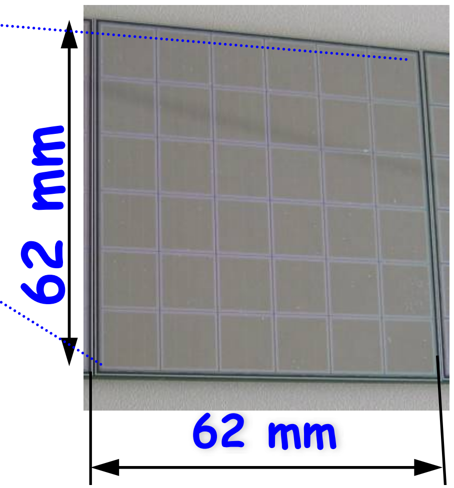

Silicon wafers
With 6×6 pads
(10×10 mm^2 each)

SiW EM CalorimeterPerformance

- Measure e showers between 6 GeV and 45 GeV at CERN/Fermilab
- Observe excellent linearity
- Energy resolution is $$\frac{\sigma_E}{E} = \left[\frac{16.7 \pm 0.1 \pm 0.4}{\sqrt{E[\mathrm{GeV}]}} \oplus 1.1 \pm 0.1 \pm 0.1\right]\%$$

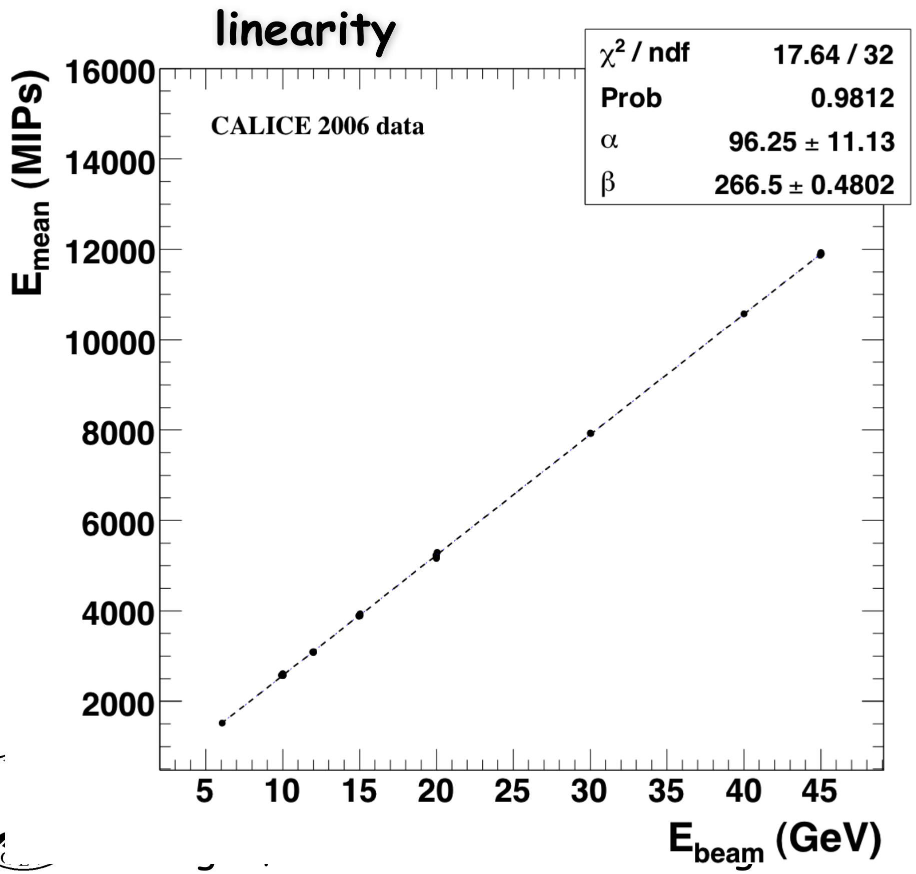

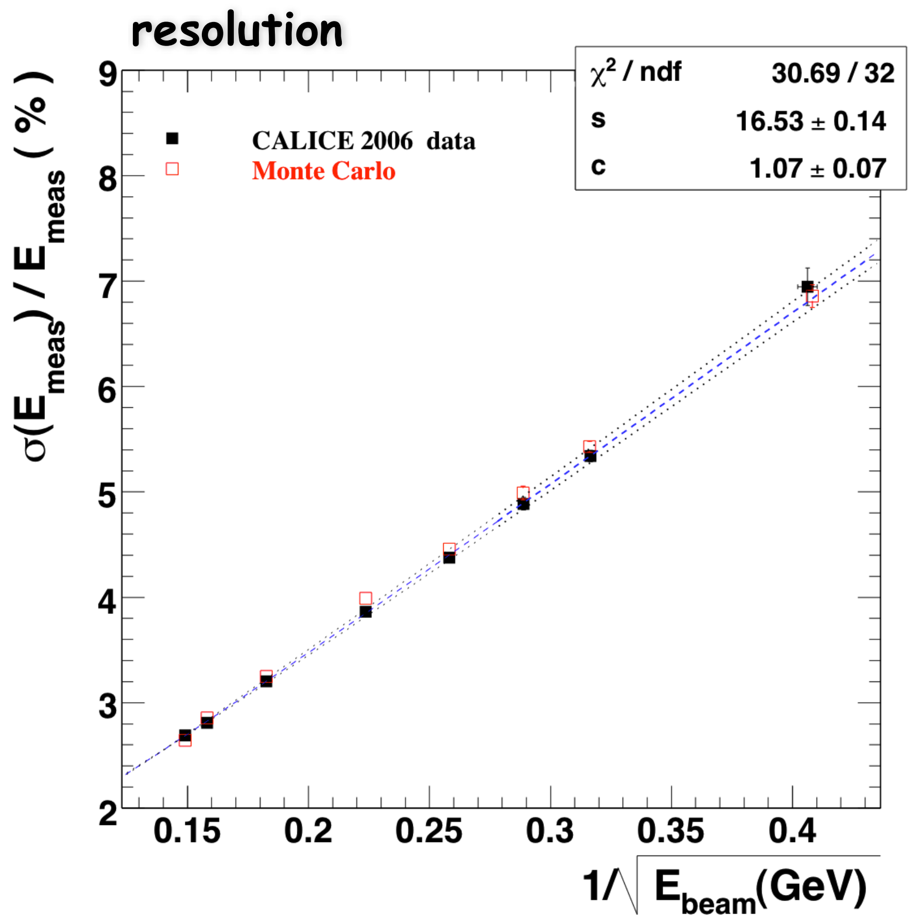

Analog Hadron Calorimeter

- 38-layer Fe-scintillator sampling calorimeter (4.5 ✧)
- Layer: 2 cm steel absorber plates + 1/2 cm scintillator tiles
  - core tiles: 3×3 cm² (10×10 matrix) increasing towards outside
- Total of 7608 tiles, each is read out with wavelength-shifting (WLS) fiber + SiPM (216 tiles/layer)

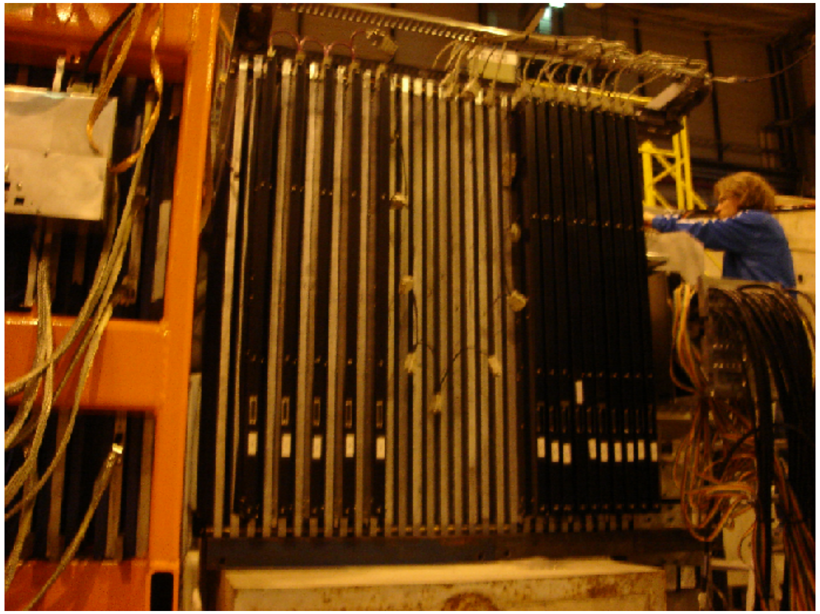

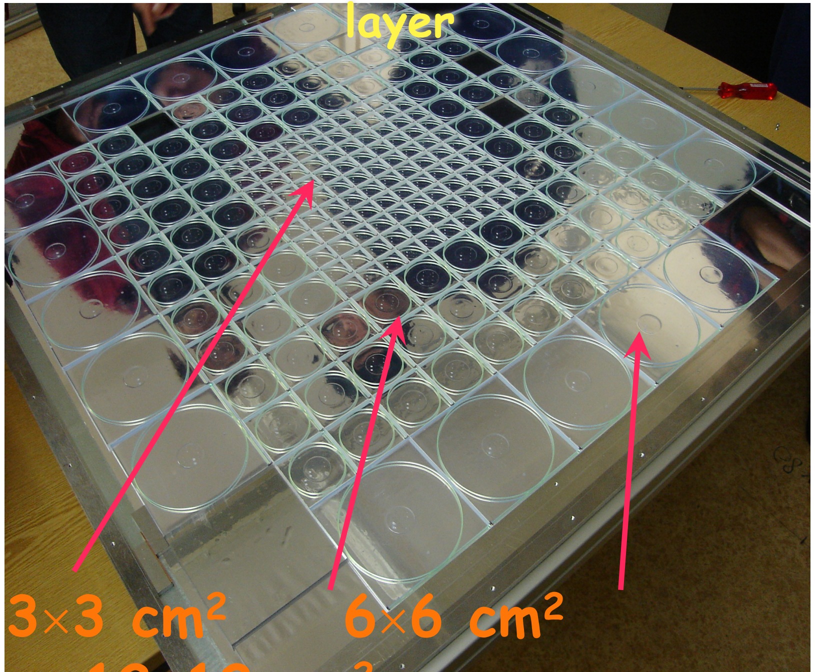

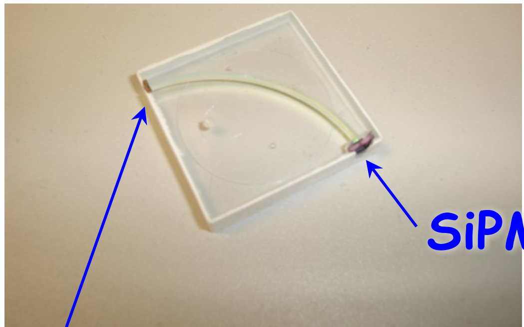

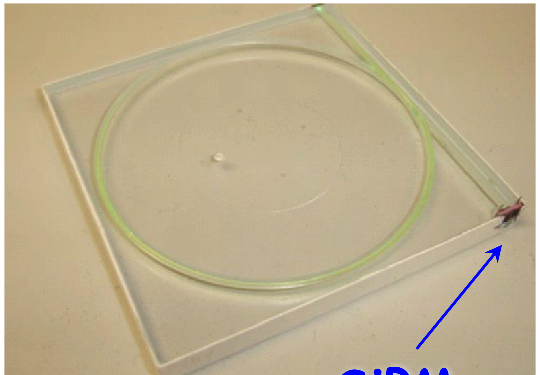

SiPMs

- The SiPM is a pixilated avalanche photodiode operated in Geiger mode

SiPM

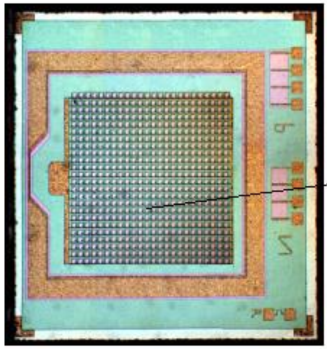

Pixel Arrangement

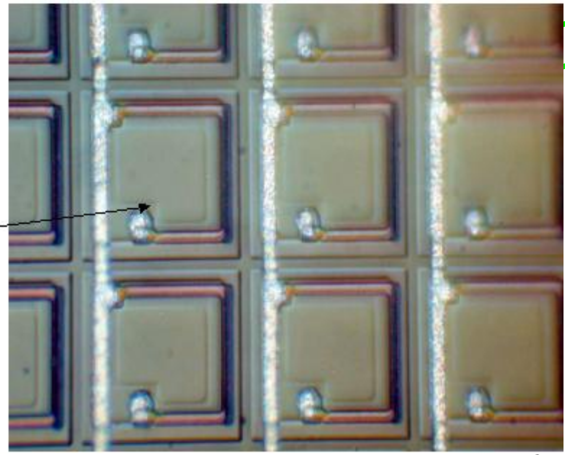

Al conductor

Si* resistor

E-field distribution

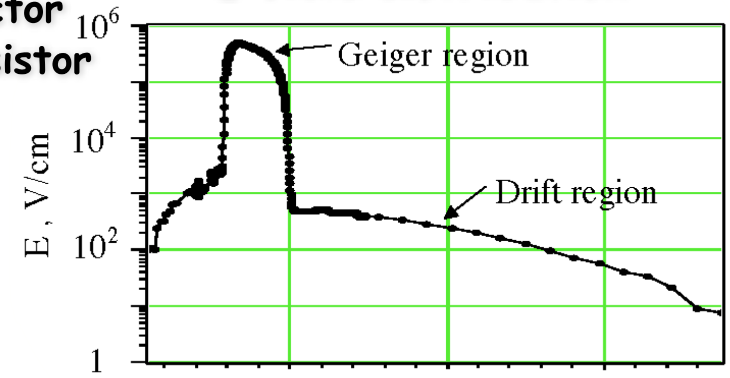

Design (sideview)

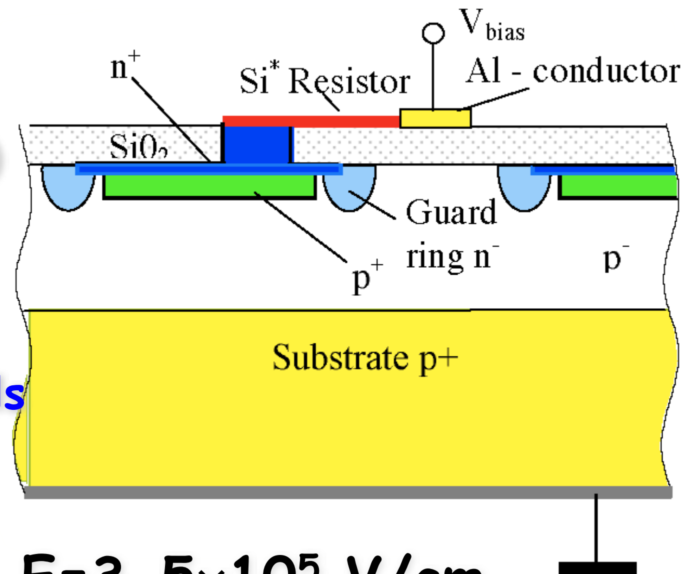

1024 pixels

$E = 3\text{-}5 \times 10^5$ V/cm

Spectrum of pe

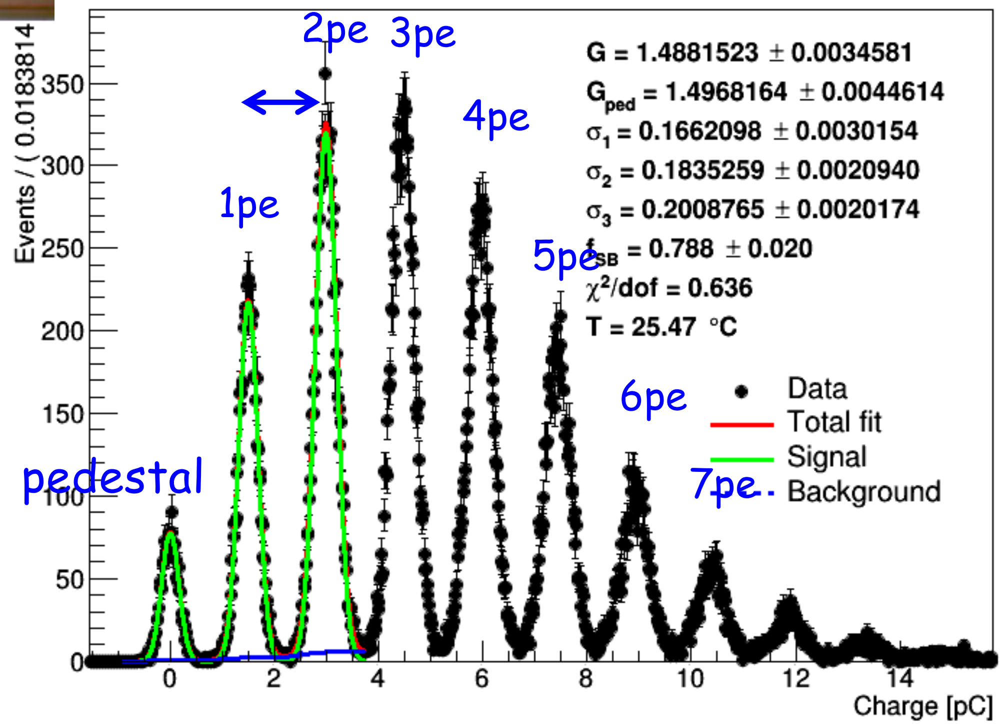

Performance of Analog Hadron Calorimeter

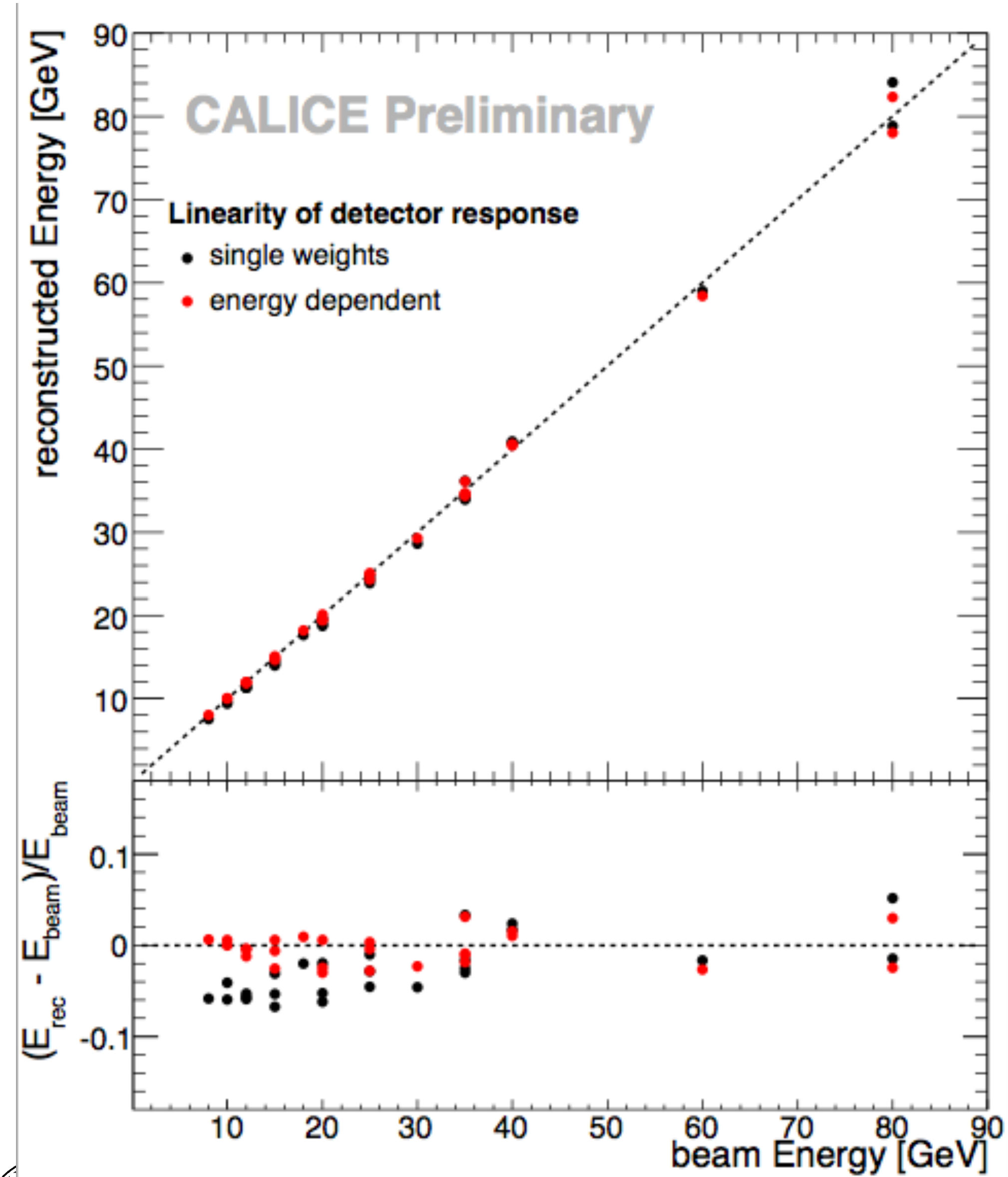

- Response of the hadron tile calorimeter is linear

- Resolution with appropriate energy weighting yields

$$\frac{\sigma_E}{E} = \left[\frac{48.8 \pm 0.2}{\sqrt{E[\mathrm{GeV}]}} \oplus 0.0 \pm 0.23\right]\%$$

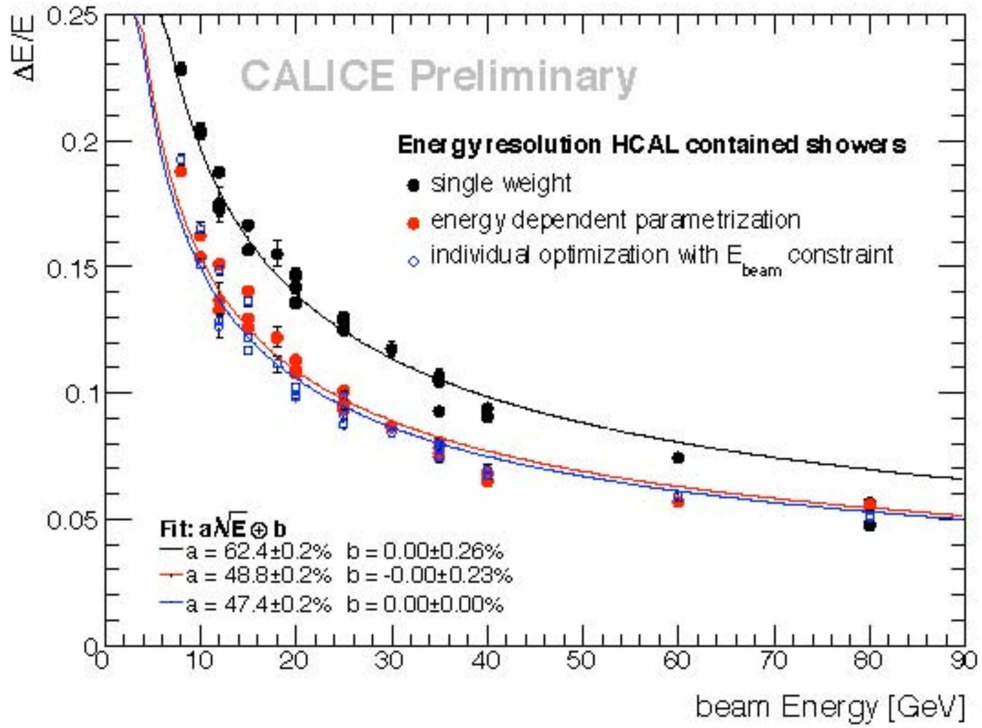

Particle Identification Detectors

Cherenkov Radiation

- Below the excitation energy a charged particle can radiate a photon
  - particle: mass m, velocity $\vec{v}=\vec{\beta}c$, energy $E=\gamma mc^2$, momentum $\vec{p}=\gamma\vec{\beta}mc$
  - medium: refractive index n, dielectric constant $\varepsilon=\varepsilon_1+i\varepsilon_2$, & $n^2=\varepsilon_1$
  - photon: energy $\hbar\omega$, momentum $\hbar\vec{k}$

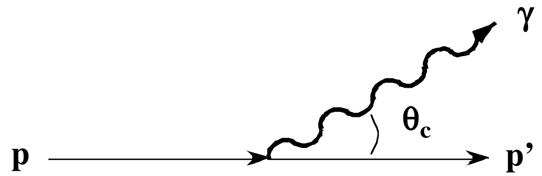

- Energy-momentum conservation
  ($p' = p - p_\gamma$) yields for $\hbar\omega \ll \gamma mc^2$:

$$\omega = \vec{v}\cdot\vec{k} = vk\cos\theta_c$$

- Dispersion relation provides link
  between photon energy & momentum

$$\omega^2 = \frac{k^2c^2}{\varepsilon}$$

- Combination of both equations yields Cherenkov condition

$$\sqrt{\varepsilon}\,\frac{v}{c}\cos\theta_c = 1 \quad\rightarrow\quad \beta\cdot\cos\theta_c = 1/n$$

- The number of Cherenkov photons is wave length dependent

$$\frac{dN}{d\lambda} = \frac{2\pi\alpha}{\lambda^2} L\sin^2\theta_c$$

Most photons are radiated
In the UV region

Concept of Ring Imaging Cherenkov Counters

- Cherenkov counters have been used in fixed target experiments in which particles are parallel to the optical axis of detector
- To use this technology in a colliding-beam experiment, a new approach was suggested
- A spherical mirror of radius R_M centered at IR focuses the Cherenkov cone produced in the radiator between the sphere radius R_D & the mirror into a ring-shaped image on the detector sphere R_D
- Usually $R_D = 1/2R_M$
- Both SLD and Delphi used this approach

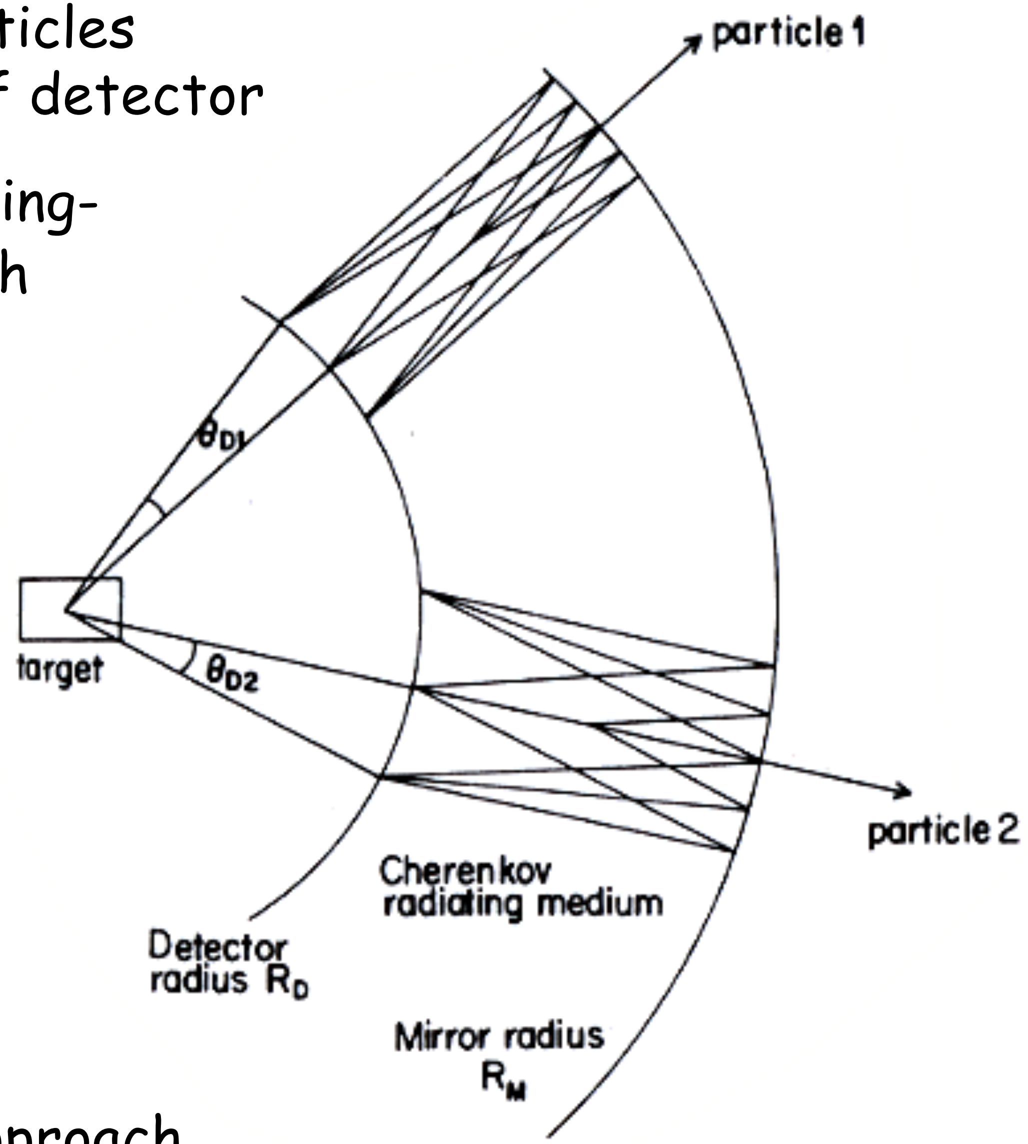

Ring Imaging Cherenkov Counters

- Since focal length of mirror is $R_M/2$, Cherenkov cones of opening angle $\theta_c=\arccos[1/(\beta n)]$ emitted along the particle's path in the radiator are focused into a ring with radius r on the detector sphere

- For $R_D=R_M/2$, the opening angle θ_D of this ring equals θ_c in first approximation

- For this special geometry, the radius of ring image yields θ_c via

$$\tan\theta_c = \frac{2r}{R_M}$$

- The uncertainty in momentum separation is

$$\frac{\Delta p}{p} = \frac{\Delta\gamma}{\gamma\beta^2} \quad \text{with} \quad \frac{\Delta\gamma}{\gamma} = \gamma^2\beta^3 n \sin\theta_c \Delta\theta_c$$

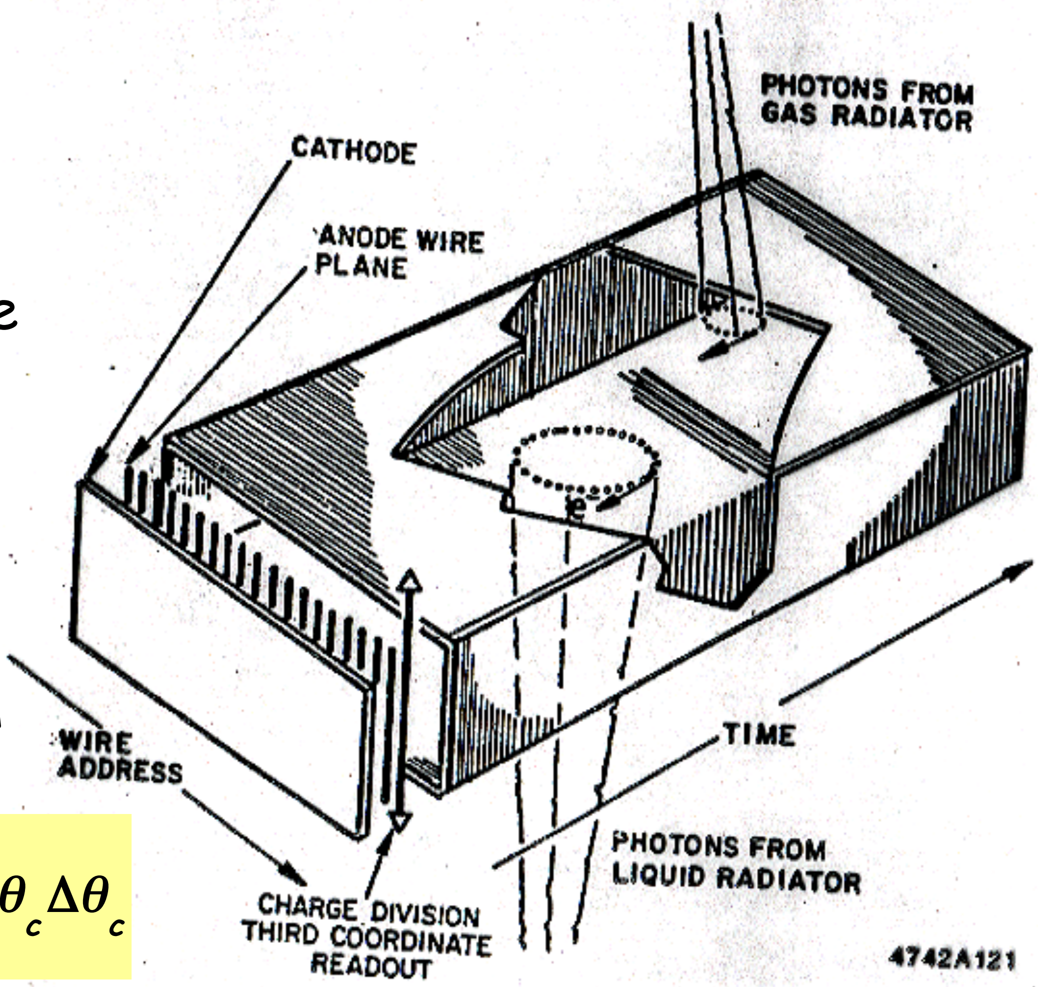

Particle Identification with DELPHI RICH

- Particle separation in DELPHI RICH
- Observation of a ring

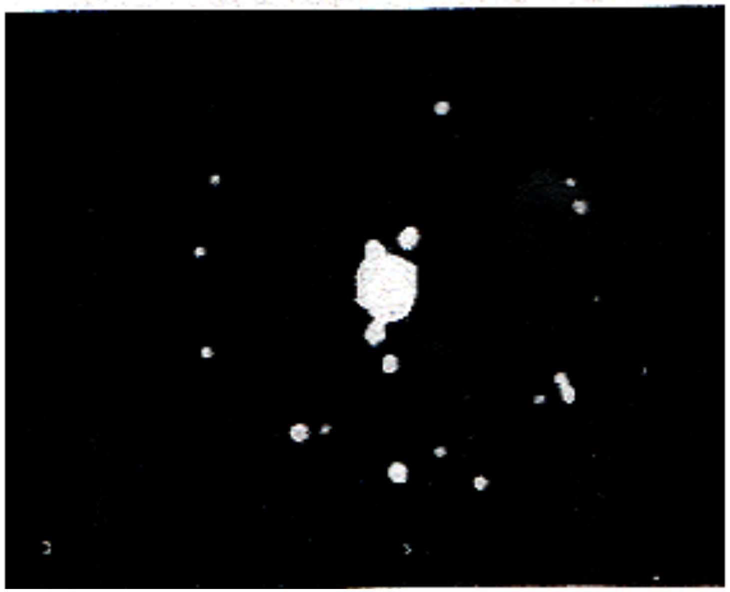

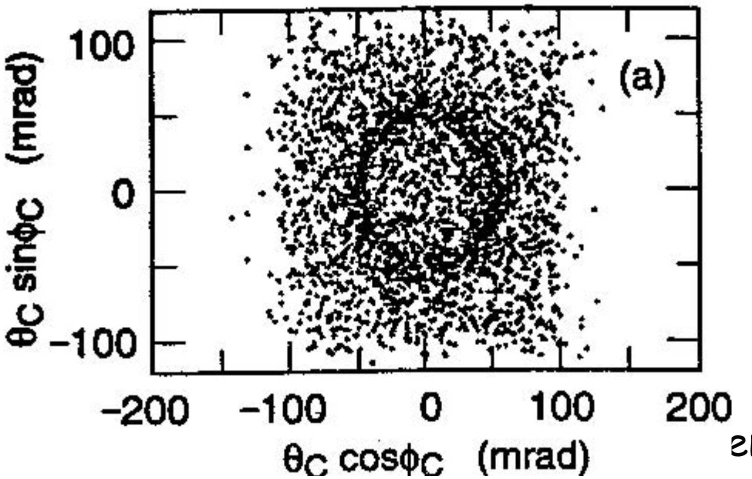

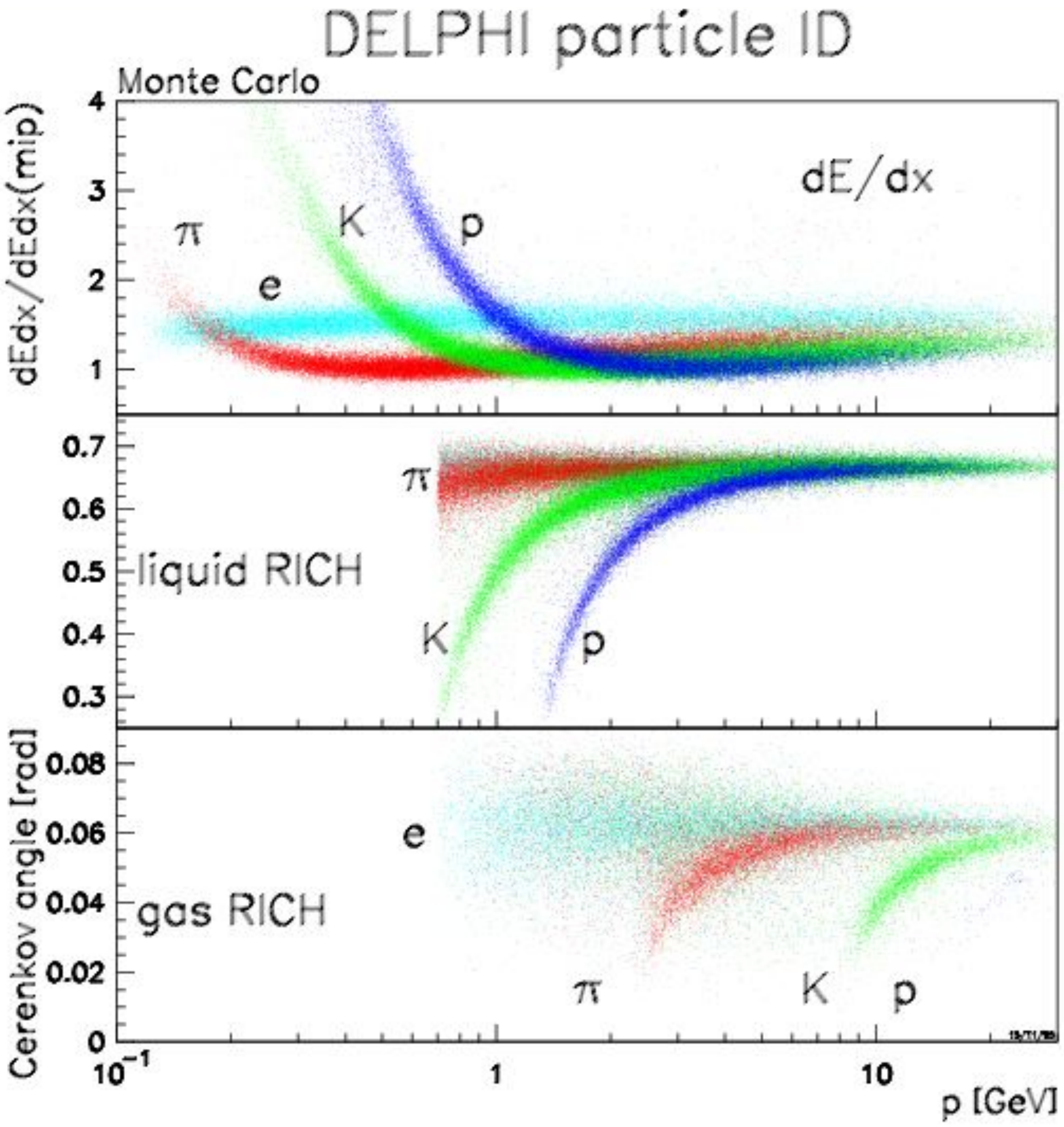

Transition Radiation

- Transition radiation arises from rapidly changing refractive indices: foil-gas → multiple layers to increase yield

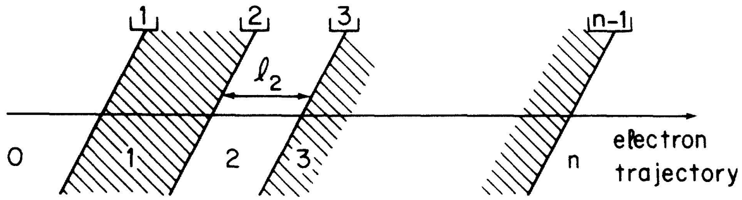

- Formation zone inside foil $\zeta < l_1$ $$\zeta = \frac{2c}{\omega}\left(\frac{1}{\gamma^2} + \frac{\omega_p^2}{\omega^2} + \theta^2\right)^{-1}$$
  ω_p: plasma frequency (styrene~20eV)
  θ: polar angle of radiation
  ω: X-ray frequency

- Number of photons: $$\frac{dN}{d\omega} \propto \frac{2\alpha}{\pi\omega} ln\left(\frac{\gamma\omega_p}{\omega}\right)$$

- For a particle with $\gamma = 10^3$, radiated photons are in soft X-ray range 2-40 keV

- Due to absorption low X-ray range is removed

-

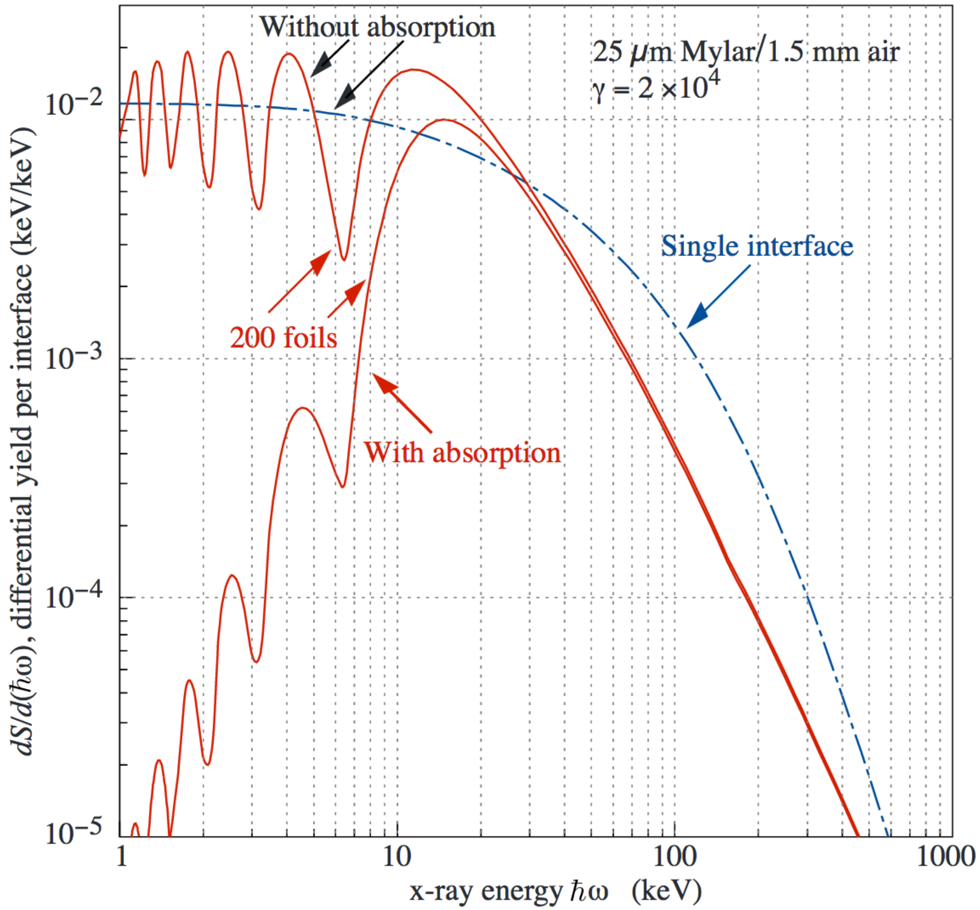

Transistion Radiation Detectors

- Pulse height spectrum in 1000 Li foils & Xe chamber

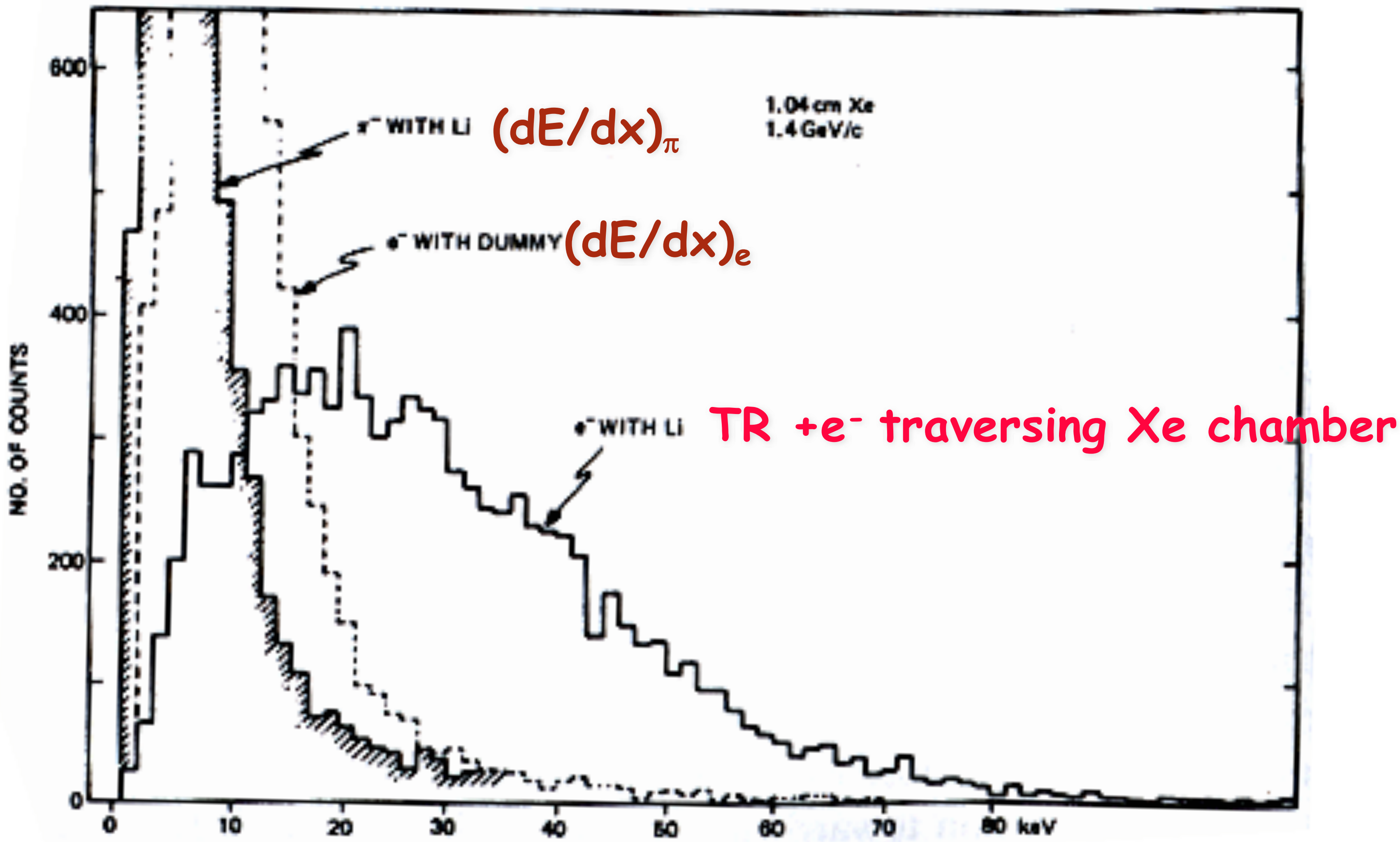

Pulse height spectrum from a Xe-filled proportional chamber of 1.04 thickness behind a Transition radiator (1000 Li foils of 51 μm thickness) exposed to 1.4 GeV/c e⁻/π beams

ATLAS Transition Radiation Tracker

- The ATLAS TRT consists of 36 layers of straw tubes, 4 mm in diameter with position resolution of 200 μm interspersed with Xenon as radiator

- Separation between hadrons and electrons via transition radiation turns on when $\beta\gamma$>~1000

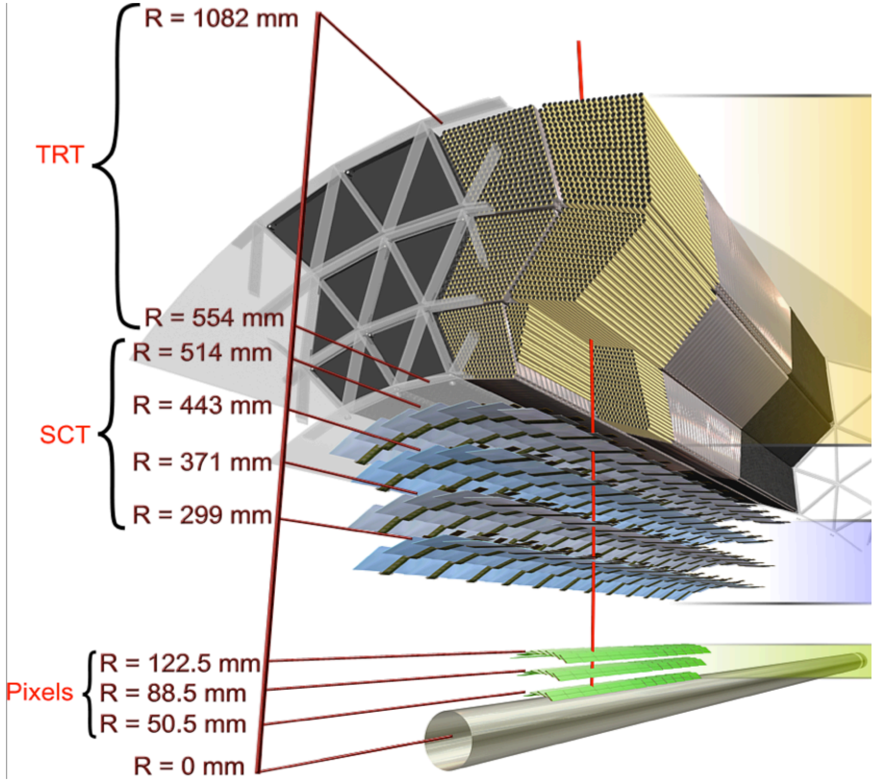

Endcaps

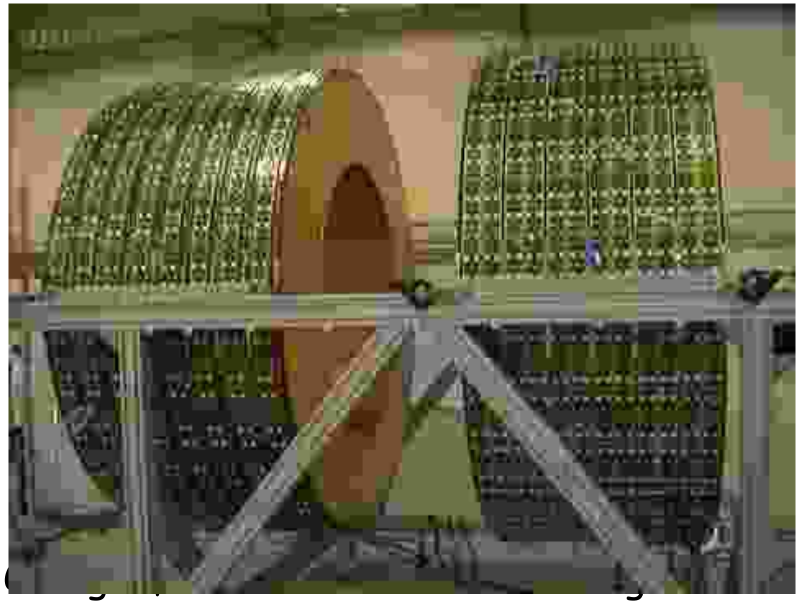

Barrel

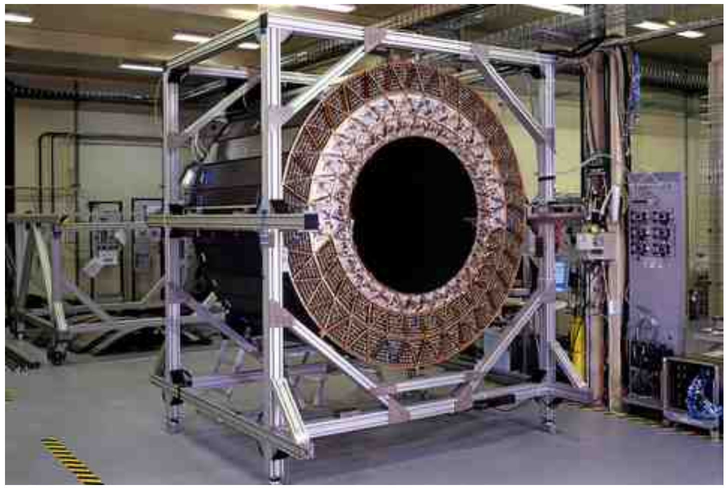

Performance of ATLAS TRT

❒ Time over threshold distribution

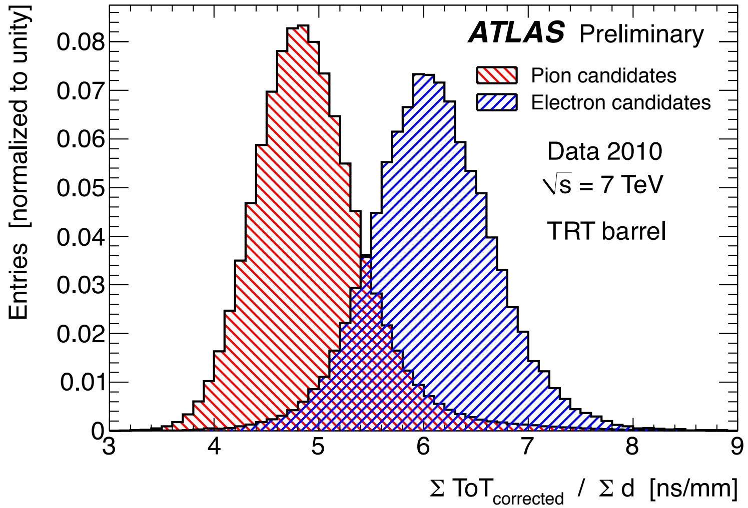

❒ High threshold probability vs p

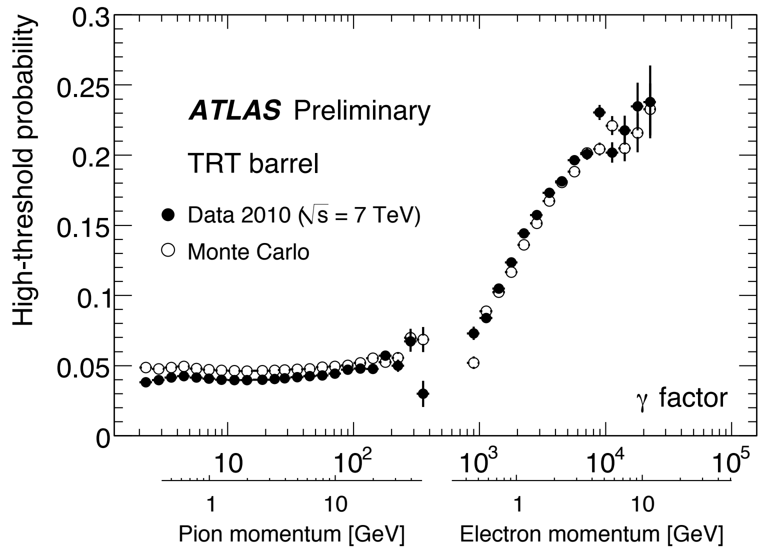

❒ Efficiency vs distance to straw center

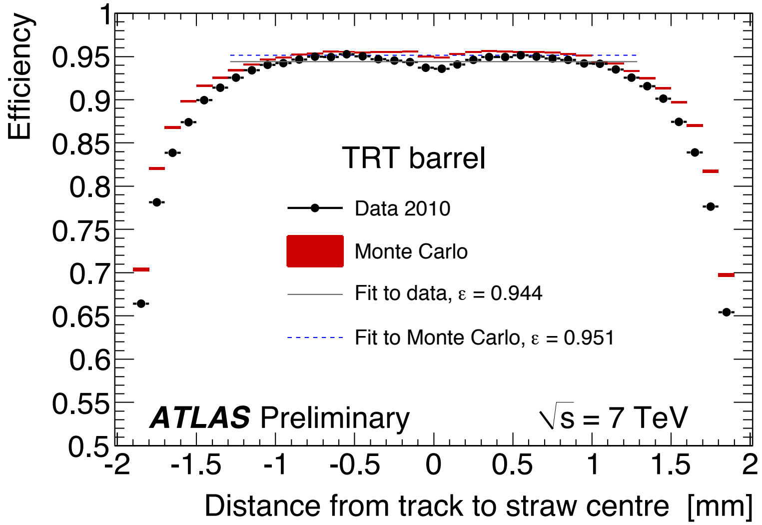

❒ Pion misidentification probability